UNIVERSITY OF OKLAHOMA

GRADUATE COLLEGE

SYNERGISTIC INTERACTIONS OF XANTHAN AND GUAR GUM POLYMERS

A THESIS

SUBMITTED TO THE GRADUATE FACULTY

in partial fulfillment of the requirements for the

Degree of

MASTER OF SCIENCE

By

ABHISHEK GOVINDU
Norman, Oklahoma
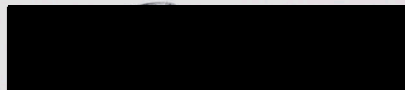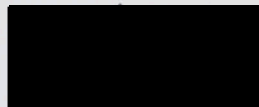2015

SYNERGISTIC INTERACTIONS OF XANTHAN AND GUAR GUM POLYMERS

A THESIS APPROVED FOR THE
MEWBOURNE SCHOOL OF PETROLEUM AND GEOLOGICAL ENGINEERING

BY

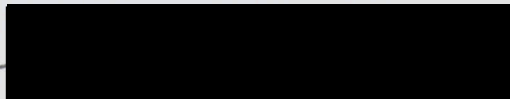_____
Dr. Subhash Shah, Chair

_____
Dr. Ramadan Ahmed

_____
Dr. Maysam Pournik

ACKNOWLEDGEMENTS

TABLE OF CONTENTS

LIST OF TABLES

LIST OF FIGURES

ABSTRACT

Polymers such as xanthan and guar gum are widely used in the oilfield and food industry as viscosifiers. In hydraulic fracturing operation, guar gum polymer solution is used as fracturing fluid to create fracture in a target zone that contains hydrocarbon. Fracturing fluid viscosity helps transport propppant down the well and into the fracture. If the fluid is not viscous enough, the proppant is deposited at the mouth of the fracture and fracture closes. However, high concentration of polymer in the fluid leads to gel damage in the fracture and reduces its conductivity.

Poor fracture conductivity could lead to expensive re-fracturing operation or abandonment. One way to avoid gel damage/polymer residue problem is to use surfactant or surfactant based fluid. These fluids form micelles that are similar to polymer structure and, thereby, increase the viscosity. This micelle structure breaks down when it comes in contact with hydrocarbon. However, surfactant based fluids are expensive and can form emulsion. The trend in the oil industry is to reduce the polymer content in the fracturing fluid and to crosslink it. Crosslinking is necessary so as to increase the viscosity of the low polymer concentration linear gel. Despite these measures, gel damage to fracture conductivity is a concern and affects productivity of a well.

Blends of xanthan and guar gum are used in the food industry to prepare fluids that have superior viscosity then either parent polymer. This synergy between these

polymers can be used to prepare new fracturing fluids that have desirable viscosity at low polymer concentration, thereby, solving the problem of proppant placement and fracture conductivity. In addition, prepared fluids would be cheaper than high concentration guar gum fluids as they require addition of less polymer.

In this study, the effect of polymer concentration, ratio of xanthan to guar polymer, and temperature on the synergy of xanthan and guar gum polymers is investigated. Particle settling behavior in these complex fluids under static conditions has been studied as well. Results show that increase in polymer concentration increases the strength of synergistic interaction while increase in temperature decreases it. Based on the results a 40 lbm/Mgal guar gum/xanthan fluid blend was identified as a suitable fracturing fluid. This blend showed better viscosities at low shear rates than both 40 and 60 lbm/Mgal guar gum fluids. In addition, it is less expensive than 60 lbm/Mgal guar gum fluid.

CHAPTER 1

INTRODUCTION

1.1 Overview

Fluid viscosity is an important parameter that affects the success of hydraulic fracturing operations. This fluid property plays a major role in providing the following:

1. Sufficient width for proppant to enter the fracture.

2. Carrying proppant from the wellbore to tip of the fracture.

3. Generating required pressure to control the growth of fracture height.

4. Fluid loss control (in cases where a gel filter cake cannot form, the fracturing fluid viscosity is the main mechanism for fluid loss control).

It is also essential that the fluid used, besides exhibiting the desired viscosity, must be safe to handle, environmental-friendly, non-damaging to fracture conductivity and reservoir permeability. These are some of the primary concerns that need to be addressed when selecting a suitable fracturing fluid.

An ideal fracturing fluid, in addition to the above detailed parameters, should also be:

1. Cost effective, such that the performance of the fluid does not drive up the fracturing costs to unacceptable levels.

2. Compatible with the formation so it does not interact adversely or cause damage to the formation mineralogy and formation fluids.

3. Able to break easily so that the viscosity reduces after fracturing and proppant placement, ensuring easy flow back and cleanup of fracture.

4. Not lead to water blocks, which are caused by an increase in water saturation in the near-wellbore area, thereby, decreasing the relative permeability to hydrocarbon.

5. Easy to mix even under very adverse conditions.

To summarize, an ideal fracturing fluid would be the one that would have an easily measured, controlled viscosity, controllable fluid loss characteristics, non-damaging to the fracture and non-interactive with the formation fluids, be completely safe to handle and to the environment. Unfortunately, this is not practical and currently used fracturing fluids compromise on many of these ideal properties. Typically, cost is the driving force, even though this sometimes leads to choices, which can be disastrous to the productivity of the well. Regardless, cost is a very important parameter, other being the viscosity.

As stated above, fluid viscosity is critical for a successful fracturing job. This viscosity should be stable at high temperature, pump rates, and shear rates. It is important to note that even though fluid viscosity is a major parameter guiding fracture design, excessive viscosity increases costs and raises treating pressures. It is, therefore, important that fracturing fluids show pseudoplastic or shear thinning rheological behavior. A shear thinning fluid would have low viscosities at high shear rates encountered when pumping the fluid down to the target zone, and high

viscosities at low shear rates such as when carrying the proppant through the fracture.

Another major concern with conventional guar gum based fracturing fluids is that they leave residue and damage the proppant pack. To counter this, polymer concentrations used for fracturing have been reduced and the fluids are formulated such that the lower concentration polymers still yield required rheology to transport proppant after crosslinking. However, even after adding enzymes and oxidizers to break down the molecular structure of polymer gel, the effect of these breakers is still not enough to eliminate the damage to the proppant pack. Therefore, there is a need to reduce the number of additives used to formulate the fluid to reduce residue in the fracture. One solution is to use surfactants, which form worm-like micelles in aqueous solution. These micelles have a gross structure similar to polymer chains, which increases the viscosity of fluid. Surfactants do not need additives to break down as they completely breakup once in contact with hydrocarbon. However, surfactants are expensive as compared to polymers and are known to form emulsions with certain crude oils.

This study presents an alternate solution to counter the problem of polymer residue by utilizing the synergy of xanthan gum and guar gum fluids. These polymers are used in the food industry to thicken and impart desirable texture to sauces, yogurts, chewing gum, toothpastes, etc. They are being replaced by their blends, which show better rheology than either xanthan or guar fluids, are cheaper and have better

texture due to their synergy. The aim of this study is to investigate this phenomenon, so as to formulate a fracturing fluid that is cheaper and shows higher viscosities at low polymer concentrations and low shear rates without addition of chemicals.

1.2 Statement of Problem

Polymers are used to increase the viscosity of fracturing fluid to a value that is determined to be sufficient to transport proppant effectively into hydraulically created fractures. After placing the proppant, reducing the viscosity of fluid is essential to promote flowback of fracturing fluid so minimum obstruction occurs as hydrocarbons move from formation to wellbore. Breaking the fluid and obtaining good proppant pack conductivity will result in high returns once the well starts producing. Reducing gel damage to the proppant pack and formation leads to minimal flow restrictions and directly impacts the return of oil and gas to wellbore (Almond 1984).

Due to their abundance, relative low cost, proppant-carrying ability, guar gum and its derivatives are extensively used as fracturing fluids today. However, these polymers have insoluble residue, carried over from manufacturing process and also generated during breaking of the fluid. Broken linear or crosslinked guar gels damage the proppant pack and significantly reduce its conductivity (Devine et al. 1999). It is, therefore, beneficial to reduce the polymer concentration in fracturing fluid to mitigate problems of polymer residue. This presents another problem, as poor or insufficient fracturing fluid viscosity will lead to premature screen-out,

where proppant drops out in wellbore or fracture, impairing fluid's ability to extend the fractures deeper into the formation. A third concern is that high viscosity of fluid would result in higher friction pressure losses when pumping down the tubing.

Delayed crosslinkers, introduced in 1982, are used to strengthen the viscosity of low concentration polymer fluids. Using these chemicals would delay the crosslinking reaction so viscosity of fluid will not increase until shortly before it reaches the bottom of wellbore and enters the fracture. Low viscosity of low concentration polymer fluids will not result in significant increase in friction pressure losses as fluid is pumped to the bottom of wellbore. Despite these measures, damage to proppant pack due to polymer residue remains a concern in the industry. In addition, using delayed crosslinkers and addition of more chemicals in formulating fracturing fluids poses environmental and cost concerns.

1.3 Objectives

The principle aim of this study is to strengthen the rheological properties of low concentration guar gum polymer fluids by utilizing synergy of guar gum-xanthan gum polymers. Therefore, the objectives are to:

1. Develop complex fluid composed of guar gum and xanthan gum polymers that lower cost and show better performance than conventional guar based fracturing fluids.

2. Formulate the fluid such that it has better shear thinning properties than guar gum polymer fluids.

3. Ensure the developed fluid has higher low shear rate viscosity than guar gum polymer fluids.

4. Improve understanding of particle settling in complex fluids.

1.4 Scope and Methodology

This study involves experimental investigations and theoretical study to achieve above stated objectives. Experimental work involved rheological studies of complex fluids at ambient temperature (77 °F) to determine strength of synergy of xanthan and guar gum polymers in fresh water at two different concentrations – 40 lbm/Mgal (0.48 *wt%*) and 60 lbm/Mgal (0.71 *wt%*). Rheology of complex fluids at 150 °F was studied to determine their sensitivity to temperature. Shear thinning property and relative high low shear rate viscosity of the developed complex fluids was compared with component guar gum polymer fluid. Cost analysis was performed as well and based on these investigations a complex fluid with a polymer concentration of 40 lbm/Mgal was identified as a viable fracturing fluid.

To design successful fracturing treatments it is important to understand particle settling characteristics in complex fluids as these affect proppant distribution in fracture. Therefore, experimental work involved studying terminal settling velocity of particle in complex and base (guar gum and xanthan gum) fluids. The scope of settling velocity study was: (1) to determine if settling velocity correlations

settling velocity study was: (1) to determine if settling velocity correlations available in the literature for polymer fluids are applicable for complex fluids, and (2) to relate terminal settling velocity to fluid viscosity and identify complex fluid with relative high low shear rate viscosity and better shear thinning property than component guar gum fluid. Particle settling under static and dynamic conditions was theoretically studied, taking into account factors such as wall effects and particle-particle effects. Based on this study, experimental single particle settling velocity data was compared with Shah (1982) correlation.

CHAPTER 2

LITERATURE REVIEW

2.1 Fracturing Fluids

There is a wide variety of fracturing fluids available today with an even more impressive range of additives. The fracturing fluids can be broadly categorized into:

1. Water based fluids – Fluids that use water as the base fluid.

2. Oil based fluids – Fluids that use oil as the base fluid for water sensitive formations.

3. Energized fluids – Fluids that use immiscible gases with water such as Nitrogen, and Carbon dioxide.

4. Multi-phase emulsions – Fluids that use immiscible material with water such as propane or diesel such that water is the internal phase.

5. Acid fluids – Fluids that use a weak acid as the base fluid.

The additives can be categorized as:

1. Gelling agents – Additives that increase the viscosity of solution.

2. Cross-linkers – Additives that increase the viscosity of a linear gel.

3. Breakers – Additives that reduce the viscosity of fluid after fracturing treatment.

4. Fluid loss additives – Additives that aid in fluid loss by building a filter cake on the fracture face as the fluid loses to the formation.

5. Bactericides – Additives that kill micro-bacterial organisms that could degrade the fluid.

6. Surfactants and non-emulsifying agents – Additives that prevent formation of emulsions and water blocks.

7. Clay control additives – Additives that prevent swelling of clay on contact with water.

8. Temperature stabilizers – Additives that prevent loss of viscosity of polymer gel at high temperature.

The first fracturing fluid used was developed during the Second World War and composed of gasoline gelled with palm oil and cross-linked with napthenic acid, commonly called Nalpalm. These fluids were highly hazardous and expensive, leading to the development of safer, cheaper, water based fluids. Most of the fracturing fluids used today are water based fluids. The components of a typical cross-linked water based fluid are: polymer, water, cross-linker, buffer, and gel-stabilizer or breaker. Each component is critical to the development of desired fracturing fluid properties. Polymers in fracturing fluids act as viscosifiers and thereby provide desired viscosity to:

1. Generate fracture width.

2. Suspend proppants.

3. Control fluid loss to formation.

4. Reduce friction pressure in tubing.

Guar gum and cellulosic derivatives are the most commonly used polymers in fracturing fluids. Usually these polymers in water are cross-linked with metal-based

cross-linkers. The first cross-linked guar fluid used a borate cross-linker and was patented by Lord Kern with Sinclair (later ARCO) on October 16, 1962. Metal-based cross-linking agents developed by DuPont for plastic explosive applications were found to be useful for formulating fracturing fluids for high temperature applications. Fluids formulated using cellulosic derivatives are residue-free and help minimize fracturing fluid damage to formation. However, these derivatives are difficult to disperse due to their rapid rate of hydration. Fluids formulated using guar gum and its derivatives are easily dispersed but produce some residue when broken. Strong oxidizing agents such as sodium or ammonium per sulfate are added to these fluids to break the polymer as the temperature increases. The first patent on borate gel breakers was issued to Tom Perkins, Sinclair, December 29, 1964.

Buffers are used in conjunction with polymers such that optimal pH for polymer hydration can be attained. When this optimal pH is reached, the fluid or the polymer exhibits the maximum viscosity. Usually weak acid/weak base blends are used as buffers in fracturing fluids. The ratios of these blends are adjusted so the desired pH can be attained. Some buffers dissolve slowly to delay the cross-linking effect.

Gel stabilizers are added to fracturing fluids to inhibit chemical degradation as the fluid travels from the wellbore to the fracture tip. Some commonly used gel stabilizers are methanol, Tri Ethanol Amine (TEA), and various inorganic sulfur compounds. Some stabilizers interfere with cross-linking. Therefore, it is important to identify compatibility of individual components in the fracturing fluid. TEA and

sulfur compounds are preferred over methanol as it is expensive, flammable, and

toxic.

2.2 Guar gum

Guar gum is a galactomanan obtained from the endosperm of the *Cyamopsis*

tetragonolobus seed. Galactomanans are polysaccharides consisting of a mannose

backbone with galactose side groups. The principal backbone is a chain of (1-4)-β-

D-mannopyranosyl units, with single (1-6)-α-D-galactopyranosyl units linked to the

principal chain. The molecular weight of the polymer ranges from 1.2×10^6 to $2.0 \times$

10^6 g/mol. Figure 2.1 shows the structure of the guar gum polymer. This figure

shows two mannose units (forming the backbone) and one linked galactose

molecule (side group).
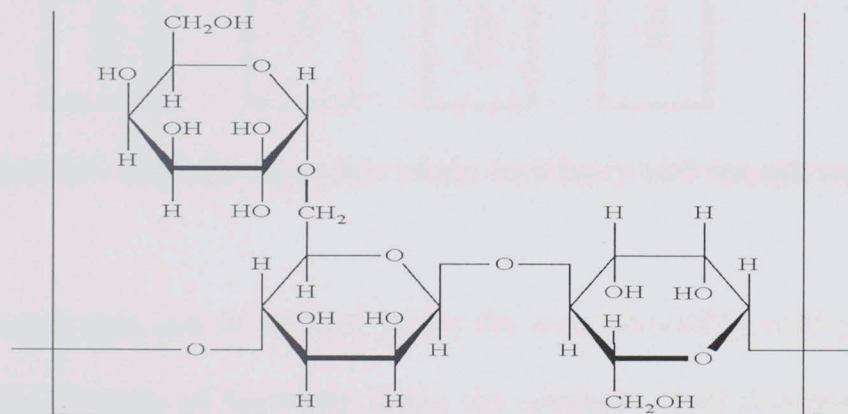
Figure 2.1: Structure of guar gum polymer (Curr et al. 2012)

The mannose to galactose ratio is 1.2 to 1.8 and can change depending on

temperature at which guar is dissolved in water. The distribution of galactose

ramifications is not constant, i.e., there are smooth (no ramifications, i.e., mannose

unit is not linked to a galactose molecule) and hairy regions. Hairy regions are when one galactose molecule is linked to every mannose unit. The interaction among galactomanan molecules, with themselves or with other polysaccharides (synergy) is enhanced by the presence of smooth regions. Figure 2.2 explains the smooth and hairy regions of a guar gum polymer.

$$\left[\begin{array}{c} -O-C_6O_4H_9-O-C_6O_4H_{10}-O-C_6O_4H_9-O-C_6O_4H_{10}-O- \\ | \qquad\qquad\qquad\qquad\qquad | \\ C_6O_6H_{11} \qquad\qquad\qquad\qquad C_6O_6H_{11} \end{array} \right]_n$$

$$\left[\begin{array}{c} \ldots - \text{Mannose} - \text{Mannose} - \text{Mannose} - \text{Mannose} - \ldots \\ | \qquad\qquad\qquad\qquad | \\ \text{Galactose} \qquad\qquad\qquad \text{Galactose} \end{array} \right]_n$$

Smooth   Hairy   Smooth   Hairy
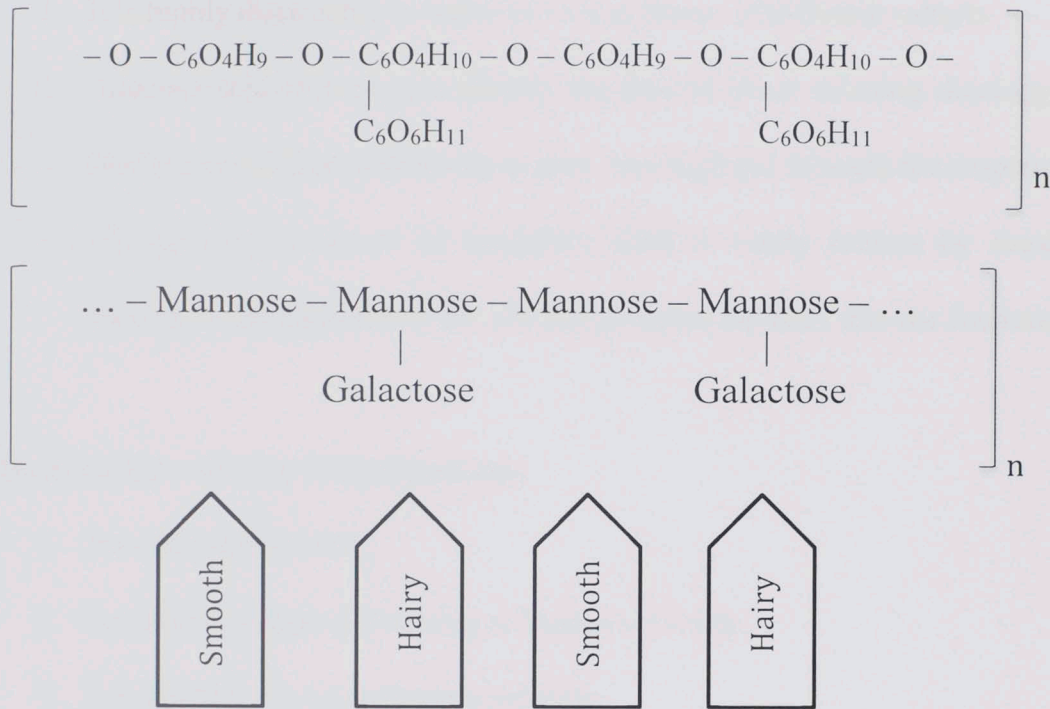
Figure 2.2: Guar gum polymer chain with hairy and smooth regions

Although guar gum and its derivatives are the most commonly used polymers to increase the viscosity of fracturing fluids, the conductivity of fractures created is low because of residual unbroken gel in the fracture. It is, therefore, desirable to reduce the polymer concentration of fracturing fluids without compromising on viscosity. One method of achieving this is to cross-link. Cross-linking increases the performance of these polymers by yielding higher viscosities without increasing the

polymer concentration. Low polymer concentration cross-linked gels lower costs and help minimize formation damage.

Advantages of using guar gum as a viscosifier for hydraulic fracturing operations are:

1. It is highly dispersible in water as well as brines of different salinity.

2. Aqueous solutions of guar display the desired shear thinning rheology and can be cross-linked with borax to give very high gel strength for suspension.

3. The polymer structure of fracturing fluid is easily broken by breakers, serving as the ideal carrier for placing proppant far back into the fractures.

Disadvantages of using this polymer are:

1. Poor thermal stability.

2. Sensitivity to high pH leading to loss of viscosity.

3. Susceptibility to bacterial fermentation.

4. Residual damage.

2.3 Xanthan gum

Xanthan gum is a bio-polysaccharide synthesized by *Xanthomonas campestris*, and is used as a thickener in many industries other than petroleum, such as pharmaceutical, cosmetic and food. The primary structure of xanthan consists of repeated pentasaccharide units formed by two glucose units, two mannose units, and one glucuronic acid unit, in the molar ratio 2.8:2.0:2.0. Its main chain consists of β-

D-glucose units linked at the 1 and 4 positions. Trisaccharide side chains contain a D-glucuronic acid unit between two D-mannose units linked at the O-3 position of every other glucose residue in the main chain. The trisaccharide branches appear to be closely aligned with the polymer backbone. The resulting stiff chain may exist as a single, double, or triple helix (Morris, 1977; Milas and Rinaudo, 1979), which interacts with other polymers to form a complex structure. Figure 2.3 shows the polymer structure of xanthan gum. The molecular weight distribution ranges from 2 x 10^6 to 20 x 10^6 g/mol. This molecular weight distribution depends on the association between chains, forming aggregates of several individual chains.

$$[- Glucose - Glucose -]_n$$
$$|$$
$$Mannose$$
$$|$$
$$Mannose - Glucuronic$$
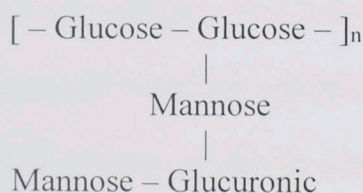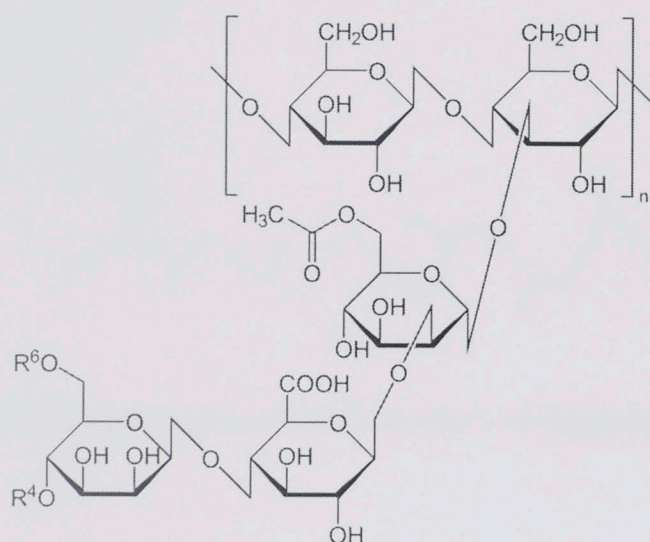
Figure 2.3: Structure of xanthan gum polymer (Makela & Makela 2013)

Dissolution temperature, or the temperature at which xanthan gum is dissolved in an aqueous medium, determines the conformation of the polymer structure. At low dissolution temperature, xanthan shows ordered conformation, while at higher temperature xanthan shifts to a disordered structure. Figure 2.4 shows examples of ordered and disordered conformations of single helix xanthan gum structure.

Ordered   Disordered
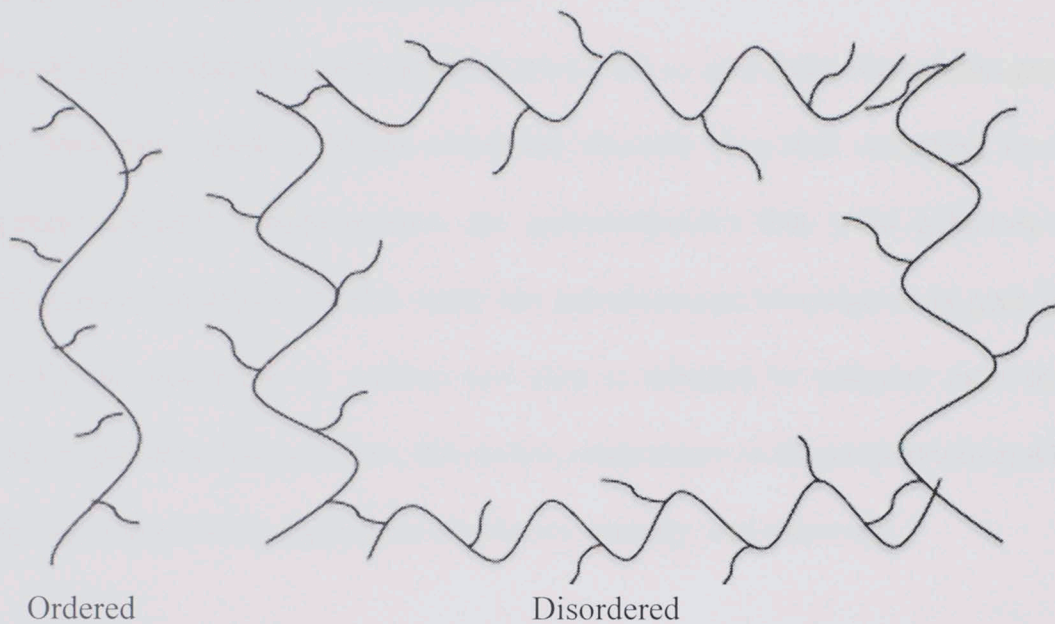
Figure 2.4: Ordered and disordered conformations of single helix xanthan gum

Xanthan gum in aqueous solution exhibits non-Newtonian, shear-thinning behavior. It is extensively used in the oil industry as a viscosifier and friction-reducing additive in drilling, completions and workover operations. It is highly desirable as a drilling mud, and produces flat velocity profile in annular flow, which is required for efficient lifting of cuttings in lower density muds. Even at very low shear rates, xanthan behaves as a pseudoplastic fluid, yielding high viscosities. This unique rheology (high low shear rate viscosity or LSRV) often offsets xanthan's high cost

as compared to other viscosifiers. Xanthan is anionic, with tolerance for salinity and fair tolerance for hardness ions. Temperature tolerance varies with water-phase components, but it starts to degrade around 200 to 250 °F. Extreme pH or hardness is not well tolerated and it is susceptible to bacterial attack.

2.4 Synergy of xanthan and guar gum

Mixtures of xanthan gum and galactomanans such as guar gum, locust bean gum or tara bean gum, show a higher combined viscosity than that occurring in each separate polymer. Galactomanans are polysaccharides that yield galactose and mannose on hydrolysis. In this study the galactomanan investigated is guar gum. Synergistic interaction of xanthan and guar is affected by polymer ratio in the mixture, polymer concentration, dissolution temperature or the temperature at which polymer is dissolved, temperature of mixture, salinity, and shear rate.

Synergistic interaction between xanthan and guar was first reported by Rocks (1971). Since then many theories have been proposed to explain synergy of xanthan and guar. It is important to note that the nature of this synergistic interaction is not entirely understood. Some researchers claimed that the higher viscosity or gelation of xanthan and guar mixture is due to their incompatibility (Kovacs, 1973 and Schorsch et al., 1995). However, there is considerable evidence and literature that supports intermolecular binding between xanthan and guar (Cairns et al., 1986; Miles et al., 1987; Cheetham & Mashimba, 1988; Cheetham et al., 1986; Cheetham & Punruckrong, 1989; Foster & Morris, 1994; Goycoolea et al., 1994; McCleary &

16

Neukom, 1982). The intermolecular binding mechanism between xanthan and guar is still controversial, and over the years different models have been proposed. They are described below:

1. Dea et al. (1977) and Morris et al. (1977) proposed that the intermolecular binding occurs between the ordered (helical) xanthan and unsubstituted or poorly substituted guar backbone. This strength of the intermolecular binding is dependent on the galactose content (Dea & Morrison, 1975).

2. Tako et al. (1984) and Tako (1991) proposed that the intermolecular binding occurs between side chains of xanthan and guar backbone. They suggested that the side chains of xanthan are inserted into adjacent substituted regions of the guar backbone, which had an extended two-fold ribbon like conformation.

3. Cairns et al. (1986) and Cairns (1987) proposed that the intermolecular binding occurs between the disordered xanthan and guar. They suggested that disordering of xanthan helical structure is essential for gelation. They proposed that xanthan had a disordered, extended two-fold cellulose like conformation when interacting with guar. Cheetham et al. (1986) and Cheetham & Mashimba (1988, 1991) proposed that the interaction occurs between the disordered segments of xanthan chains and guar.

4. Mannion et al. (1992) proposed two different mechanisms. At room temperature, the interaction with ordered xanthan gives weaker elastic gel with little dependency on the galactose content of guar. The second

17

mechanism requires heating the xanthan–guar mixture. The heat disordered xanthan segment gives a stronger gel that is highly dependent on galactose side chains of guar.

5. Zhan et al. (1993) disagreed with two-mechanism theory and stated that there can only be one mechanism governing xanthan-guar synergy. They suggested that the extent of disorder induced in xanthan prior to mixing with guar is the main factor for synergistic interaction.

It is clear that the nature of synergistic interaction is not clearly understood despite various investigations and experimental studies since 1971. Investigating the mechanism of synergy between xanthan and guar gum polymers is beyond the scope of this study. Rather it is important to understand how this synergy can be utilized for the oil and gas application. Based on experimental results of previous investigators a number of inferences can be drawn.

Weak interaction of xanthan gum and guar gum polymer mixtures is due to presence of side chains on every other unit or every two to four units of guar gum molecule (Tako and Nakamura 1984). Rheological behavior of mixtures having a total polymer concentration of 0.2% was investigated. No synergistic interaction at room temperature was observed. This might be due to side chains on guar gum molecule preventing the insertion of trisaccharide side-chains of xanthan gum molecule into the backbone of guar gum molecule. At room temperature de-acetylated xanthan and guar gum showed synergistic interaction. This might be because the xanthan

molecules are more flexible and could associate with guar gum molecules better when free from intermolecular association caused by the acetyl group. At low temperatures, xanthan and guar gum mixture displayed synergy and had higher viscosity than either polymer. Maximum synergy was observed when the ratio of xanthan and guar gum was 2:1. At temperatures of 25 °C and above, the synergy of native xanthan and guar gum starts to decrease. For de-acetylated xanthan and guar gum mixture, at temperatures of 30 °C and above, the synergistic interaction starts to weaken. This might be due to Brownian motion of the gums in aqueous solution.

Use of xanthan-hydroxypropyl guar mixture as fracturing fluids in low to moderate temperature wells to counter poor clean up and proppant pack damage was recommended (Clark et al. 1985). Rheology of 15 lbm/Mgal xanthan gum and 15 lbm/Mgal hydroxypropyl guar mixtures was studied. The aim was to investigate if synergy of these polymers can be utilized for effective proppant transport and replace crosslinked guar gum fluids, which are associated with excess viscosity and poor cleanup. A special apparatus was used to measure single particle settling velocity of proppant in blends, which had a rotatable inner cylinder to provide external shear to the fluid. This external shear is in addition to the internal shear caused by the settling of the particle. The particles used were sieved glass beads of mesh size 30. It was found that xanthan and hydroxypropyl guar at ratio of 3:4 showed the best synergy. Settling velocity of glass bead in this blend was studied at fluid temperatures, ranging from 25 to 85 °C. Suspension ability of the polymer blend improved significantly as the temperature was increased above 50 °C. At 85

°C, the settling velocity in the blend was 500% less than those in 40 lbm/Mgal hydroxypropyl guar.

Strength of synergy between xanthan and guar gum polymer fluids increases with increasing polymer concentration and decreases with increasing temperature (Casas et al. 2000). Three concentrations of food grade xanthan and guar gum polymers were investigated: 1, 1.5 and 2 kg/m^3. Ideal dissolution temperature to prepare component polymer fluids was identified in the study. Highest viscosity was obtained at 1:1 (wt./wt.) ratio of xanthan gum (dissolved at 40 °C) and guar gum (dissolved at 80 °C) at 2 kg/m^3 concentration. Decrease in apparent viscosity of these polymers with increase in temperature is reversible and is explained by molecular interaction of these polymers in solution, which get weaker as temperature increases. The solubility of guar gum is temperature dependent. At low temperatures (< 25 °C), the fraction of guar gum dissolved is 88% with a mannose/galactose ratio in the dissolved polymer is 1.23. This ratio increases with increasing dissolution temperature. At 80 °C, it was found that the more than 91% polymer is dissolved and the mannose/galactose ratio is 1.43. This change in mannose/galactose ratio affects viscosity, which increases, reaching a maximum at a dissolution temperature of 60 °C. Dissolution temperature of these polymers is the most influential variable for synergy. It was found that the highest viscosity was achieved when xanthan gum was dissolved at 40 °C and guar gum was dissolved at 80 °C.

Optimal ratio range for improved synergy between non-acetylated xanthan and guar gum was found to be 1:4 to 1:2 (Fischer et al. 2001). Non-acetylated xanthan is a xanthan variant where the acetyl group on the first mannose unit of the side chain is not present. Removal of this acetyl group aids in the binding process with guar by making the double helix configuration less stable and allowing the single helix xanthan backbone to bind to the unsubstituted guar backbone. Therefore, non-acetylated xanthan produces stronger synergy with guar than xanthan gum. Various polymer concentrations were investigated: 10, 15, 20 and 25 lbm/Mgal. The higher the polymer concentration, higher is the viscosity of polymer blends. Synergistic interaction is adversely affected by presence of salt, particularly K^+ and Ca^{+2}. KCl is normally used as a controlling agent in fracturing fluids. This can be countered by substituting KCl with Tetra Methyl Ammonium Chloride (TMAC) for clay control. Chelating agent can be used to chelate Ca^{+2} ions. Different chelating agents were investigated: Tri-Sodium Nitrilo Tri-Acetic Acid (NTA), Tri-Ethanol Amine (TEA) and Tetra-Sodium Ethylene Di-Amine Tetra-Acetic Acid (EDTA). It was found that a combination of NTA with TEA or EDTA works best in chelating Ca^{2+} ions, as long as concentration of NTA is adjusted according to the hardness of water. At temperature above 100 °F, the overall viscosity of blends reduced considerably, making it necessary to crosslink.

As pointed out by various investigators, the synergistic interaction between xanthan and guar is not clearly understood. Some report no synergy between xanthan and guar at room temperature while others report weak synergy at temperatures below

25 °C. It is important to note that the structure of polymer plays a major role in this synergistic interaction and that all investigators used different formulation of xanthan or guar. Some used food grade while others used non-acetylated or de-acetylated xanthan.

2.5 Particle Settling Behavior in Newtonian and Non-Newtonian Fluids

It is important to have reliable knowledge of terminal settling velocity of spherical particles in fluids for process design calculations in different industrial settings. Typical examples are design of slurry pipelines, settling tanks, separators, fluidized bed reactors, falling ball viscometers, etc. In the oil and gas industry, flow around submerged particles occurs during transport of cuttings and transport of proppant in a fracture. Particle motion in fluids can be characterized by three flow regimes: creeping, intermediate and turbulent.

2.5.1 Particle Settling in Newtonian Fluids

Many investigators have studied particle motion in Newtonian fluids extensively. When flow around spherical particle is in creeping flow regime, the analytical equation derived by Stokes (1851) can be used to calculate its terminal settling velocity. For flow in intermediate and turbulent region various empirically derived correlations exist by different investigators (Clift et al. 1978; Chhabra 2006) to estimate drag coefficient (C_D), which is then used to calculate terminal settling velocity. Lapple and Shepherd (1940) produced a standard curve to estimate drag coefficient using particle Reynolds number by compiling average values of

experimental data of different investigators. Using this curve, terminal settling of a particle in a Newtonian fluid can be estimated by trial and error method. To avoid this tedious process $\sqrt{C_D N_{Rep}^2}$ and particle Reynolds number can be plotted on a logarithmic scale to produce a straight line, which can then be used to estimate drag coefficient and calculate terminal settling velocity (Shah 1982). This method has been tested with experimental data by previous investigators and shows good agreement.

2.5.2 Particle Settling in Non-Newtonian Fluids

Particle settling in non-Newtonian fluids has been extensively studied and reported by various investigators due to their wide occurrence in chemical and petroleum processes. Chhabra (1986, 1990, 2006) critically reviewed and reported chemical industry literature available on particle settling in non-Newtonian fluids prior to 1990.

An empirical correlation relating drag coefficient and generalized particle Reynolds number for spherical particles falling at their terminal settling velocity in hydroxyethyl cellulose (HEC), carboxymethyl cellulose (CMC), and polyethylene oxide (PEO) fluids was developed and the rheological data of these fluids was fitted with Ellis fluid model (Dallon 1967). Chhabra (1990) used Dallon's experimental data and refitted the fluids with power law fluid model covering the flow behavior index, n, ranging from 0.64 to 0.94. Prakash (1983) developed an empirical correlation between drag coefficient and particle Reynolds number from

23

experimental data of spherical particles in CMC solutions that shows a dependence on the power law flow behavior index. It was noted that confining walls could have influenced data but no wall correction was applied.

Peden and Luo (1987) reported experimental data of spheres falling in aqueous solutions of CMC and HEC as well. Two constants in their empirical correlation showing the relationship between drag coefficient and particle Reynolds number were reported to be functions of power law flow behavior index but the dependence was found to be irregular. In addition, their correlation does not reduce to expected limiting behavior for Newtonian fluids. Although, Koziol and Glowacki (1988), Reynolds and Jones (1989) and Machac et al. (1995), have also reported similar results, none of their correlations have been tested using independent experimental data.

Kelessidis and Mpandelis (2004) produced a five-parameter implicit model to predict the settling velocity of single particle in pseudoplastic fluids. Their equation is similar to one proposed by Heider and Levenspiel (1989) for Newtonian fluids using non-linear regression and has five constants. Predictions from this model were compared with limited CMC fluid data with power law constant, n > 0.74. It was found that 80% of the data fall within 30% deviation. Kelessidis (2004) reported an explicit equation to predict terminal velocity of solid sphere falling through pseudoplastic fluids. However, this model as well was tested with limited data and only for n > 0.56.

All these studies mentioned a dependence of drag coefficient on power law behavior index. This dependence was in addition to the one accounted for in definition of generalized particle Reynolds number. However, the study of Lali et al. (1989) disputed these findings and claimed that their data of drag coefficients of spheres moving through power law fluids correlated well with Newtonian standard drag curve. Chhabra (1990) gathered a large body of experimental data available in the literature and reexamined them to explore the possibility of using the Newtonian standard drag curve for power law fluids. Specifically, he considered data of Dallon (1967), Prakash (1983), Machac et al. (1987), Lali et al. (1989) and his own gathered data (Chhabra 1980). He found that Newtonian drag curve provides a satisfactory representation of the drag coefficient – generalized particle Reynolds number data for power law fluids. His study covered fluids with power law index values between 0.55 and 1.00 and generalized particle Reynolds number range of 1 – 1000. Mean error reported was 30% but maximum errors of up to 70% were encountered as well.

Novotny (1977) studied particle transport using vertical fractures. He stated that shear rate in fracture consisted of two components: a horizontal component related to fluid motion and a vertical component related to particle settling, and presented an equation that required only knowledge of shear rate to predict settling velocity. Harrington et al. (1979) showed that terminal settling velocity of proppant in non-Newtonian crosslinked fracturing gels is 78% lower than calculated values obtained using Stokes (1851) equation for creeping flow. Hannah and Harrington (1981)

subsequently showed that it was not possible to predict the settling velocity with just shear rate.

Shah (1982, 1986) proposed a new method to analyze particle-settling velocity in non-Newtonian fluids. He demonstrated the effect of fluid behavior index, n, on drag coefficient for particle settling in non-Newtonian fluids. Previous authors had employed conventional coordinates – drag coefficient versus particle Reynolds number. Although this works well with Newtonian fluids, it tends to obscure the effect of power law behavior index. This can be seen from the data of Shah (1982, 1986), which scattered around the Newtonian standard drag curve with no discernable trend and with significant deviations. However, when this data was plotted as C_D^{2-n} versus N_{Repg} it showed a family of curves as a function of n. This indicates the dependence of drag coefficient on power law flow behavior index. For Newtonian fluids (n = 1), it reduces to the Newtonian standard drag curve. To avoid trial and error method to evaluate drag coefficient and, thereby, terminal settling velocity of particle, he plotted settling velocity data as $\sqrt{C_D^{2-n} N_{Repg}^2}$ versus N_{Repg} and proposed correlations for particle settling in power law fluids. The inadequacy of Newtonian model to correlate the data of single solid spherical particle moving in power liquids was demonstrated (Shah et al. 2007). They recommend using Shah (1982) model, as it is an improvement to existing models in the literature to predict spherical particle settling velocity in power law liquids.

2.5.3 Particle Settling in Fluids with Yield Stress

Particle settling behavior in complex fluids with yield stress is different from fluids without yield stress. Various investigators have tried to come up with drag coefficient correlations as a function of modified particle Reynolds number such that when yield stress is assigned a zero value, the correlations reduce to Newtonian standard drag curve. However, this has attained limited success with most of the data scattered around the Newtonian standard drag curve.

Spherical particle settling data in Bingham plastic fluids was reported by Valentik and Whitmore (1965). Graphical relations between settling velocity of spherical particle and diameter of unsheared envelope of fluid surrounding the particle were given. These relations were not based on the actual diameter of the spherical particle. They suggested using particle Reynolds number – drag coefficient correlations developed for Newtonian fluids to estimate drag coefficient provided diameter of unsheared envelope and plastic viscosity are used to calculate particle Reynolds number. However, the model did not have any physical basis and no method was given to predict the unsheared envelope of fluid surrounding the particle.

An expression to determine drag coefficient of spherical particle in Bingham plastic fluids using modified particle Reynolds number that incorporated yield stress was given using fifty data points (Du Plessis and Ansley 1967). Ansley and Smith (1967) modified particle Reynolds number and developed a correlation parameter

on the basis of stress analysis of surrounding fluid due to forces acting on falling spherical particle. They proposed two correlations to predict drag coefficient in creeping and turbulent flow region as a function of this parameter. These correlations could not predict drag coefficient in the intermediate zone. Further, the correlating parameter developed could not be reduced to particle Reynolds number when yield stress was assigned a zero value. Based on visualization studies of slowly flowing Bingham plastic fluids around bodies of different shapes it was found that drag is not simply due to increase in effective volume of the body as suggested by Valentik and Whitmore (1965) (Brookes and Whitmore 1969).

A theoretical model was developed to predict drag coefficient as a function of modified Reynolds number using data of Valentik and Whitmore (1965) (Dedegil 1987). However, this model as well could not reduce to Newtonian standard curve when yield stress in modified particle Reynolds number was assigned a zero value. Fluids that exhibit yield stress can completely suspend small or fine particles. Maximum diameter a particle can have to stay suspended in fluid with yield stress was given (Dedegil 1987).

2.5.4 Particle Settling in Fluids Under Dynamic Conditions

Proppant transport and settling in a fracture is an example of particle settling under dynamic conditions. Since it is important to understand the phenomenon affecting proppant placement in a fracture, studies were undertaken using Newtonian oils as the fluid medium in a transparent, vertical, clear, plastic fracture model (Kern et al

1959). These experiments confirmed that separation from fluid and banking of proppant occurs in a vertical fracture due to gravity. Using a similar apparatus, proppant transport in both Newtonian and non-Newtonian fluids was studied (Babcock et al 1967). Proppant transport in horizontal fractures was investigated and it was established that proppant formed dunes similar to that formed in river beds (Wahl 1963). Using experimental data of these investigators, mathematical models were developed that would predict final placement of proppant on completing a fracturing job.

These models were proven to be insufficient to predict proppant settling in crosslinked gels, introduced to the industry in mid to late 1960s. Due to high viscosity of these fluids, tests run in vertical fracture models showed no separation of proppant. However, the residence time allowed in these tests was too short and this could have led to erroneous results. This uncertainty has led to some researchers using established correlations for non-crosslinked, non-Newtonian fluids, based on Stokes law, and applying them for crosslinked gels. Others have treated these gels as perfect support fluids by assuming no proppant separation.

Feeling a need to understand proppant settling in crosslinked gels under dynamic conditions, Hannah and Harrington (1978) used a concentric cylinder tester and attempted to match experimental data of particle settling with predictions of non-Newtonian form of Stokes Law. To simulate dynamic conditions, outer cylinder of was rotated while inner cylinder remained stationary. This experimental setup is

similar to the one used by Novotny (1977). However, their experimental data did not agree with theoretical predictions. Using a similar tester, with a different aspect ratio, rotating inner cylinder and stationary outer cylinder, settling rates of proppant in crosslinked gels was measured (Harrington et al 1979). Experimental data of proppant settling velocities were plotted on a logarithmic scale against apparent viscosity and a straight line was obtained. This line was parallel to but 78% lower than Stokes line on a similar plot leading them to develop an empirical constant to predict settling velocity. However, this empirical constant is fluid specific and cannot be generalized.

Particle settling experiments in non-Newtonian fluids under static and dynamic conditions were conducted and a correlation was developed which is dependent on power law fluid parameter, n (Shah 1982). The experimental data of Hannah and Harrington (1978) show good agreement with the correlation predictions.

2.5.5 Wall Effects

The drag experienced by a free falling particle in a fluid or its terminal settling velocity in a bounded fluid is not the same as in infinite fluid. Bounding walls exert a retarding effect on terminal velocity of particles in a viscous medium and this has been studied both theoretically and experimentally for centuries (Newton 1687; Munroe 1888; Ladenburg 1907). This retarding effect is brought about by upwards counter flux of fluid, which balances downwards flux of the solid and that of the dragged down fluid. The smaller the area available for the counter flux, i.e., the

smaller the container cross-section area as compared to the particle size, the more critical the phenomenon. For perfectly spherical particles falling in a cylindrical tube, the diameter ratio of particle diameter to cylinder diameter is an important parameter that can be used to quantify wall effects.

In creeping flow regime, both fully theoretical and empirical correlations have been proposed to estimate wall factor, which is the ratio of bounded terminal settling velocity to unbounded terminal settling velocity (Francis 1933, Haberman and Sayre 1958, Clift et al. 1978, Iwaoka and Ishii 1979). Theoretical analysis is not available for terminal Reynolds number outside the creeping flow regime and empirical correlations are used to estimate the wall factor. Based on 3000 experimental observations, the effect of cylindrical column diameter on single particle settling velocity for Reynolds number range of 0.054-20000 was published (Whitmore 1961). Experimental observations suggest that wall effect phenomenon becomes less critical with increasing Reynolds number (Munroe 1988). For intermediate flow regime Fidleris and Whitmore (1961) gave multiple correlations for different Reynolds numbers and selected values of diameter ratio (0.1-0.6). They concluded that in intermediate region wall factor is a function of both diameter ratio and particle Reynolds number in an unbounded medium. Wall factor is independent of Reynolds number in the creeping and turbulent region.

For non-spherical particles in creeping flow regime, wall effect correction factor has been correlated with geometric parameters, shape and orientation (Johnson et al.

1987, Leith 1987, Sheaffer 1987, Lee and Leith 1989, Cheng 1991). Similar approaches to develop correction factors based on Reynolds number, shape and orientation of non-spherical particles have been published and gained wide acceptance in the literature (Finn 1953, Jones and Knudsen 1961, List and Schmeanauer 1971, Kasper et al. 1985, Unnikrishnan and Chhabra 1991, Sharma and Chhabra 1991, Swamee and Ojha 1991). Generalized correlations have been developed for non-spherical particles in cylindrical columns by Haider and Levenspiel (1989) and Thompson and Clark (1991) to account for wall effects on drag coefficient.

2.5.6 Particle-Particle Effect

In addition to effect of container boundaries, particle settling is affected by presence of other surrounding particles. When the particles are near each other, the motion of a particle is impeded by other particles and settling process is called hindered settling. Static sedimentation experiments to evaluate the settling behavior of non-flowing slurries were conducted by Kirkby and Rockerfeller (1985). They found that proppant clustering phenomenon results in average static-slurry settling velocities considerably greater than those of single particles. Setting of single particles and suspensions in static HPG fracturing fluids was studied by Dunand and Soucemarianadin (1985). They concluded that in fluids with identical single particle settling velocities, the average settling rate of a concentrated suspension in a static non-Newtonian fluid is two to three times higher than in a corresponding Newtonian fluid. Empirical correlations have been developed by various investigators that

relate hindered settling velocity to single particle settling velocity in a particular fluid (Steinour 1944, Richardson and Zaki 1954, Slattery 1962). An experimental study was undertaken to simulate the behavior of proppant-laden fluids in a fracture and observe proppant settling behavior under controlled test conditions (McMechan and Shah 1991). It was concluded that at low slurry concentrations, clustering occurs in linear gels leading to higher settling velocities than single particle settling velocity. As concentration is increased beyond a critical value, hindered settling effects are dominant.

CHAPTER 3

THEORETICAL STUDY

This section details a theoretical study undertaken to understand Newtonian fluids, non-Newtonian fluids, and particle settling in Newtonian and non-Newtonian fluids. Fluids are constituents of matter that experience continuous deformation when stress is applied to them. Therefore, the stress applied to a fluid can be expressed in terms of the rate of deformation or shear. Viscosity of a fluid is its ability to resist shear deformation when shear stress is applied to it.

3.1 Newtonian and non-Newtonian Fluid Rheology Models

Newtonian fluids are simple fluids that adhere to Newton law of viscosity. Shear stress is related to the shear rate by a constant, for a given pressure and temperature, which is the viscosity of the Newtonian fluid (Eq. 3.1). Water, oil, alcohol, etc. are examples of fluids considered as Newtonian and viscosity is a fluid dependent property. These fluids have simple internal structure with low molecular weight and dissipate energy due to collision of small molecules.

$$\tau = \mu\dot{\gamma} \qquad (3.1)$$

where,

τ = shear stress, lbf/ft^2

$\dot{\gamma}$ = shear rate, 1/s

μ = Newtonian viscosity, lbf/ft^2-s

Newtonian fluids are the simplest mathematical models of fluids that account for viscosity. No real fluid fits this definition perfectly but many common liquids and gases can be assumed to be Newtonian for practical calculations under ambient conditions.

Non-Newtonian fluids do not adhere to Newton law of viscosity. These fluids have dissolved molecules that give rise to non-Newtonian behavior. There are many classifications among non-Newtonian fluids based on how shear stress is related to shear rate. For the scope of this study, non-Newtonian fluids discussed are pseudoplastic or shear thinning fluids. Shear thinning is an effect where fluid's viscosity decreases with an increasing rate of shear. Viscosity is no longer a constant at all shear rates and is shear dependent. Hence, the term 'apparent' is used to differentiate from Newtonian viscosity and to denote its shear dependency. Power law fluid model can be used to describe the relationship of shear stress and shear rate of a shear thinning fluid (Eq. 3.2).

$$\tau = K\dot{\gamma}^n \qquad\qquad (3.2)$$

where,

n = flow behavior index (<1 for shear thinning fluid), dimensionless

K = fluid consistency index, lbf/ft^2-s^n

At a given pressure and temperature, n and K are constant for a given composition of fluid. As was the case with Newton's law of viscosity, no real fluids fit power

law rheology model perfectly. For practical considerations, this rheology model is adequate to describe fluid properties of different fluids used in the oil and gas industry.

3.2 Particle Settling in Newtonian Fluids

Consider a spherical particle of mass 'm' moving through static Newtonian fluid. The major forces acting on the particle are: gravity (F_g), buoyancy (F_b), and viscous drag (F_v). These forces are shown in Fig. 3.1. Applying force balance in the vertical direction:

$$m \frac{dv}{dt} = F_g - F_b - F_v \tag{3.3}$$
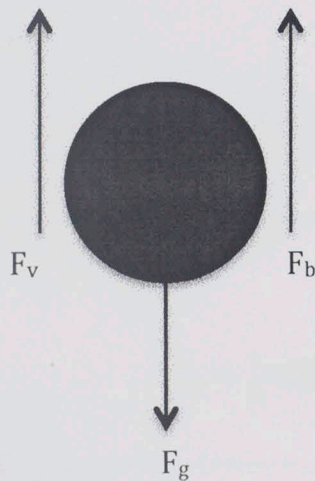
Figure 3.1: Forces acting on a single particle in Newtonian fluid

The measure of force of gravity on the particle is given by its weight (Eq. 3.4).

$$F_g = mg \qquad (3.4)$$

Mass of the particle can be expressed in terms of its density and volume.

$$F_g = \frac{1}{6}\pi D_p{}^3 \rho g \qquad (3.5)$$

where in consistent units,

F_g = gravity force

D_p = diameter of particle

ρ_p = density of particle

g = acceleration due to gravity

Buoyancy is the upward force exerted by volume of fluid displaced by partially submerged or fully submerged particle. The measure of this force is given by the weight of the displaced fluid.

$$F_b = m \frac{\rho}{\rho_p} g \qquad (3.6)$$

Expressing the mass of the particle in terms of its volume and density, Eq. 3.6 reduces to:

$$F_b = \frac{1}{6}\pi D_p^3 \rho g \qquad (3.7)$$

where in consistent units,

F_b = buoyancy force

ρ = density of fluid

Viscous drag force is the measure of fluid resistance and acts opposite to relative motion of a particle moving with respect to surrounding fluid. For creeping flow regime, viscous drag force is given by Stokes' Law (Eq. 3.8). This equation is only valid for smooth spherical particles in a homogeneous Newtonian fluid under steady state conditions.

$$F_v = 3\pi\mu D_p v \qquad (3.8)$$

where in consistent units,

F_v = viscous drag force

μ = Newtonian fluid viscosity

v = velocity of particle

When a particle is released into a static fluid, its velocity increases with time due to the net force acting on the particle (Eq. 3.3). As the particle accelerates, the drag force increases and reduces the net force acting on the particle. In steady state, the net force acting on the particle is zero and it travels at its maximum attainable velocity or terminal settling velocity. Therefore, at steady state:

$$F_g - F_b - F_v = 0 \qquad (3.7)$$

Since Eq. 3.8 is only valid under steady state conditions, the particle velocity 'v' in the equation can be denoted by 'v_t', particle terminal settling velocity.

Substituting the constituent forces in this equation and re-arranging it, terminal settling velocity can be expressed as:

$$v_t = \frac{D_p^2(\rho_p - \rho)g}{18\mu} \qquad (3.8)$$

38

Under steady state conditions, the viscous drag force can be expressed in terms of drag coefficient as:

$$F_v = \frac{1}{2}\rho v_t{}^2 A C_D \qquad (3.9)$$

where in consistent units,

A = surface area of particle projected on a plane perpendicular to flow direction

C_D = drag coefficient, dimensionless

Drag coefficient is a dimensionless number used to quantify the drag or fluid resistance to relative motion of particle.

From Eq. 3.8 and 3.9, drag coefficient in creeping flow or Stokes region can be expressed as:

$$C_D = \frac{24\mu}{\rho D_p v_t} \qquad (3.10)$$

The variables in Eq. 3.10 represent the ratio of inertial forces to viscous forces, which is defined as particle Reynolds number, N_{Rep}. This is a dimensionless quantity used quantify the relative importance of these two types of forces for given flow conditions. It is expressed as:

$$N_{Rep} = \frac{\rho D_p v_t}{\mu} \qquad (3.11)$$

Therefore, for a single particle settling at its terminal velocity in a Newtonian fluid under steady state conditions and when the flow regime is in Stokes region (creeping flow), the drag coefficient can be analytically given as:

$$C_D = \frac{24}{N_{Rep}} \qquad (3.12)$$

Particle Reynolds number can be used to characterize different flow regimes observed.

Creeping flow regime: $N_{Rep} < 0.1$.

Intermediate flow regime: $2 < N_{Rep} < 500$.

Turbulent flow regime: $500 < N_{Rep} < 200{,}000$.

Analytic equations to quantify drag coefficient are not available as particle Reynolds number increases beyond creeping flow regime range. However, based on extensive experimental data, empirical correlation for drag coefficient exists in the intermediate range and is given as:

Intermediate flow regime
$$C_D = \frac{18.5}{N_{Rep}^{0.6}}$$
(3.13)

At very high Reynolds numbers, value of drag coefficient is approximately constant:

Turbulent flow regime:
$$C_D \approx 0.44$$
(3.14)

Lapple and Shepherd (1940) gathered experimental data of many investigators and produced a curve representing the relationship of drag coefficient and particle Reynolds number for solid sphere motion in Newtonian fluids (Fig. 3.2). Using this plot, by trial and error, the terminal settling velocity of a particle with known diameter and density in a fluid can be determined. This difficulty arises, as both drag coefficient and particle Reynolds number are functions of terminal settling velocity.
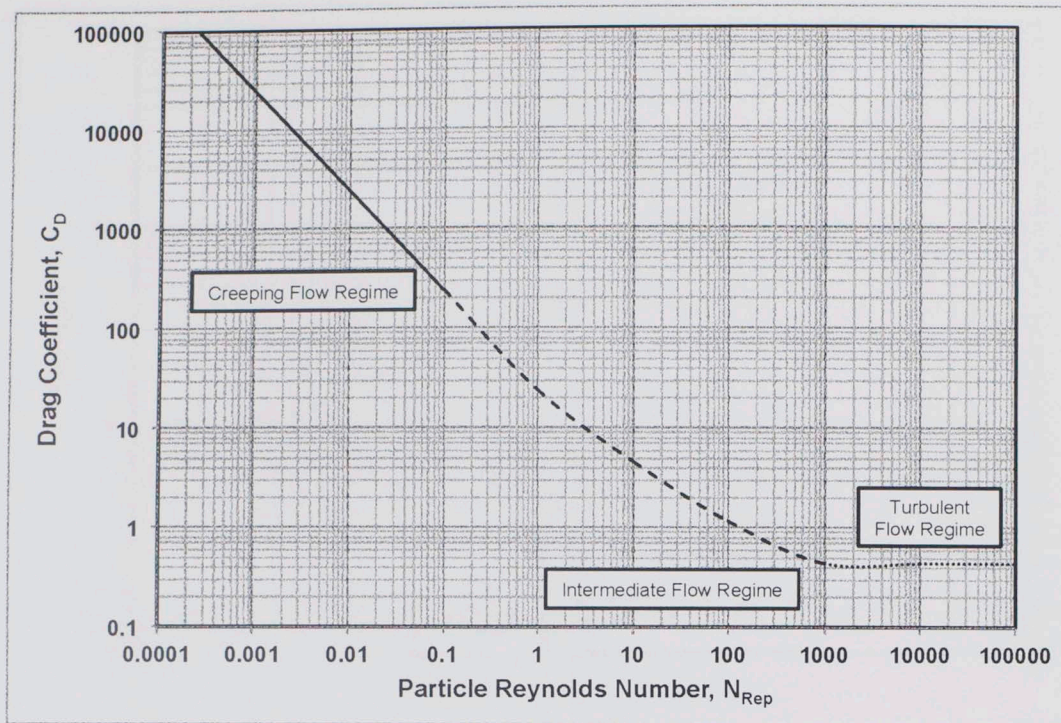
Figure 3.2: Standard Newtonian Drag Curve (redrawn, Lapple and Shepherd 1940)

Shah (1982) proposed that to avoid the difficulty of trial and error procedure, the data represented in Fig. 3.2 might be plotted with $\sqrt{C_D N_{Rep}{}^2}$ as y-axis and particle Reynolds number as x-axis (Fig. 3.3). As y-axis is now independent of terminal settling velocity term and is a function of particle diameter, density, and fluid properties, it can be easily calculated. Using this value, the corresponding x-axis quantity can be determined. Once, particle Reynolds number is obtained, terminal-settling velocity can be calculated using Eq. 3.11.
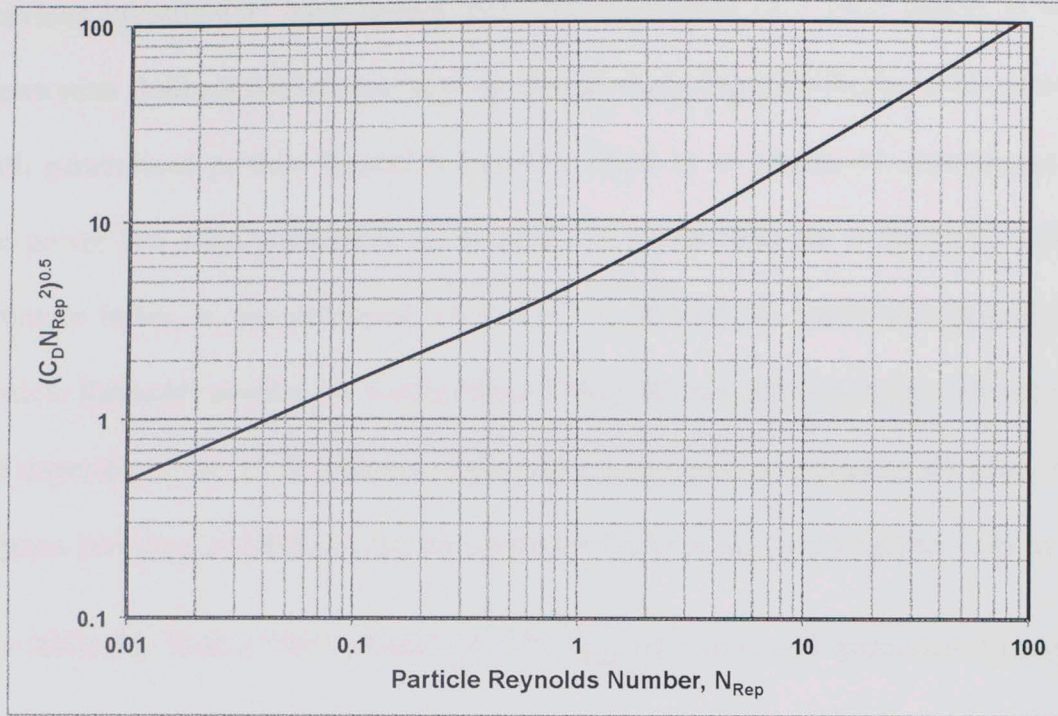
Figure 3.3: $\sqrt{C_D N_{Rep}{}^2}$ **vs. particle Reynolds number (redrawn, Shah 1982)**

3.3 Particle Settling in Non-Newtonian Fluids

A simple but incorrect approach to determine terminal-settling velocity in non-Newtonian fluids is to use modified analytic and empirical equations developed for particle settling in Newtonian fluids. To account for non-Newtonian behavior of the fluid, Newtonian viscosity term in particle Reynolds number is replaced with apparent viscosity, which is a function of shear rate. The prefix 'generalized' is added to particle Reynolds number to indicate that the fluid is non-Newtonian. For a fluid that fits power law rheology model, generalized Reynolds number is given as:

$$N_{Repg} = \frac{\rho v_t D_p}{K \dot{\gamma}^{n-1}} \tag{3.15}$$

where,

N_{Repg} = generalized particle Reynolds number, dimensionless

42

Previous investigators have shown that drag coefficient of a solid sphere in non-Newtonian fluid cannot be estimated by simply replacing particle Reynolds number with generalized particle Reynolds number. There is an additional dependence on the power law fluid parameter, n. A family of curves that are a function of flow behavior index, n, are produced when C_D^{2-n} is plotted on y-axis and generalized particle Reynolds number on x-axis (Shah 1982). With increasing Reynolds number the dependence on 'n' diminishes. This plot can be used to represent all three flow regions and drag coefficient can be estimated by trial and error method. To avoid this difficulty Shah (1982) plotted $\sqrt{C_D^{2-n}N_{Repg}^2}$ on y-axis and generalized particle Reynolds number on x-axis. This plot reduces to the standard Newtonian drag curve shown in Fig. 3.3 when n is unity. The y-axis term is independent of terminal settling velocity term and can be easily calculated using particle and fluid properties. Terminal settling velocity of a particle can be calculated by estimating particle Reynolds number from Eq. 3.16, 3.17 and using it in Eq. 3.18.

$$\sqrt{C_D^{2-n}N_{Repg}^2} = A(N_{Rep})^C + B \qquad (3.16)$$

$$\sqrt{C_D^{2-n}N_{Repg}^2} = \sqrt{\left[\frac{(3.5778)^{2-n}(0.02615)}{36^{2(n-1)}}\right]\left[\frac{d_p^{n+2}\rho^n(\rho_p-\rho)^{2-n}}{K^2}\right]} \qquad (3.17)$$

$$v_t = \left[\frac{(36)^{n-1}KN_{Repg}}{0.1617d_p^n\rho}\right]^{1/(2-n)} \qquad (3.18)$$

where,

A, B, C = correlation constants.

This correlation is valid for: $0.281 < n < 1.000$ and $0.01 < N_{Repg} < 500$. The correlation constants, A, B and C, are functions of flow behavior index and can be

estimated using Fig. 3.4. Particle shear rate used in this correlation is the maximum

shear rate and is given in consistent units as:

$$\dot{\gamma} = \frac{3v_t}{D_p} \qquad (3.19)$$
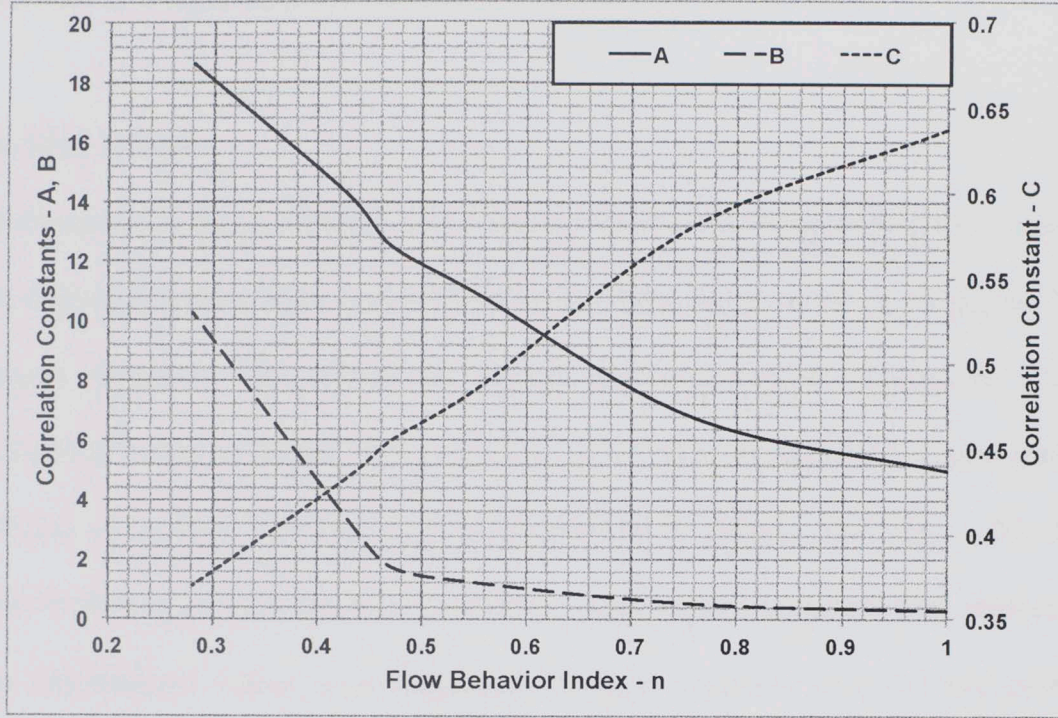
Figure 3.4: Correlations Constants – A, B and C (redrawn, Shah 1982)

3.4 Particle Settling in Fluid Under Dynamic Conditions

Hannah and Harrington (1981) have reported dynamic proppant transport data in

linear fracturing gels. Their experimental data did not agree with modified form of

Stokes' Law. This is because there is an additional dependence of drag coefficient

on power law parameter, n, as described in the previous section. This data when

plotted as $\sqrt{C_D^{2-n} N_{Repg}^2}$ versus generalized particle Reynolds number showed good

agreement with Shah (1982) correlation. Experimental data generated for particle

44

settling under dynamic conditions with different diameter particles and power law fluids agree well with this correlation developed from static particle settling data (Shah 1982). Due to shear thinning of the fluid under dynamic conditions, particle settling is faster than under static conditions. However, in a fracture this effect is opposed by exaggerated wall effects, which retard particle settling.

3.5 Wall Effects

As discussed in the previous chapter, various empirical correction factors to account for wall effects have been reported and widely used by previous investigators. This section discusses wall effects on smooth spherical particle settling in a long cylindrical column of fluid. The correction factor (f) is the ratio of terminal settling velocity of particle in bound fluid to its velocity in infinite fluid (Eq. 3.20). It is independent of particle Reynolds number in creeping and turbulent flow regions. In the intermediate region, it is dependent on both diameter ratio (λ) and particle Reynolds number in infinite fluid ($N_{Rep\infty}$).

$$f = \frac{v_t}{v_{t\infty}} \qquad (3.20)$$

where in consistent units,

f = correction factor, dimensionless

v_t = terminal settling velocity in bound fluid

$v_{t\infty}$ = terminal settling velocity in infinite fluid

$$\lambda = \frac{D_p}{D_c} \qquad (3.21)$$

where in consistent units,

λ = diameter ratio, dimensionless

45

D_p = diameter of particle

D_c = diameter of cylinder

Chaabra et al. (2003) reviewed a large number of experimental data on wall effects and recommended using the Haberman and Sayre (1958) equation (Eq. 3.22) for creeping regime, the Di Felice (1996) equation (Eq. 3.23) for intermediate region, and Newton (1687) equation (Eq. 3.24) for turbulent regime. These equations have been developed empirically from experimental data.

Creeping:
$$f = \left(\frac{1-2.105\lambda+2.0865\lambda^3-1.7068\lambda^6}{1-0.75857\lambda^5} \right); \lambda \leq 0.8 \qquad (3.22)$$

Intermediate:
$$f = \left(\frac{1-\lambda}{1-0.33\lambda} \right)^\alpha ; \frac{3.3-\alpha}{\alpha-0.85} = 0.1N_{Re p\alpha}; 0.08 \leq \lambda \leq 0.7 \qquad (3.23)$$

Turbulent:
$$f = (1-\lambda^2)(1-0.5\lambda^2)^{0.5}; 0.11 \leq \lambda \leq 0.83 \qquad (3.24)$$

3.6 Hindered Settling

Presence of multiple particles in a fluid leads to mutual interference in the motion of particles. The settling velocity of particles is considerably less than that of a single particle in fluid. This is because the particle is settling through a slurry or suspension of particles rather than a simple fluid. Therefore, accounting for bulk density and viscosity of slurry in Eq. 3.8 would give the maximum hindered settling velocity of a particle in fluid.

$$v_H = \frac{D_p^2(\rho_p-\rho_b)g}{18\mu_b} \qquad (3.25)$$

where in consistent units,

v_H = maximum hindered settling velocity

ρ_b = bulk density

μ_b = bulk viscosity

Bulk density of slurry can be calculated by dividing the mass of fluid and suspended particles with the volume occupied by the slurry. Bulk viscosity is a function of shear rate and in case of suspensions it is an indefinite and indeterminate value. However, the interference caused by the presence of many particles is a function of the volume fraction of slurry (ϕ) occupied by the fluid. Therefore, the viscosity of the fluid may be multiplied by a factor determined as a function of volume fraction (ϕ) to determine bulk viscosity of slurry. For spherical particles the following relationship was developed (Steinour 1944):

$$\frac{\mu_b}{\mu} = \frac{10^{1.82(1-\phi)}}{\phi} \tag{3.26}$$

Since bulk density is a function of volume fraction (ϕ), particle density and fluid density, it is simpler to express hindered settling velocity in terms of some function, $f(\phi)$, and terminal settling velocity of single particle in fluid:

$$v_H = v_t f(\phi) \tag{3.27}$$

This function of volume fraction was empirically determined by Steinour (1944) as:

$$f(\phi) = \frac{v_H}{v_t} = \frac{\phi^2}{10^{1.82(1-\phi)}} \tag{3.28}$$

If $\phi < 0.7$, the following simpler relationship can be used:

$$v_H = v_t \frac{\phi^3}{1-\phi} \tag{3.29}$$

CHAPTER 4

EXPERIMENTAL SETUP

The various experimental setup, equipment, chemicals, and the procedure followed to gather experimental data are detailed in this section. A number of precautions were taken and the recommended mixing procedures were followed carefully when preparing xanthan and guar gum polymer solutions. Based on the literature review, the factors that affect synergy of xanthan and guar fluids are:

1. Ratio of xanthan/guar gum in the blend

2. Polymer concentration

3. Dissolution temperature of xanthan and guar gum in fresh water

4. Temperature of the blend

5. Salinity of water used to prepare xanthan and guar fluids

In this study, the effects of polymer concentration, ratio of xanthan and guar fluids in the blend, and temperature of the blend have been investigated. Xanthan and guar gums were dissolved at 25 °C or 77 °F in fresh water. The water used to prepare these fluids was tap water supplied by the City of Norman.

Two polymer concentrations (40 and 60 lbm/Mgal) were investigated. Eight blends of xanthan and guar gum fluids were prepared for each polymer concentration. Temperature and pH were closely monitored. The viscometer readings were recorded at a constant temperature of 25 °C or 77 °F. The volumetric ratios of xanthan/guar gum fluids investigated and the nomenclature used are shown in Table

48

4.1. To study the effect of temperature, a rheology study of some of these blends at each polymer concentration was undertaken at an elevated temperature of 150 °F.

Table 4.1 Nomenclature of xanthan/guar gum fluid blends

Volumetric ratio of xanthan/guar gum fluids	Nomenclature
0:1	40 lb Guar Gum
1:4	Blend (1:4 X:G 40 lb)
1:3	Blend (1:3 X:G 40 lb)
1:2	Blend (1:2 X:G 40 lb)
2:3	Blend (2:3 X:G 40 lb)
1:1	Blend (1:1 X:G 40 lb)
3:2	Blend (3:2 X:G 40 lb)
3:1	Blend (3:1 X:G 40 lb)
4:1	Blend (4:1 X:G 40 lb)
1:0	40 lb Xanthan Gum
0:1	60 lb Guar Gum
1:4	Blend (1:4 X:G 60 lb)
1:3	Blend (1:3 X:G 60 lb)
1:2	Blend (1:2 X:G 60 lb)
2:3	Blend (2:3 X:G 60 lb)
1:1	Blend (1:1 X:G 60 lb)
3:2	Blend (3:2 X:G 60 lb)
3:1	Blend (3:1 X:G 60 lb)
4:1	Blend (4:1 X:G 60 lb)
1:0	60 lb Xanthan Gum

4.1 Equipment

A model 35 Fann viscometer shown in Fig. 4.1 with number 1 spring was used to measure rheology of fluids. Table 4.2 shows specifications of the viscometer. Model 35 Fann is a coaxial cylinder rotational viscometer. The test fluid is contained in the annular space between the cylinders. Rotation of the outer cylinder at known

velocities and viscous drag exerted by the fluid creates a torque on the inner cylinder or bob. This torque is transmitted to the spring and its deflection is the dial reading of the viscometer.
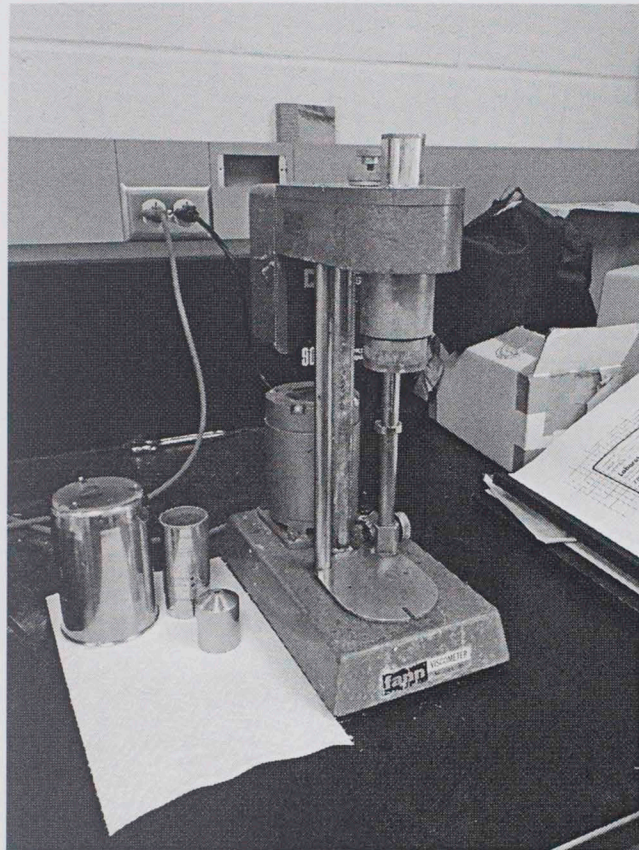
Figure 4.1 Model 35 Fann Viscometer

Table 4.2 Specifications of Model 35 Fann Viscometer

Geometry	Dimensions,	Shear Rate Range,	Spring Number,
Diameter of Bob,	34.49		
Diameter of Cup,	36.83	5.11 – 1021.80	1
Ratio ($\beta = D_b/D_c$)	0.9365		

The rheology of fluids was measured at 77 and 150 °F. The fluid temperature was maintained constant using a hot water bath shown in Fig. 4.2. Fluid quality was monitored by measuring pH.
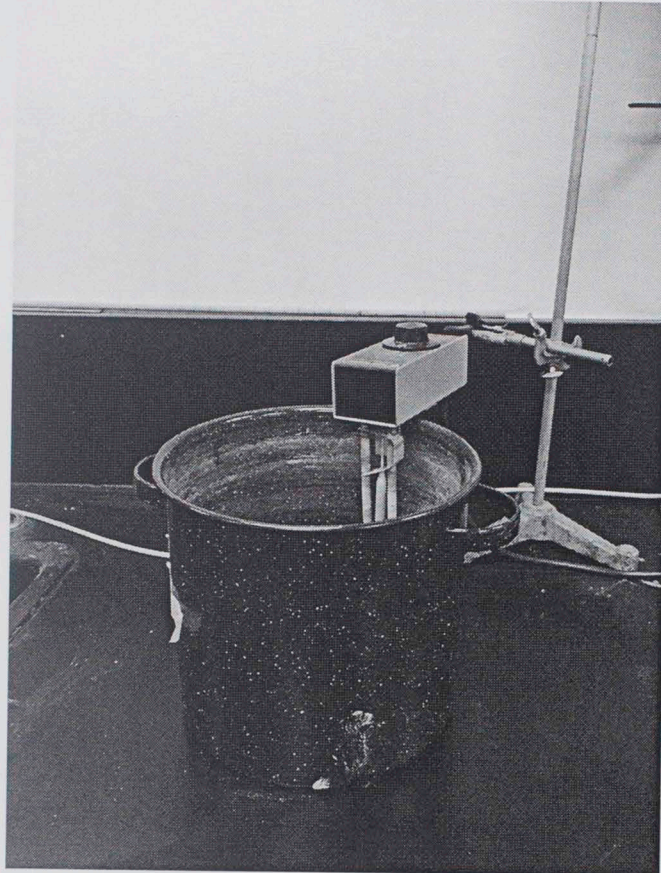
Figure 4.2: Hot water bath with an immersion heater and ring stand

Specially constructed equipment shown in Fig. 4.3 and 4.4 was used to determine terminal velocity of spherical particle in test fluids. It is a 6 ¼ ft long Plexiglas tube with an internal diameter of 3.72-in. and an outer diameter of 4-in. At the bottom of the tube, a small spigot was attached to drain the fluid after the test. A transparent scale spans the length of the tube and has graduation in both centimeters and inches. Voice recorded on camera was used as a time stamp to measure terminal settling

velocities of particles. The specifications of three particles used are given in Table 4.3.
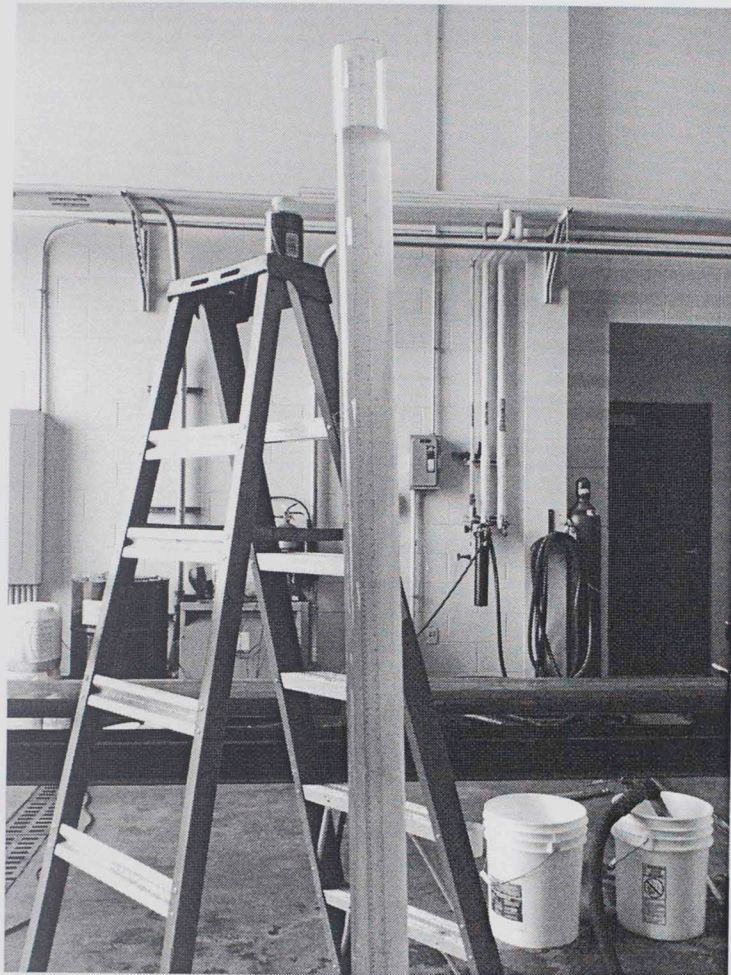
Figure 4.3: 6 ¼ ft Plexiglas Tube (OD x ID: 4.00 x 3.72 –in.) with scale

Table 4.3: Specification of Particles

Mass, g	Volume, cc	Diameter, cm	Specific Gravity
3.8385		1.434	
3.8898	1.55	1.436	2.50
3.9599		1.438	

1 – Plexiglas Tube
2 – Spherical Particle
3 – Video Camera
4 – Scale
5 – Stand
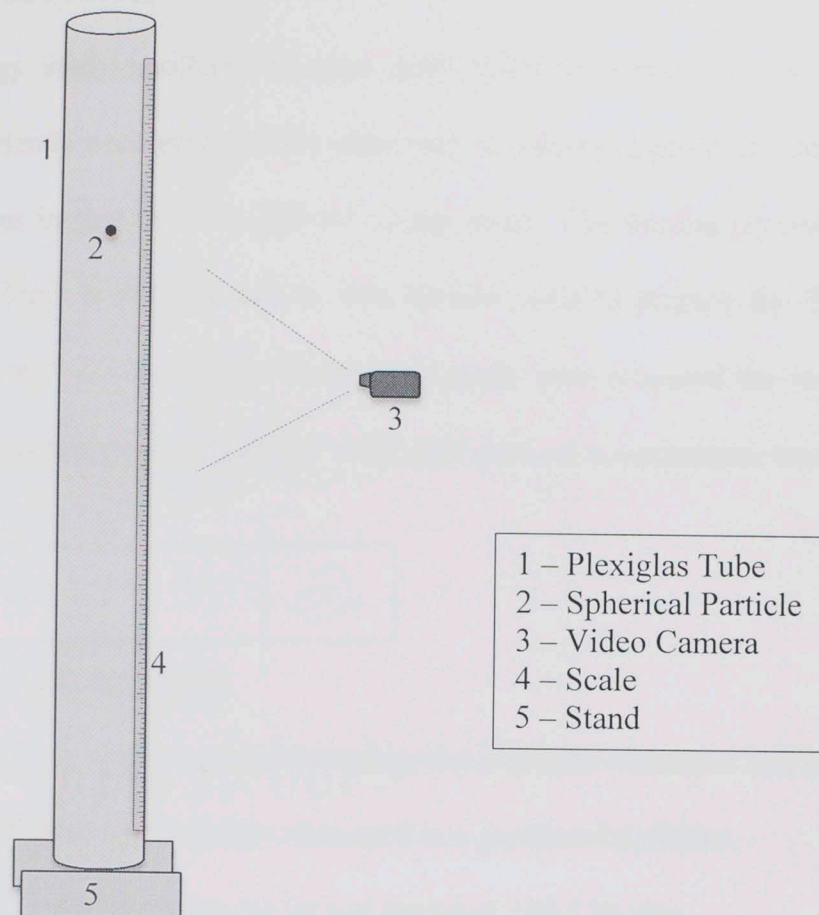
Figure 4.4: Schematic of equipment used for single particle settling tests

4.2 Chemicals Used

The xanthan gum used sold under the commercial name of FLO-VIS L® by MI SWACO. It is a light tan color liquid suspension with a specific gravity of 1.1 and has an active polymer content of 4 lbm/gal. It disperses readily in aqueous solution and hydrates rapidly. The guar gum used was commercially sold as BJ Services Gelling Agent. It is a pale yellow, almost whitish, powder with a slight odor. It disperses readily in aqueous solution and yields high viscosity rapidly.

4.3 Experimental Procedure

For the rheology study xanthan and guar gum polymers were made in 500 ml batches. Their blends were prepared the same way by adding appropriate amount of guar and xanthan in that order to 500 ml of tap water. The mixing procedure for these polymer fluids is detailed below. The blender used to prepare the fluids is shown in Figure 4.4. All the fluids for rheology study were prepared the same day so as to ensure that the properties of tap water and ambient temperatures were same for all the samples.

Xanthan Fluid Mixing Procedure:

1. Desired amount of xanthan gum suspension was carefully measured in a syringe.

2. 500 ml of tap water was carefully measured in a graduated cylinder.

3. The water was added to a blender jar and mixed at 100-120 rpm.

4. Xanthan suspension was carefully added to the vortex of water.

5. If water is mixed at very high speeds, air will be entrained in the polymer fluid.

6. The fluid was monitored carefully and blender speed was increased as required (140-150 rpm for 40 lb Xanthan Gum and 170-180 rpm for 60 lb Xanthan Gum).

7. After 30 minutes of shearing the fluid, the blender was switched off.

8. The fluid was transferred to a tri-pour and hydrated for 24 hours.
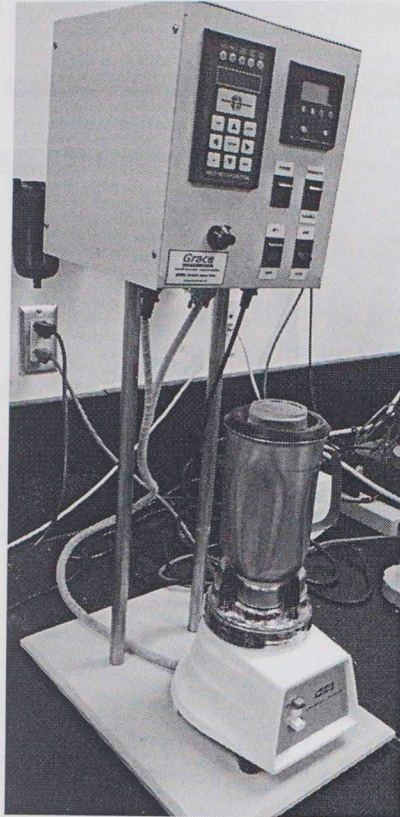
Figure 4.5: Blender used to mix fluids with manual and automatic speed controls

Guar Gum Fluid Mixing Procedure:

1. Desired amount of guar gum powder was carefully measured using an electronic scale.

2. 500 ml of tap water was carefully measured in a graduated cylinder.

3. The water was added to a blender jar and mixed at 140-150 rpm.

4. Guar gum powder was added slowly with a spoon to the vortex.

5. If the mixture is mixed at low speeds, guar will form fish eyes or stick to the blender blades. There is no danger of entrained air as was the case with xanthan gum.

6. The fluid was monitored carefully and speed was increased as required (180-190 rpm for 40 lb Guar Gum and 220-230 rpm for 60 lb Guar Gum).

7. After 30 minutes of blending, the blender was switched off.

8. The fluid was transferred to a tri-pour and hydrated for 24 hours.

Xanthan Gum-Guar Gum Blend Mixing Procedure:

1. Desired amount of guar gum powder and xanthan gum suspension were measured carefully.

2. 500 ml of tap water was carefully measured in a graduated cylinder.

3. The water was added to blender jar and mixed at 140-150 rpm.

4. Guar gum powder was added first. After it completely dispersed in the water, the rpm was lowered.

5. Xanthan gum suspension was added next. Care has to be taken as if the rpm is too high, air will be entrained in the fluid.

6. The fluid was monitored constantly and rpm increased or decreased as required.

7. After 30 minutes the blender was switched off and the fluid was transferred to a tri-pour.

8. The blend was left to hydrate for 24 hours.

Procedure for rheology study:

1. After hydrating for 24 hours, 300 ml of the fluid was poured into the viscometer cup, up to the mark on the inside wall of the cup.

2. The temperature and pH were then measured. The hot water bath was used to increase the temperature of the fluid in the sample cup.

3. While the fluid was heated, it was continuously stirred to ensure even distribution of heat.

4. Once the fluid had reached the desired temperature it was placed on the viscometer stand.

5. The stand was then raised so that bob and sleeve were immersed in the fluid.

6. Readings were then taken at different rpms (3, 6, 100, 200, 300, and 600).

Procedure for Single Particle Settling Tests:

The lower the terminal settling velocity, the higher is the viscosity of fluid. These tests, therefore, identify which fluid would show high low shear rate viscosity. In the current experimental setup, each particle was carefully released into a polymer fluid or blend so as not to impart acceleration or force. After the particle had travelled a distance of 2 ft from the top of the tube, measurements were made to calculate terminal velocity over the next 2 ft. This was done to minimize the entrance and exit effects. Since, the fluid was contained in a cylinder of 3.72-in. inner diameter it may not be considered infinite. Wall effects affect the settling velocity calculations. To minimize these effects, the ratio of the particle diameter to the cylinder diameter was maintained very low and the particles were released at the center of the tube. The Plexiglas tube is sufficiently long to ensure that the particle achieves zero acceleration motion and travels at its terminal settling velocity.

The procedure followed for the single particle settling tests is listed below:

1. The fluids used in these tests were prepared in 5 gallon buckets and blended with a Lightin blender.

2. After hydrating for 24 hours, the fluid was carefully poured into the Plexiglas tube with a tri-pour. The tube was tilted so the polymer fluid would flow into it gently.

3. Care was taken with xanthan fluids and the blends so air bubbles were not entrained.

4. Plexiglas tube was then carefully set on a stand.

5. A particle was gently wet with the polymer fluid and released at the exact center of the tube to minimize wall effects.

6. The particle was allowed to settle for two feet measured from the top of the tube.

7. Travel time of the particle over fixed equal intervals was measured using voice recording as a time stamp on a video camera. When particle has reached its terminal settling velocity, it requires the same time to travel these intervals.

8. The particle was then allowed to settle to the bottom of the tube. Measurements were made in the middle of the tube to minimize entrance and exit effects.

9. The test was repeated with two other particles of similar size and diameter.

4.4 Equations Used in Data Analysis

The equations used for fluid characterization and terminal settling velocity calculations are discussed here. The fluids studied were found to be

pseudoplastic/shear-thinning and can adequately be described by power law or Ostwald-de-Waele rheology model.

Wall Shear Stress, τ_w

Wall shear stress was calculated from the viscometer dial readings (θ) using the equation:

$$\tau_w = 0.01066N\theta_i \tag{4.1}$$

where,

τ_w = wall shear stress, lb_f/ft^2

N = spring number, dimensionless

θ_i = dial reading at i^{th} rpm

Wall Shear Rate, γ_w

Wall shear rate was calculated from the speed of the rotating sleeve of the viscometer using the equation:

$$\dot{\gamma}_w = 1.703 \, RPM \tag{4.2}$$

where,

$\dot{\gamma}_w$ = wall shear rate, 1/s

RPM = revolutions per minute of model 35 Fann viscometer

Power Law Fluid Model

Wall shear stress and wall shear rate were used to calculate the power law parameters, n, the flow behavior index, and K_v, the viscometer consistency index.

The relationship of wall shear stress and wall shear rate of a power law fluid is given as:

$$\tau_w = K_v \dot{\gamma}_w^n \tag{4.3}$$

where,

τ_w = wall shear stress, lb_f/ft^2

$\dot{\gamma}_w$ = wall shear rate, $1/s$

K_v = viscometer consistency index, $lb_f\text{-}s^n/ft^2$

n = fluid behavior index, dimensionless

Apparent Viscosity, μ_a

The viscosity of a non-Newtonian fluid is shear dependent, hence the use of the term 'apparent'. For a shear thinning fluid, the viscosity increases with decrease in shear. Apparent viscosity of a power law fluid is calculated using the equation:

$$\mu_a = 47880 K_v \dot{\gamma}_w^{n-1} \tag{4.4}$$

where,

μ_a = apparent viscosity, cP

K_v = viscometer consistency index, $lb_f\text{-}s^n/ft^2$

$\dot{\gamma}_w$ = wall shear rate, $1/s$

Terminal Settling Velocity, v_t

Terminal-settling velocity is the velocity of a particle in a fluid when its acceleration is zero. Therefore, it can be calculated using the equation of motion:

$$v_t = x/t \tag{4.5}$$

where,

v_t = terminal-settling velocity, ft/s

x = displacement of a particle, ft

t = time, s

CHAPTER 5

RESULTS AND DISCUSSION

Analysis of the rheology data involved calculating the wall shear stress and wall shear rate using the equations described in the previous chapter. It was found that the fluids investigated were adequately described by Ostwald-de-Waele or power law model. Logarithmic plots of wall shear stress and wall shear rate or rheograms were made to estimate the power law parameters. The slope of the straight line is the flow behavior index and the intercept at unity wall shear rate is the fluid consistency index.

Terminal settling velocity of three particles with similar size, density and mass in polymer fluids and blends was measured. The experimental results were compared with predictions of Shah (1982) correlation. Terminal velocity data was also used to compare the rheology of blends and polymer fluids. Cost analysis of blends and polymer fluids was undertaken to determine a blend that optimized on price and performance.

5.1 Rheology Studies

Rheology of 40 and 60 lb/Mgal polymer fluids and complex fluids was studied at ambient (77 °F) and elevated temperature (150 °F). The aim was to identify the complex fluids that displayed higher viscosities at low shear rates, better shear thinning properties, and better temperature stability as compared to component guar

gum polymer fluid. A good shear thinning fluid would have low viscosity when pumped down to the formation (6000 – 10000 s^{-1} shear rate) and high viscosity when transporting proppant in fracture (0.01 – 500 s^{-1} shear rate). Low viscosity when pumping would result in less pump pressures and lower costs. It is also important that these fluid properties remain stable with increasing temperature as fluid is pumped down the tubing.

5.1.1 40 lb/Mgal Concentration Polymer Fluids

Model 35 Fann viscometer data of all 40 lb/Mgal polymer concentration fluids are listed in Tables A.1 – A.10 in Appendix A. Power law fluid parameters, flow behavior index and fluid consistency index, of control polymer fluids and eight complex fluids are listed in Table 5.1. Based on volume percentage of 40 lb/Mgal xanthan gum polymer added, viscosity at low shear rates and shear thinning, two complex fluids show strong synergy – Blend (1:3 X:G 40 lb) and Blend (3:1 X:G 40 lb).

Table 5.1: Power Law Fluid Parameters of 40 lb/Mgal Polymer Fluids

Fluid	n	K_v, lbf-s^n/ft^2
40 lb Guar Gum	0.578	0.00842
Blend (1:4 X:G 40 lb)	0.349	0.04783
Blend (1:3 X:G 40 lb)	0.306	0.06901
Blend (1:2 X:G 40 lb)	0.358	0.04158
Blend (2:3 X:G 40 lb)	0.312	0.05640
Blend (1:1 X:G 40 lb)	0.298	0.06161
Blend (3:1 X:G 40 lb)	0.228	0.08651
Blend (4:1 X:G 40 lb)	0.167	0.13078
Blend (1:0 X:G 40 lb)	0.203	0.10152
40 lb Xanthan Gum	0.141	0.11455
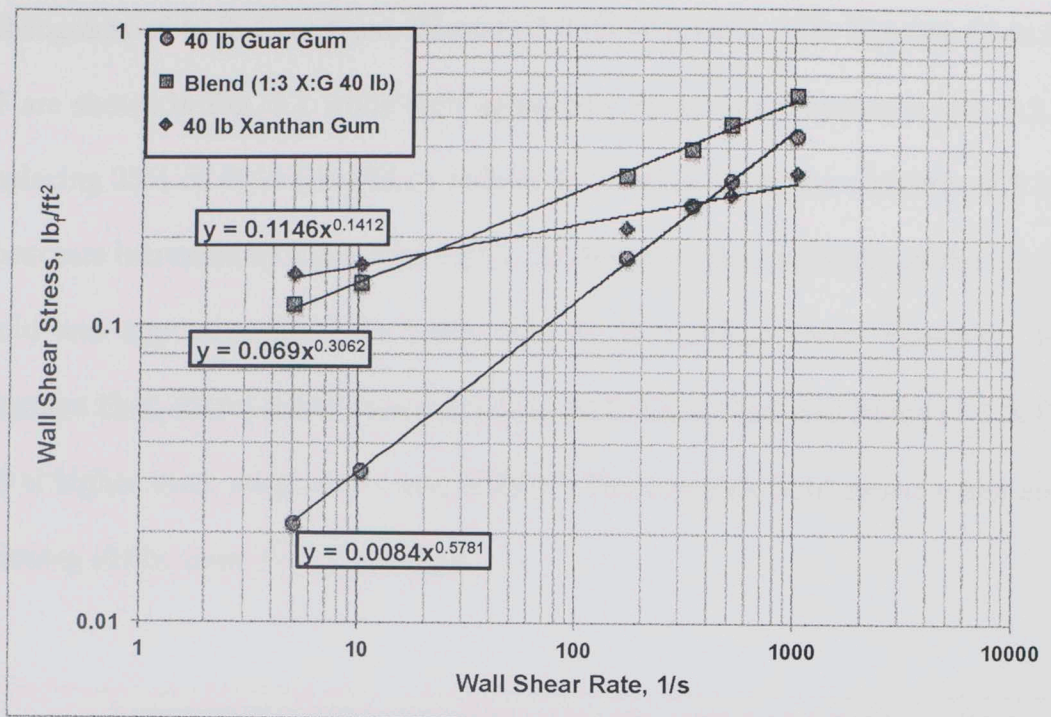
Figure 5.1: Rheograms of 40 lb Guar Gum, Blend (1:3 X:G 40 lb) and 40 lb Xanthan Gum at 77 °F

The equations shown on the figure:

$$y = 0.1146x^{0.1412}$$

$$y = 0.069x^{0.3062}$$

$$y = 0.0084x^{0.5781}$$
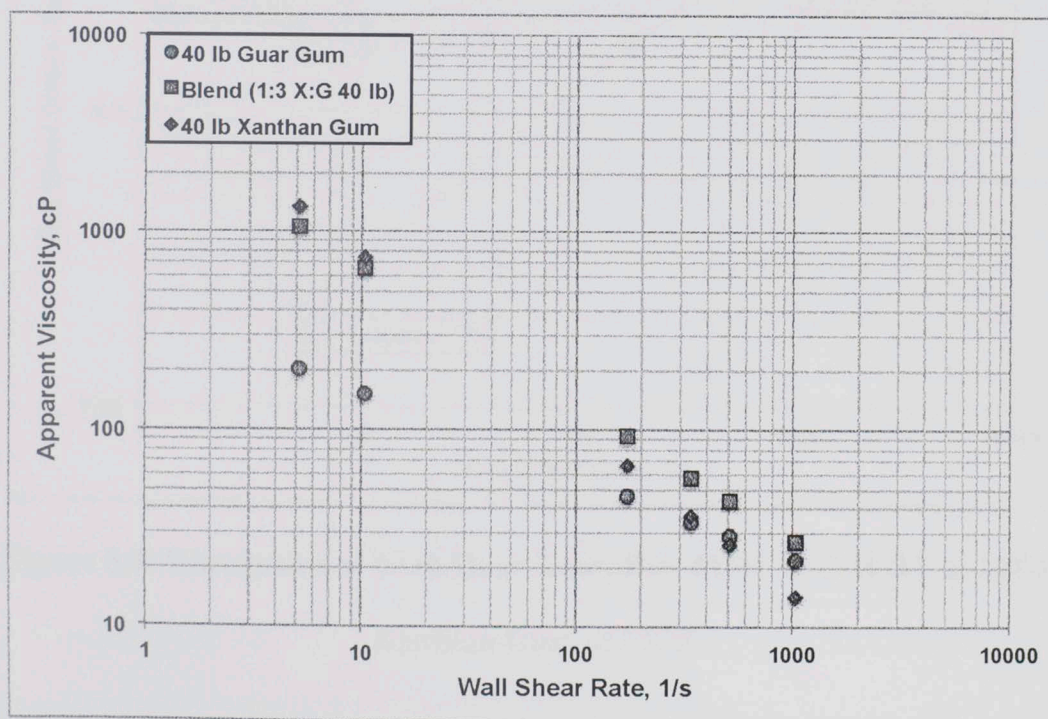
Figure 5.2: Apparent Viscosity of 40 lb Guar Gum, Blend (1:3 X:G 40 lb) and 40 lb Xanthan Gum at 77 °F

Rheograms of 40 lb Guar Gum, Blend (1:3 X:G 40 lb) and 40 lb Xanthan Gum at 77 °F are shown in Fig. 5.1 while their apparent viscosities are shown in Fig. 5.2. On replacing 25% of 40 lb Guar Gum with 40 lb Xanthan Gum, the viscosity at 5.11 s^{-1} shear rate increased by more than 420%. At this shear rate, viscosity of the complex fluid was approximately 20% lower than 40 lb Xanthan Gum. However, 40 lb Xanthan Gum shows lower viscosities than 40 lb Guar Gum and Blend (1:3 X:G 40 lb) at higher shear rates of 511 and 1022 s^{-1}. The complex fluid shows better shear-thinning ability than 40 lb Guar Gum.
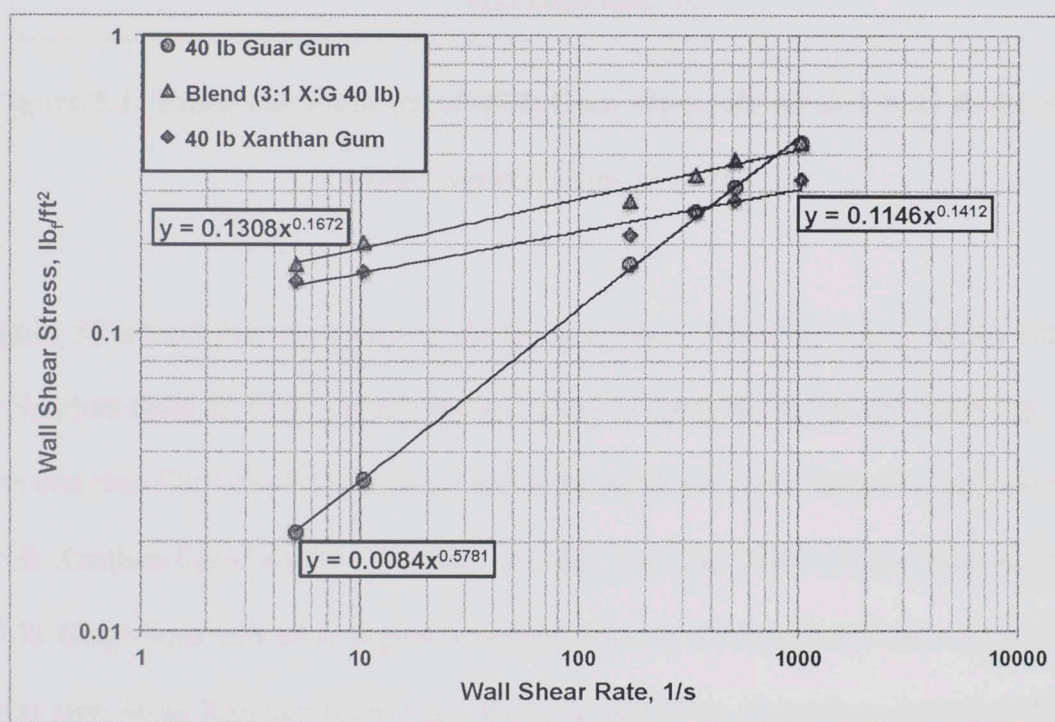
Figure 5.3: Rheograms of 40 lb Guar Gum, Blend (3:1 X:G 40 lb) and 40 lb Xanthan Gum at 77 °F
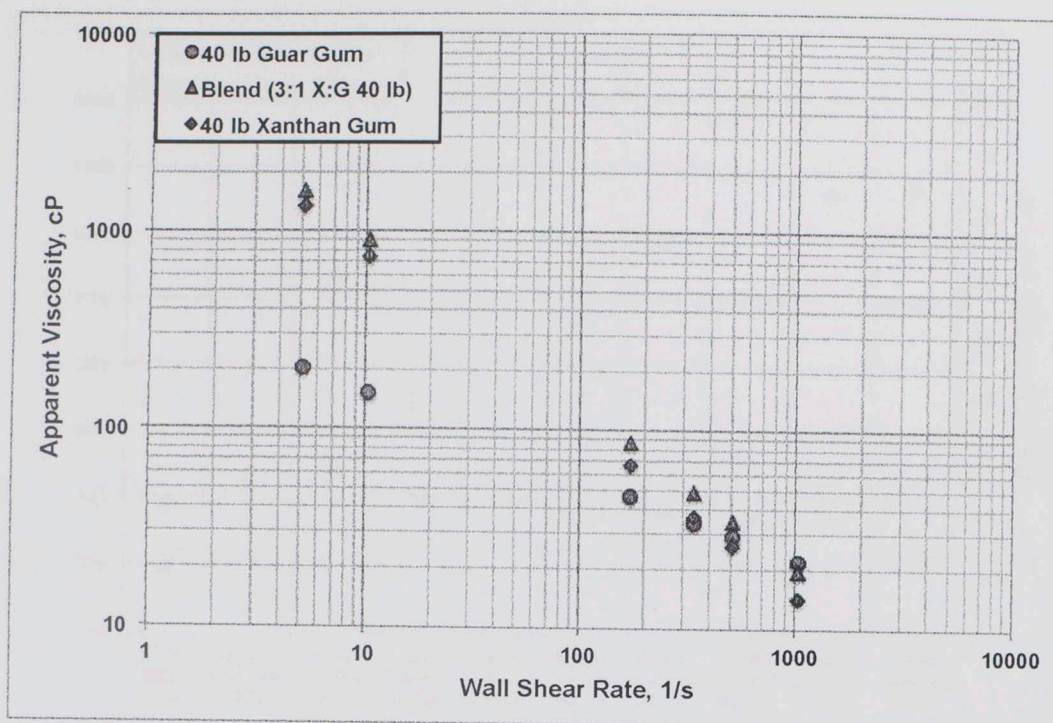
Figure 5.4: Apparent Viscosity of 40 lb Guar Gum, Blend (3:1 X:G 40 lb) and

40 lb Xanthan Gum at 77 °F

Figure 5.3 shows the rheograms of 40 lb Guar Gum, Blend (3:1 X:G 40 lb) and 40 lb Xanthan Gum at 77 °F. Apparent viscosities of these fluids are shown in Fig. 5.4. The complex fluid displayed higher viscosities at all six shear rates investigated than 40 lb Xanthan Gum. At 5.11 s^{-1} shear rate this fluid has 700% higher viscosity than 40 lb Guar Gum and 20% higher viscosity than 40 lb Xanthan Gum. At 1022 s^{-1} shear rate, 40 lb Xanthan Gum has lower viscosity than 40 lb Guar Gum and Blend (3:1 X:G 40 lb). Blend (3:1 X:G 40 lb) shows higher viscosities and better shear thinning property than Blend (1:3 X:G 40 lb). However, this complex fluid is prepared with 75% 40 lb Xanthan Gum and 25% 40 lb Guar Gum, and has three times higher xanthan fluid content than Blend (1:3 X:G 40 lb).
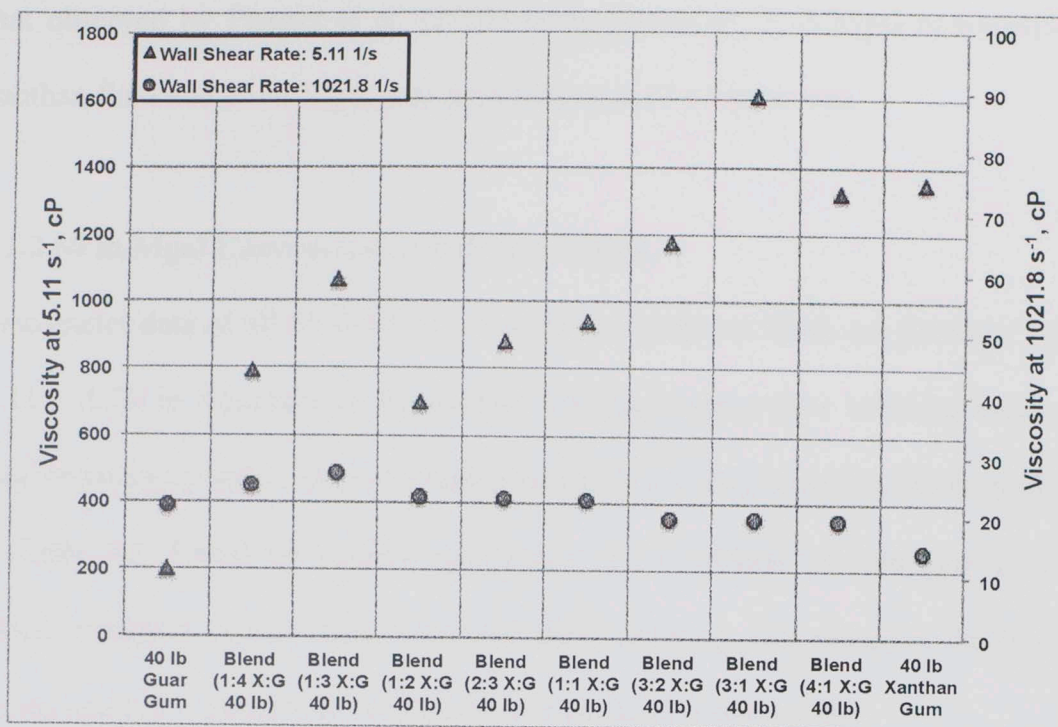
Figure 5.5: Apparent Viscosities at 5.11 and 1021.8 s⁻¹ of 40 lbm/Mgal polymer

fluids at 77 °F

To compare the viscosities of all 40 lbm/Mgal concentration polymer fluids at high and low shear rates, the rheology data at 5.11 and 1021.8 s^{-1} shear rates of these fluids has been shown in Fig. 5.17. A general trend of viscosity at both these shear rates can be observed with increasing xanthan content in complex fluids. All eight blends showed significant increase in viscosities as compared to 40 lb Guar Gum at low shear rates. Addition of xanthan fluid to 40 lb Guar Gum results in a spike in apparent viscosity at 5.11 s^{-1} shear rate. The trend of viscosity at this shear rate then stabilizes and gradually increases with increasing xanthan content. At 1021.8 s^{-1} shear rate, apparent viscosity gradually decreases with increasing xanthan content and 40 lb Xanthan Gum shows the least viscosity. The sudden spike in viscosity at low shear rates on addition of 20 – 25% xanthan to guar polymer fluid is similar to

that observed by Fischer et al. (2001) using blends of 25 lb/Mgal non-acetylated xanthan fluid and 25 lb/Mgal guar gum fluid at 0.17 s^{-1} shear rate.

5.1.2 60 lb/Mgal Concentration Polymer Fluids

Viscometer data of all 60 lb/Mgal concentration polymer fluids are listed in Tables A.11 – A.20 in Appendix A. Power law fluid parameters, flow behavior index and fluid consistency index, of control polymer fluids and eight complex fluids are listed in Table 5.2. Based on volume percentage of 60 lb/Mgal xanthan gum polymer added, viscosity at low shear rates and shear thinning, two complex fluids show strong synergy – Blend (1:3 X:G 60 lb) and Blend (1:1 X:G 60 lb).

Table 5.2: Power Law Fluid Parameters of 60 lb/Mgal Polymer Fluids

Fluid	n	K_v, lb$_f$-s^n/ft^2
60 lb Guar Gum	0.202	0.11949
Blend (1:4 X:G 60 lb)	0.197	0.19234
Blend (1:3 X:G 60 lb)	0.205	0.19921
Blend (1:2 X:G 60 lb)	0.221	0.17042
Blend (2:3 X:G 60 lb)	0.249	0.17482
Blend (1:1 X:G 60 lb)	0.272	0.14533
Blend (3:1 X:G 60 lb)	0.286	0.12975
Blend (4:1 X:G 60 lb)	0.282	0.15582
Blend (1:0 X:G 60 lb)	0.270	0.14642
60 lb Xanthan Gum	0.483	0.03074
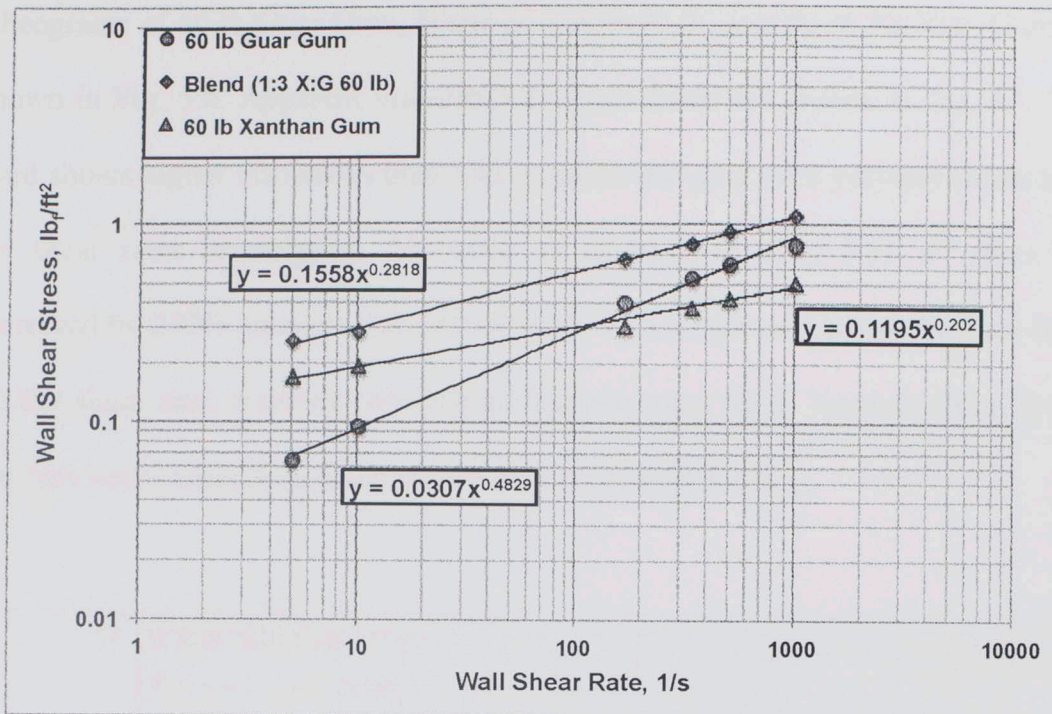
Figure 5.6: Rheograms of 60 lb Guar Gum, Blend (1:3 X:G 60 lb) and 60 lb
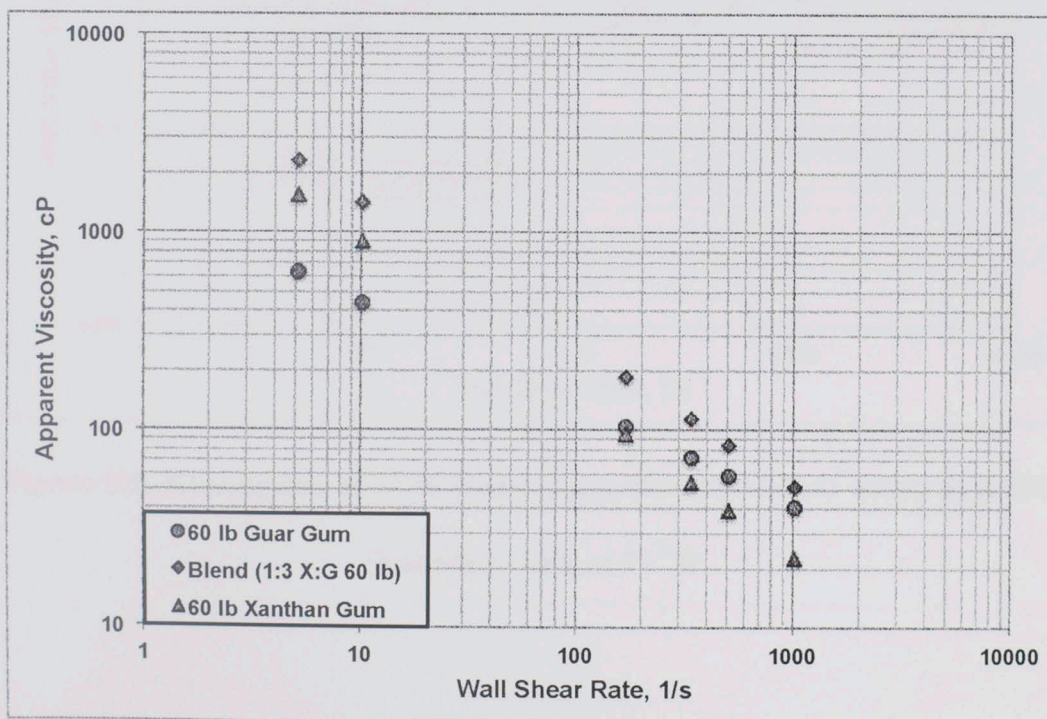
Xanthan Gum at 77 °F

Figure 5.7: Apparent Viscosity of 60 lb Guar Gum, Blend (1:3 X:G 60 lb) and

60 lb Xanthan Gum at 77 °F

Rheograms of 60 lb Guar Gum, Blend (1:3 X:G 60 lb) and 60 lb Xanthan Gum are shown in Fig. 5.6. Apparent viscosities of these fluids are shown in Fig. 5.7. This fluid shows higher viscosities than both xanthan and guar gum polymer fluids at all six shear rates investigated. Viscosity of complex fluid at 5.11 s^{-1} shear rate increased by 270% on replacing 25% of 60 lb Guar Gum with 60 lb Xanthan Gum. At this shear rate, it shows 50% higher viscosity than 60 lb Xanthan Gum. It also displays better shear thinning property than 60 lb Guar Gum.
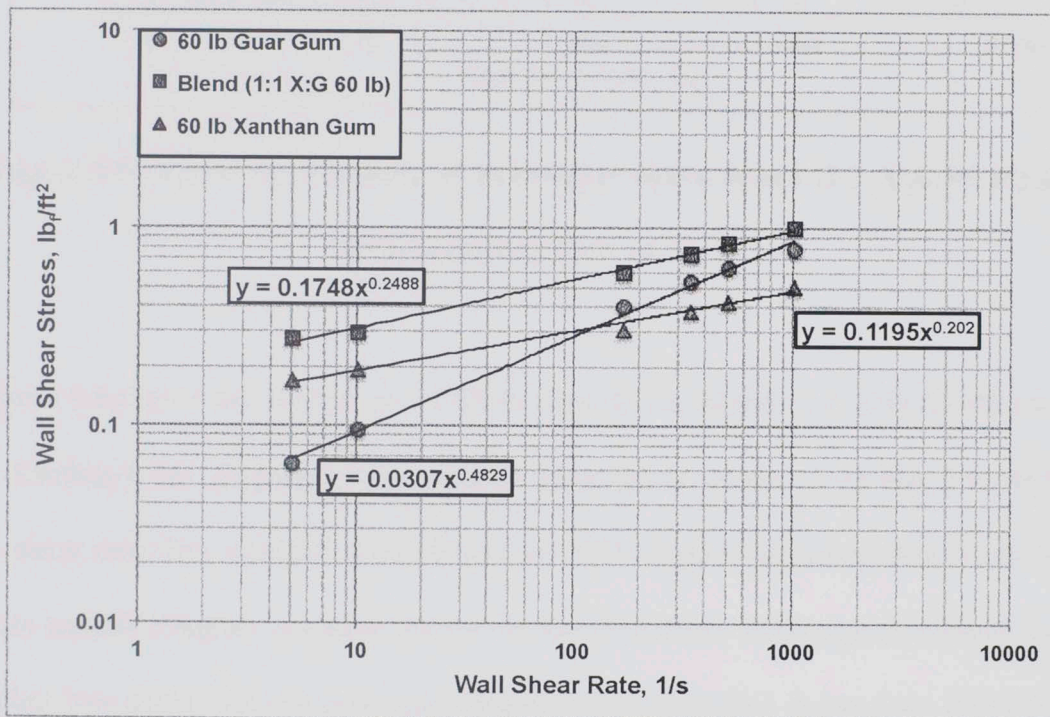
Figure 5.8: Rheograms of 60 lb Guar Gum, Blend (1:1 X:G 60 lb) and 60 lb Xanthan Gum at 77 °F
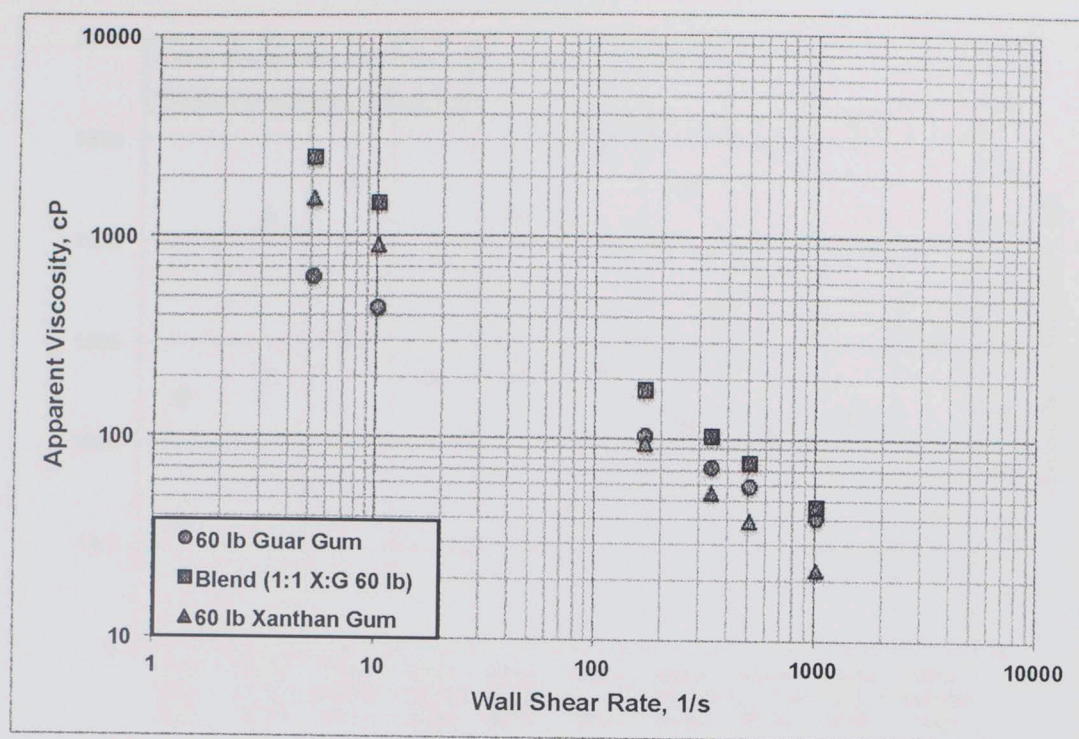
Figure 5.9: Apparent Viscosity of 60 lb Guar Gum, Blend (1:1 X:G 60 lb) and

60 lb Xanthan Gum at 77 ^{o}F

Figure 5.8 shows the rheograms of 60 lb Guar Gum, Blend (1:1 X:G 60 lb) and 60 lb Xanthan Gum. Apparent viscosities of these fluids are shown in Fig. 5.9. At 5.11 s^{-1} shear rate, this complex fluid displayed 290% higher viscosity than 60 lb Guar Gum and 60% higher viscosity than 60 lb Xanthan Gum. Although this blend shows higher low shear rate viscosity than Blend (1:3 X:G 60 lb), it requires 100% (vol.) more xanthan gum fluid to prepare.
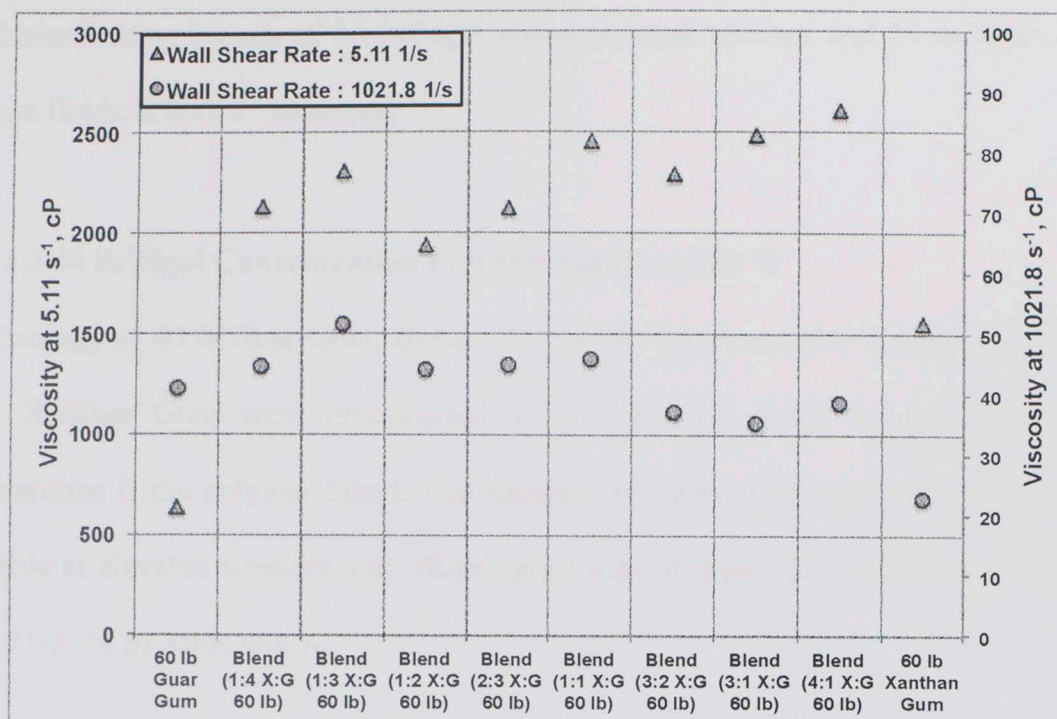
Figure 5.10: Apparent Viscosities at 5.11 s⁻¹ and 1021.8 s⁻¹ of 60 lbm/Mgal

polymers at 77 °F

To compare the viscosities of all 60 lbm/Mgal concentration polymer fluids at high

and low shear rates, the rheology data at 5.11 and 1021.80 s⁻¹ shear rates of these

fluids has been shown in Figure 5.10. All eight blends showed significant increase

in viscosities as compared to 60 lb Guar Gum and 60 lb Xanthan Gum at low shear

rates. However, all of these blends displayed considerable increase in viscosity at

1021.80 s⁻¹ shear rate compared to 60 lb Xanthan Gum. Apparent viscosity at 5.11 s⁻

¹ of complex fluids spikes and gradually increases with increasing xanthan content.

At the higher shear rate of 1021.80 s⁻¹, apparent viscosity of these fluids spikes and

gradually decreases with increasing xanthan content. Addition of xanthan imparts

better shear thinning property to 60 lb Guar Gum. The viscosity trend at the two

shear rates is consistent with the experimental results of Fischer et al. (2001)

obtained using blends of 25 lb/Mgal non-acetylated xanthan and 25 lb/Mgal guar gum fluids at 0.17 s^{-1} shear rate.

5.1.3 40 lb/Mgal Concentration Polymer Fluids at 150 °F

Rheology of 40 lb Guar Gum, Blend (1:3 X:G 40 lb), Blend (3:1 X:G 50 lb) and 40 lb Xanthan Gum were investigated at 150 °F. The study was undertaken to determine if the polymer blends that showed favorable rheological properties were stable at elevated temperatures. Rheological data of these fluids is listed in Tables A.21-A.24 in Appendix A.
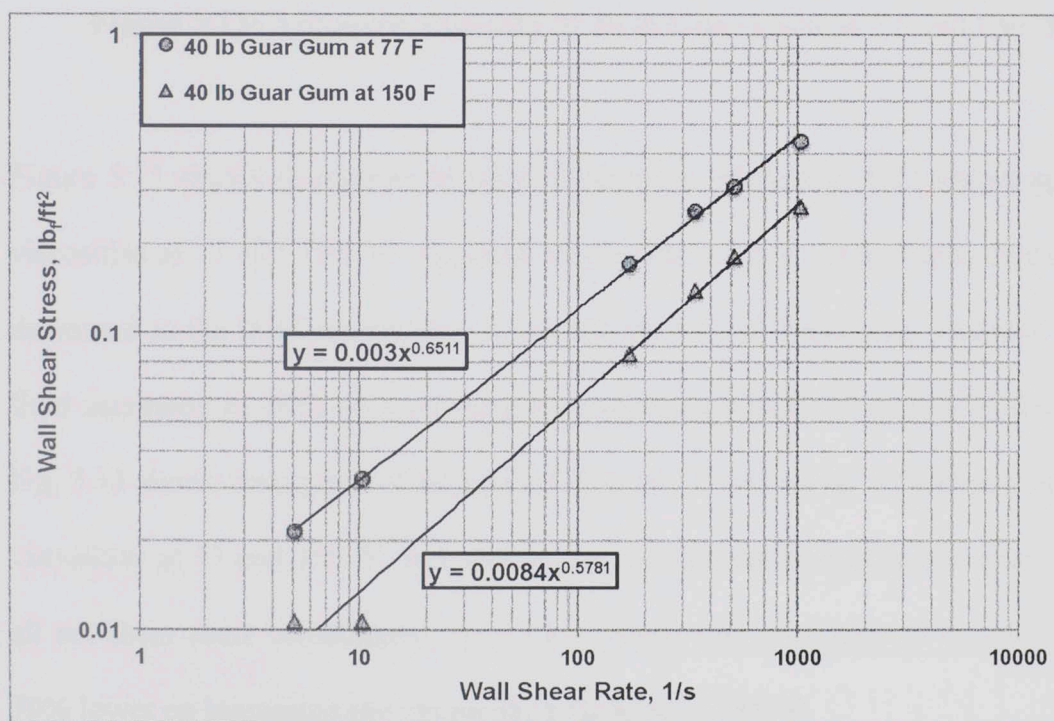
Figure 5.11: Rheograms of 40 lb Guar Gum at 77 and 150 °F
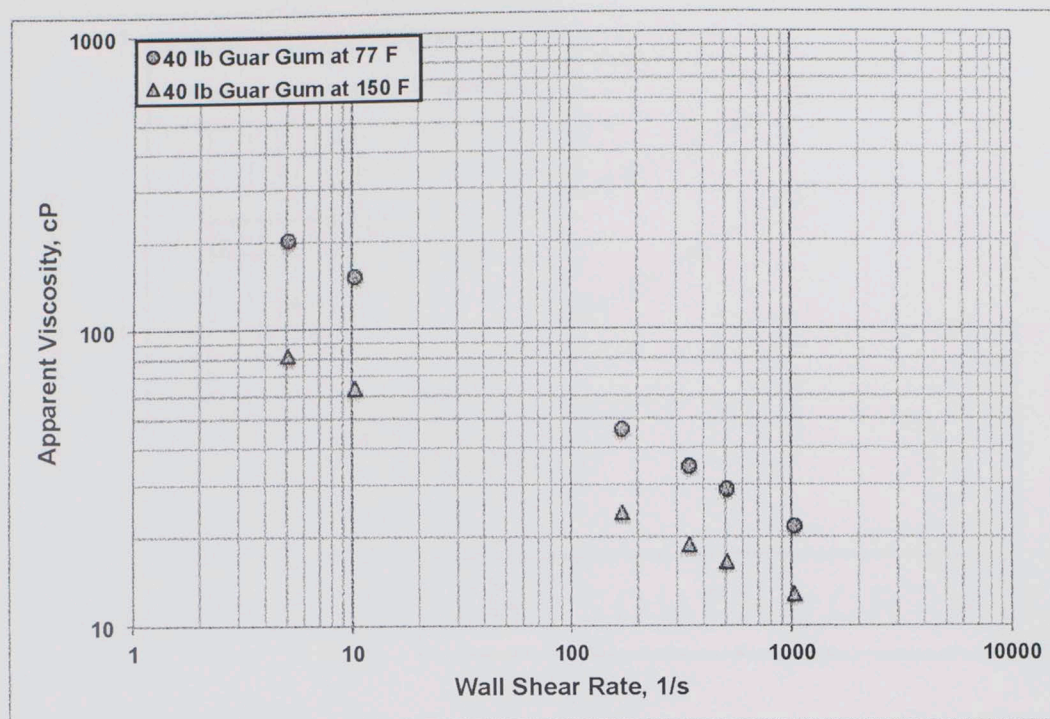
Figure 5.12: Apparent Viscosity of 40 lb Guar Gum at 77 and 150 $^{\circ}$F

Figure 5.11 shows rheograms of 40 lb Guar Gum while Fig. 5.12 shows apparent viscosities at 77 and 150 $^{\circ}$F. Apparent viscosities at all six shear rates investigated decreased as the fluid temperature increased. At 5.11 s^{-1} shear rate, viscosity of this fluid decreased by 60% on increasing the temperature from 77 to 150 $^{\circ}$F. Similarly, Fig. 5.13 shows rheograms of Blend (1:3 X:G 40 lb) while Fig. 5.14 shows apparent viscosities at 77 and 150 $^{\circ}$F. Increase in temperature resulted in lower viscosities at all six shear rates investigated. At 5.11 s^{-1} shear rate, viscosity of this blend was 70% lower on increasing the temperature from 77 to 150 $^{\circ}$F.

74
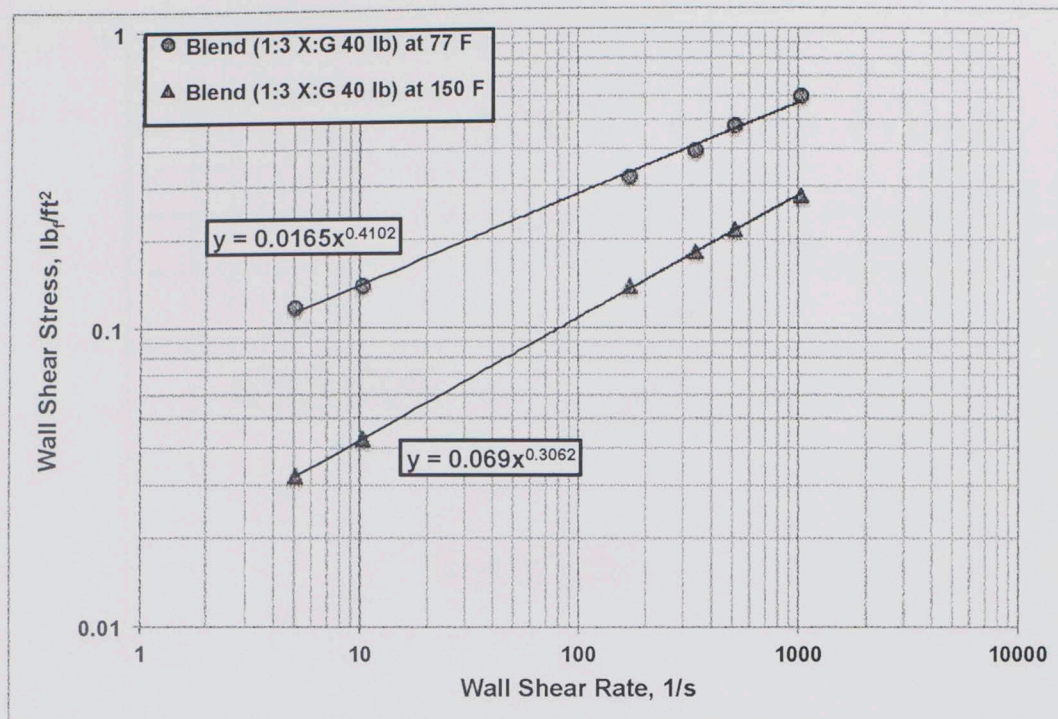
Figure 5.13: Rheograms of Blend (1:3 X:G 40 lb) at 77 and 150 $^{\circ}$F
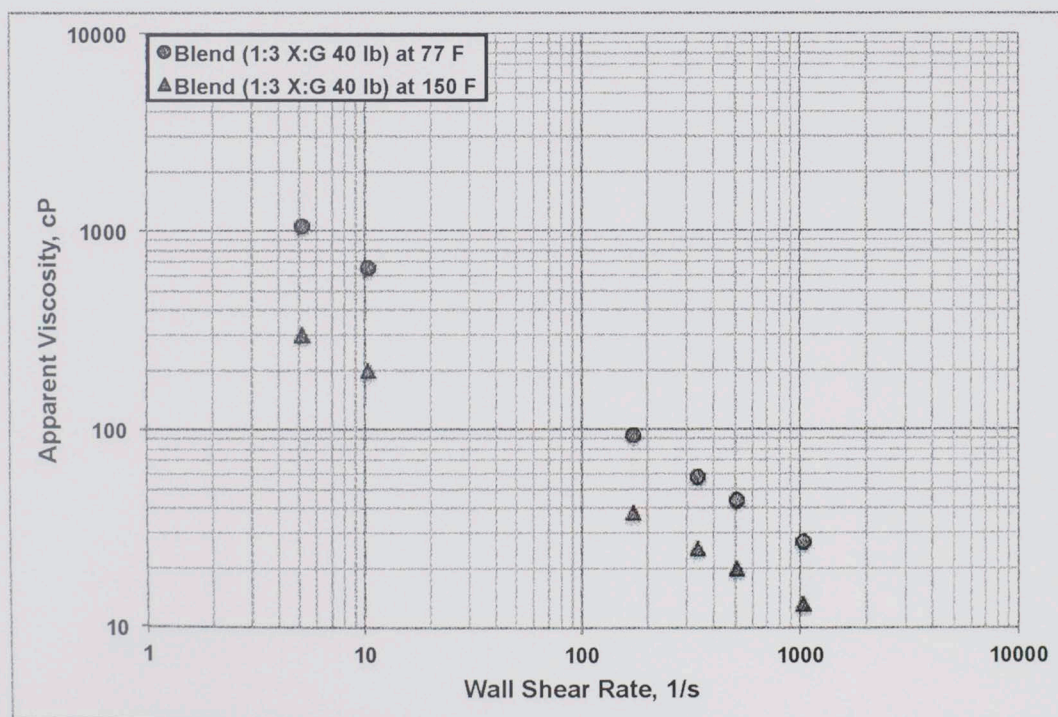
Figure 5.14: Apparent Viscosity of Blend (1:3 X:G 40 lb) at 77 and 150 $^{\circ}$F
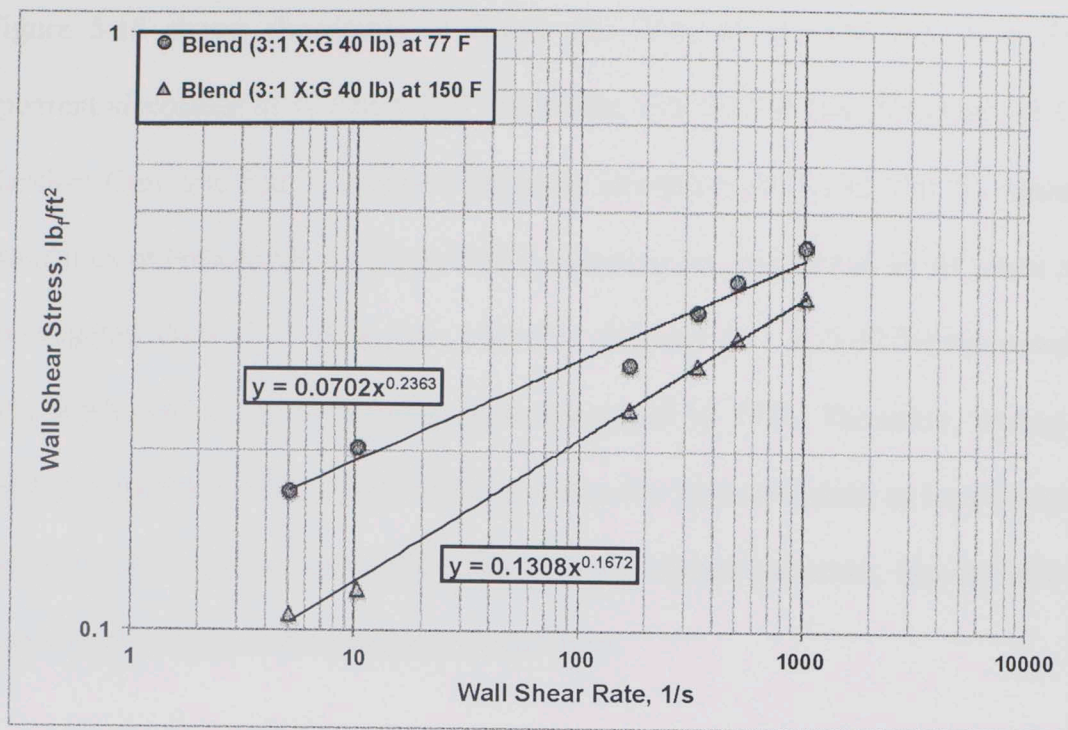
Figure 5.15: Rheograms of Blend (3:1 X:G 40 lb) at 77 and 150 °F
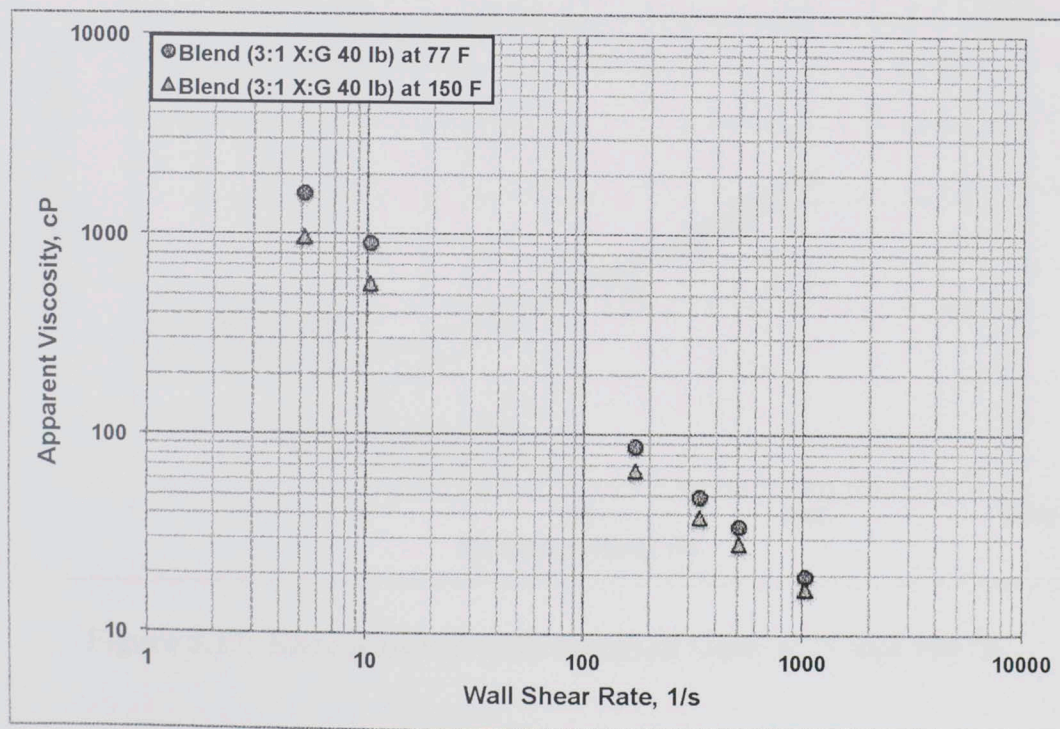
Figure 5.16: Apparent Viscosity of Blend (3:1 X:G 40 lb) at 77 and 150 °F

Figure 5.15 shows rheograms of Blend (3:1 X:G 40 lb) and Fig. 5.16 shows apparent viscosities at 77 and 150 °F. Similarly, Fig. 5.17 shows rheograms of 40 lb Xanthan Gum and Fig. 5.18 shows apparent viscosities at 77 and 150 °F. Apparent viscosities of both fluids decreased with increasing temperature at all six shear rates investigated. At 5.11 s^{-1} shear rate, viscosity of Blend (3:1 X:G 40 lb) decreased by 40% while that of 40 lb Xanthan Gum decreased by 17%. Therefore, among the fluids investigated, 40 lb Xanthan Gum shows the least deviation as temperature is increased. As xanthan gum fluid content in the blends increases, the deviation in rheology decreases with increasing temperature.
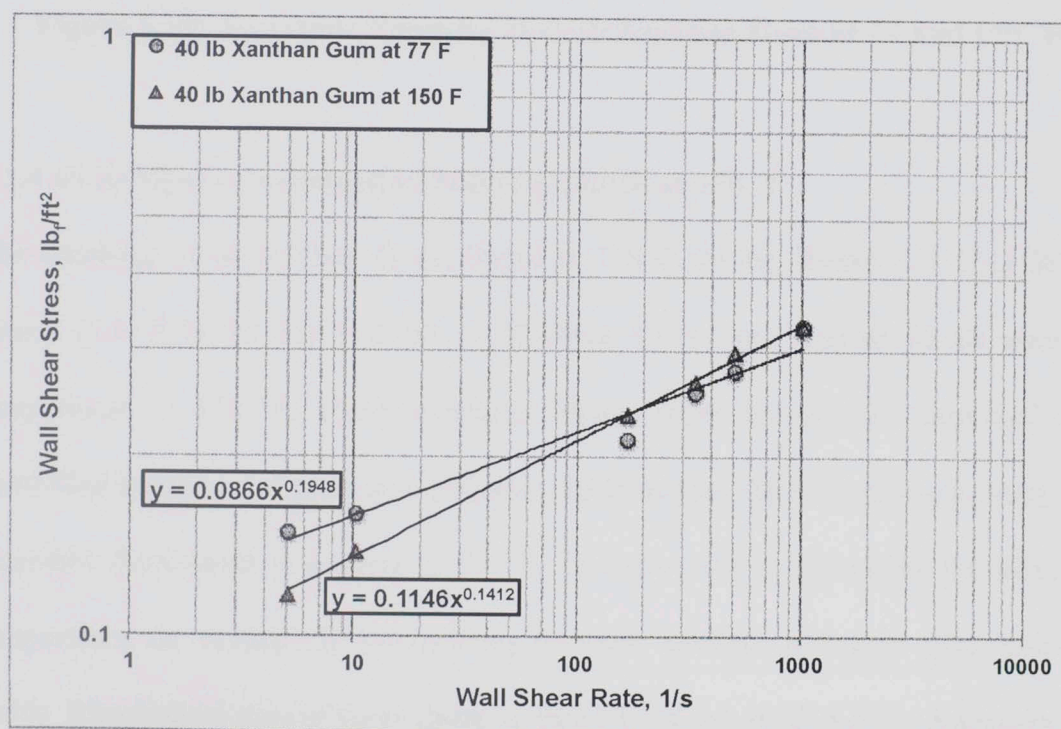
Figure 5.17: Rheograms of 40 lb Xanthan Gum at 77 and 150 °F
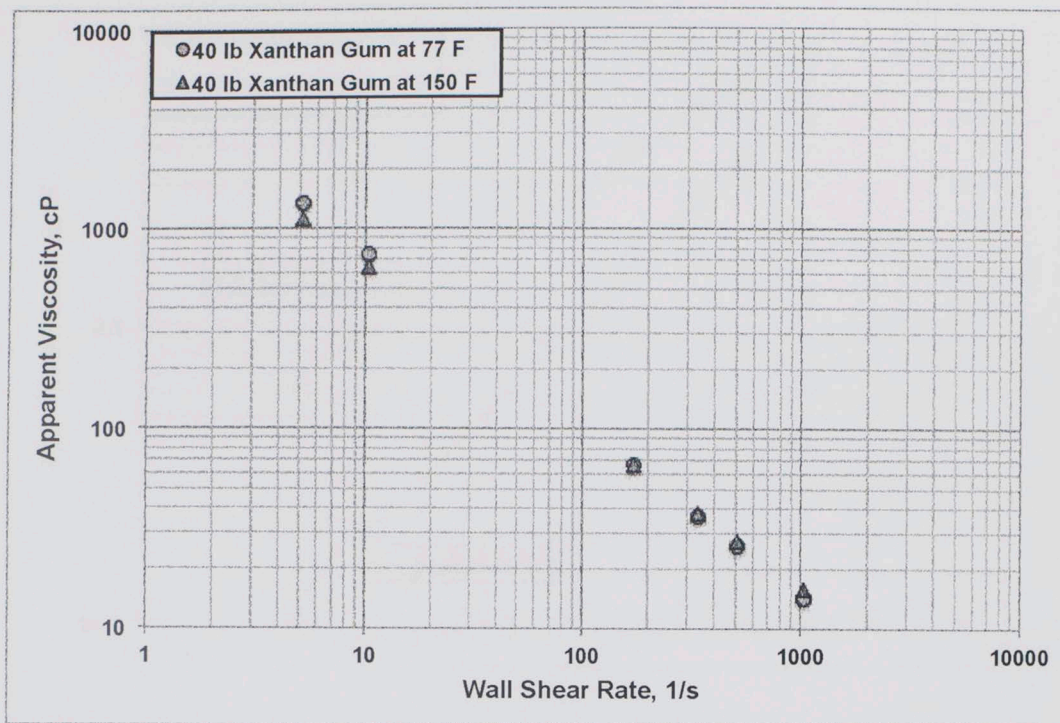
Figure 5.18: Apparent Viscosity of 40 lb Xanthan Gum at 77 and 150 °F

5.1.4 60 lb/Mgal Concentration Polymer Fluids at 150 °F

The rheology of 60 lb Guar Gum, Blend (1:3 X:G 60 lb), Blend (1:1 X:G 60 lb), Blend (3:1 X:G 60 lb) and 60 lb Xanthan Gum was studied at an elevated temperature of 150 °F. These particular blends were chosen and compared with controlled xanthan and guar gum polymer fluids as they showed strong synergy and desirable rheological properties at 77 °F. The aim was to determine the effect of temperature on synergistic interactions between xanthan and guar gum polymer fluids. Rheological data of these fluids is listed in Tables A.25-5.29 in Appendix A.

78
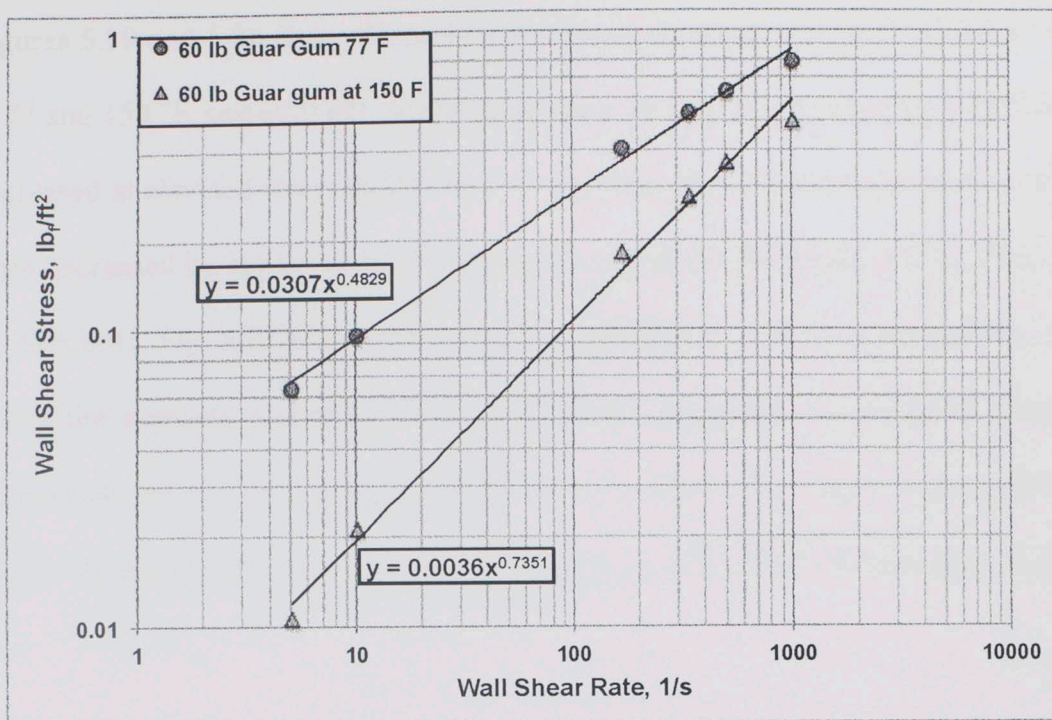
Figure 5.19: Rheograms of 60 lb Guar Gum at 77 and 150 $^{\circ}$F

The rheogram shows Wall Shear Stress, lb_f/ft^2 versus Wall Shear Rate, 1/s, with the two series:
- 60 lb Guar Gum 77 F: $y = 0.0307x^{0.4829}$
- 60 lb Guar gum at 150 F: $y = 0.0036x^{0.7351}$
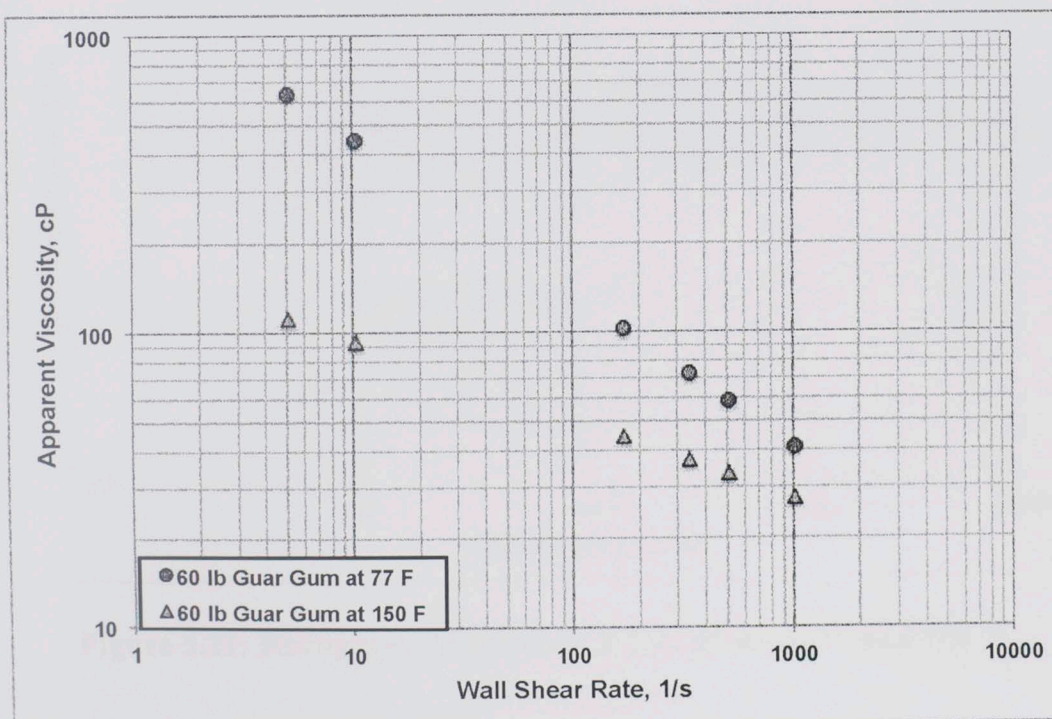
Figure 5.20: Apparent Viscosity of 60 lb Guar Gum at 77 and 150 $^{\circ}$F

Figures 5.19 and 5.20 show rheograms and apparent viscosities of 60 lb Guar Gum at 77 and 150 °F, respectively. Apparent viscosities at all six shear rates investigated decreased at elevated temperature. At 5.11 s^{-1} shear rate, the viscosity of 60 lb Guar Gum decreased by approximately 80% on increasing the temperature from 77 to 150 °F. Similarly, Fig. 5.21 shows the rheograms of Blend (1:3 X:G 60 lb) and Fig. 5.22 shows the apparent viscosities at 77 and 150 °F. Apparent viscosities of complex fluid decreased on increasing the temperature at all six shear rates investigated. At 5.11 s^{-1} shear rate apparent viscosity was 65% lower at 150 °F as compared to at 77 °F.
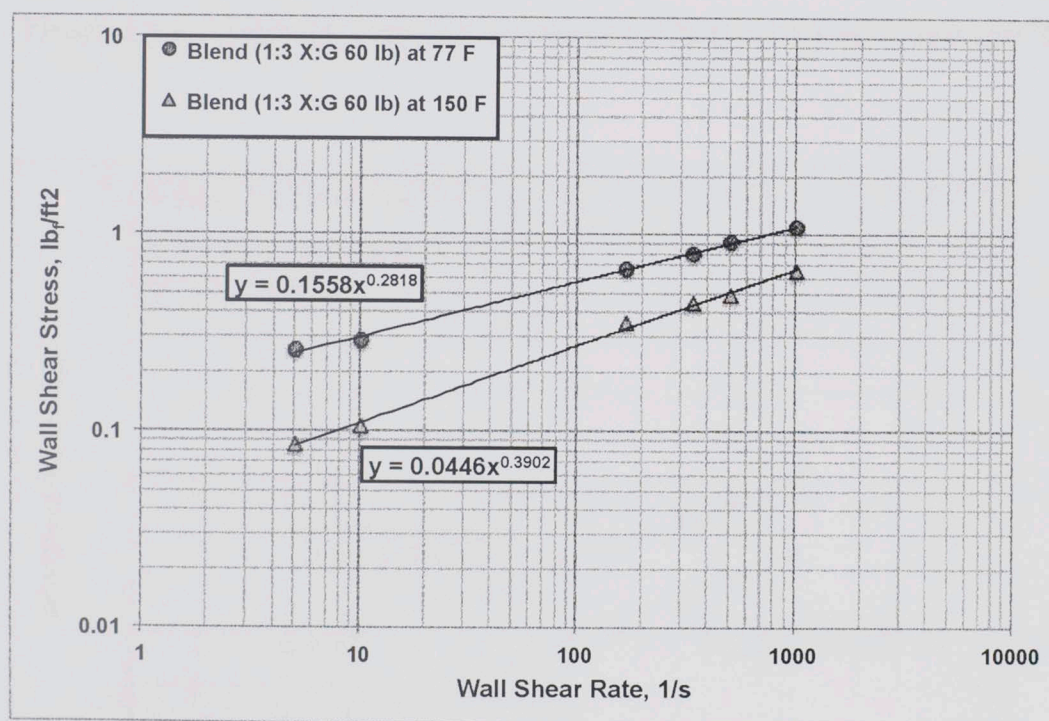
Figure 5.21: Rheograms of Blend (1:3 X:G 60 lb) at 77 and 150 °F
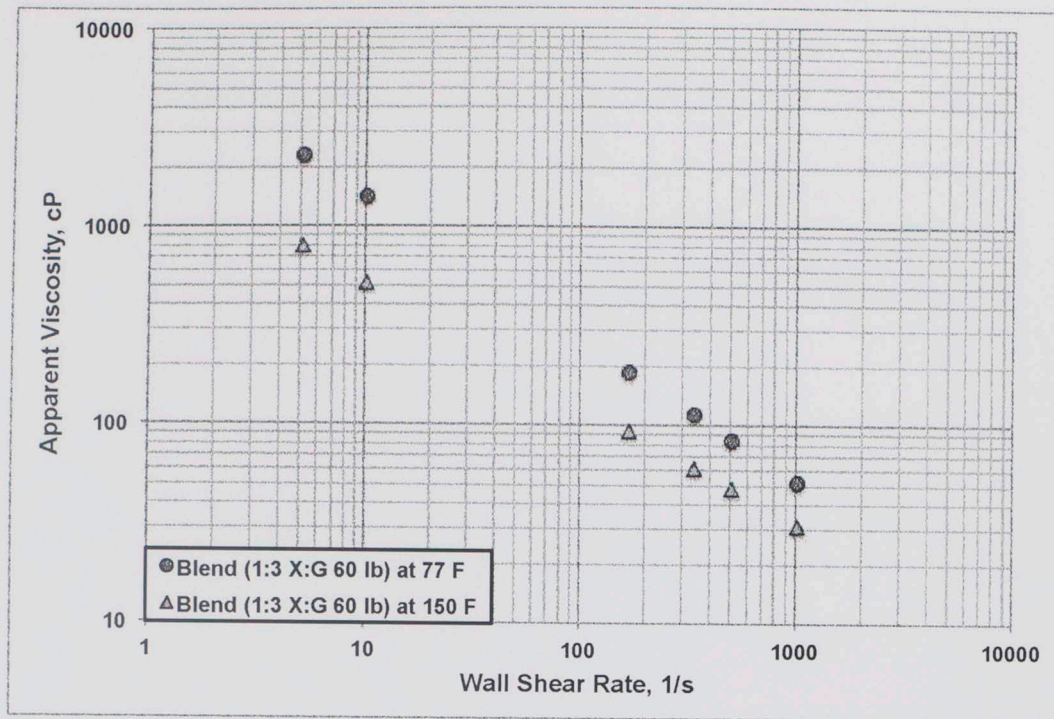
Figure 5.22: Apparent Viscosity of Blend (1:3 X:G 60 lb) at 77 and 150 ^{o}F
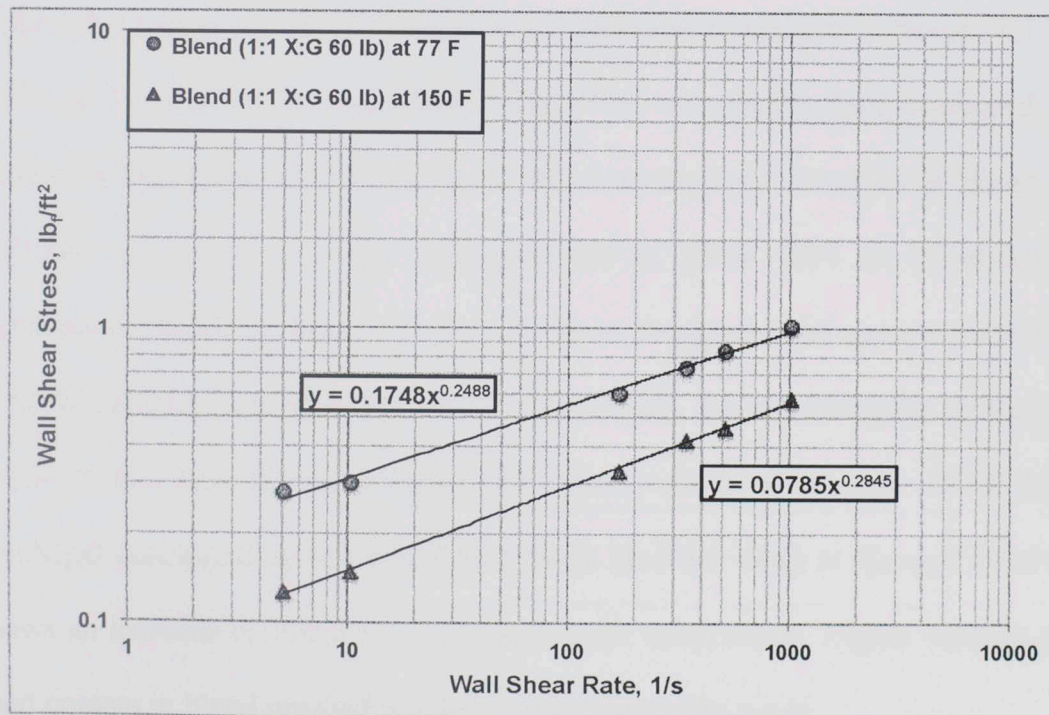
Figure 5.23: Rheograms of Blend (1:1 X:G 60 lb) at 77 and 150 ^{o}F
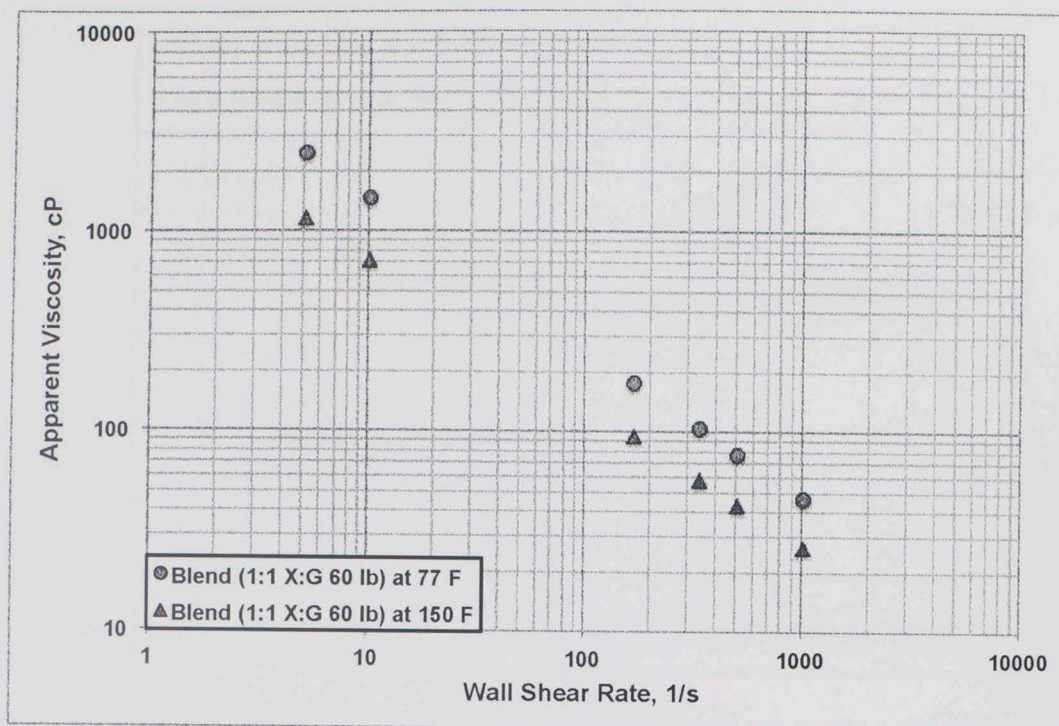
Figure 5.24: Apparent Viscosity of Blend (1:1 X:G 60 lb) at 77 and 150 °F

Figures 5.22 and 5.24 show rheograms and apparent viscosities of Blend (1:1 X:G 60 lb) at 77 and 150 °F, respectively. Viscosities of complex fluid decreased with increasing temperature at all six shear rates investigated. Viscosity of Blend (1:1 X:G 60 lb) at 5.11 s^{-1} shear rate decreased by about 50% on increasing the temperature. Similarly, Figs. 5.25 and 5.26 show rheograms and apparent viscosities of 60 lb Xanthan Gum at 77 and 150 °F, respectively. On increasing the temperature to 150 °F this fluid displayed higher viscosities at all six shear rates. Of all the 60 lbm/Mgal concentration polymer fluids, 60 lb Xanthan Gum is the only fluid that shows an increase in viscosity on increasing the temperature. Higher xanthan gum fluid content in blend resulted in it being more thermally stable.
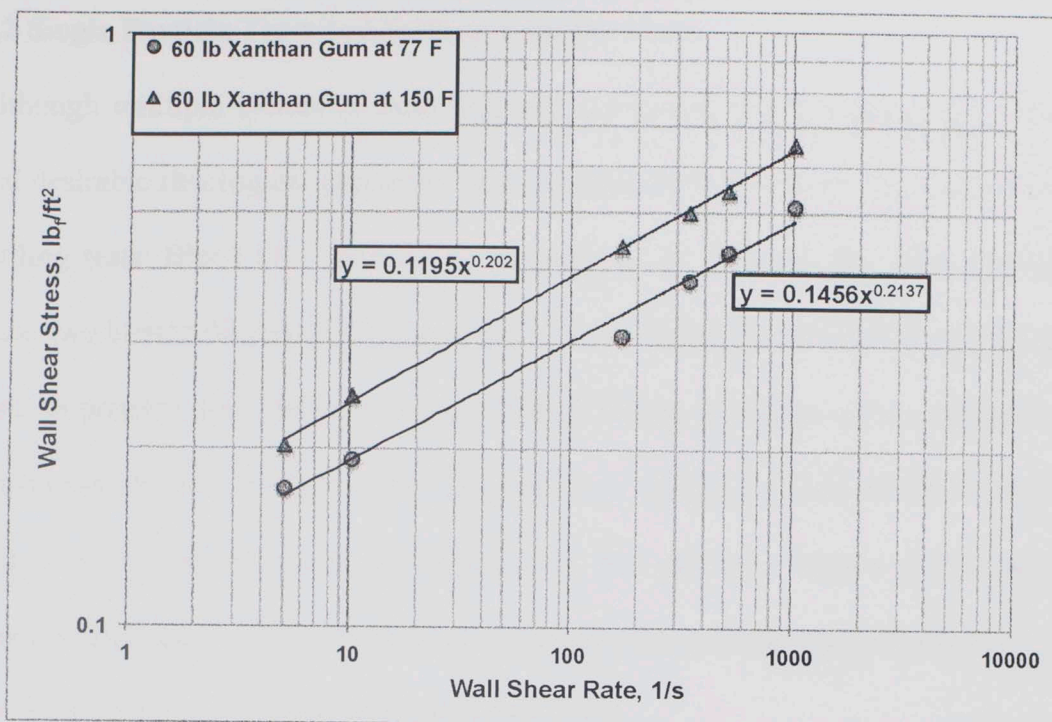
Figure 5.25: Rheograms of 60 lb Xanthan Gum at 77 and 150 °F
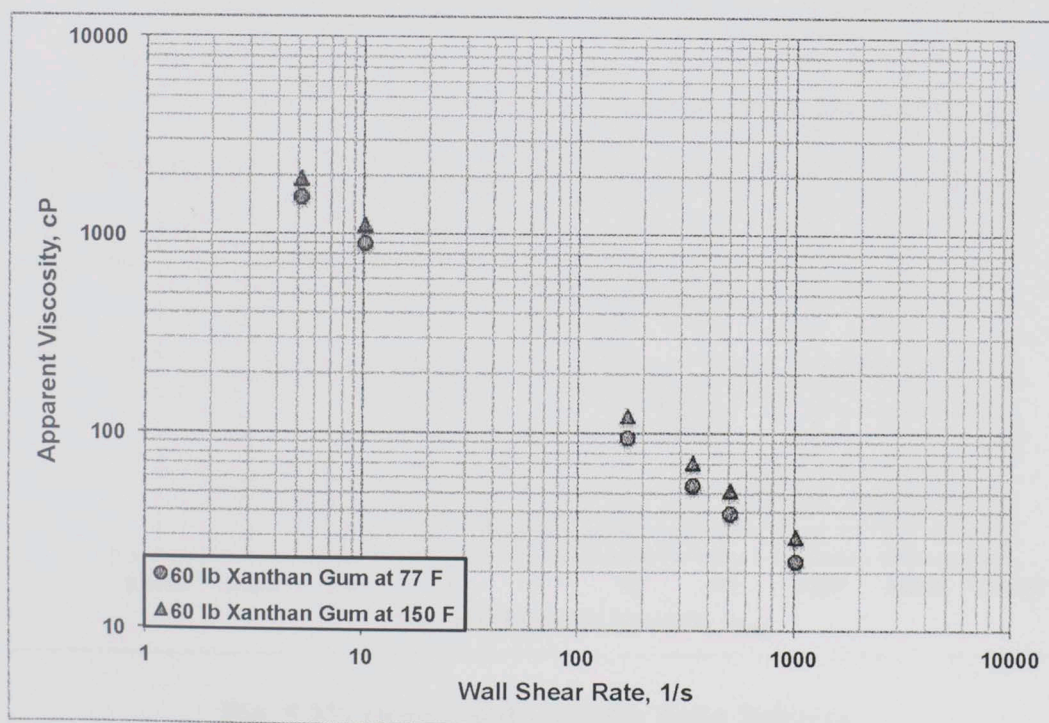
Figure 5.26: Apparent Viscosity of 60 lb Xanthan Gum at 77 and 150 °F

5.2 Single Particle Terminal Settling Velocity Tests

Although multiple blends of both polymer concentrations showed strong synergy and desirable rheological properties only two blends were chosen for single particle settling tests: Blend (1:3 X:G 40 lb) and Blend (1:3 X:G 60 lb). This is because these two blends displayed strong synergy and required less amount of xanthan gum fluid to prepare. Including the parent polymer fluids, six fluids were considered for these tests: 40 lb Guar Gum, 40 lb Xanthan Gum, Blend (1:3 X:G 40 lb), 60 lb Guar Gum, 60 lb Xanthan Gum and Blend (1:3 X:G 60 lb). Figure 5.27 compares experimental drag coefficient data with standard Newtonian drag coefficient curve for solid spheres by Lapple and Shepherd (1940).
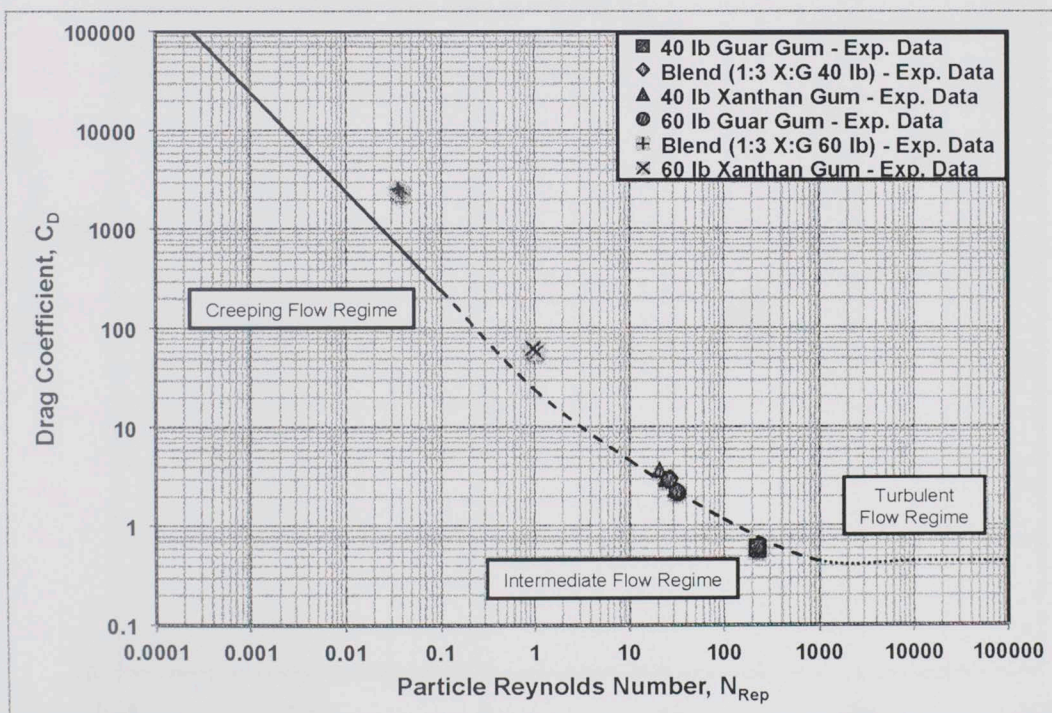
Fig. 5.27: Drag Coefficient for Solid Spheres

Experimental data are not in agreement with theoretical curve as the fluids investigated are non-Newtonian. Drag coefficient cannot be computed as a function of particle Reynolds number by simply replacing viscosity with apparent viscosity. Effect of non-Newtonian parameter, n, has to be taken into account. Figure 5.28 shows a logarithmic plot of $\sqrt{C_D^{2-n} N_{Repg}^2}$ and generalized particle Reynolds number. Figure 5.29 shows a logarithmic plot of C_D^{2-n} and generalized particle Reynolds number.
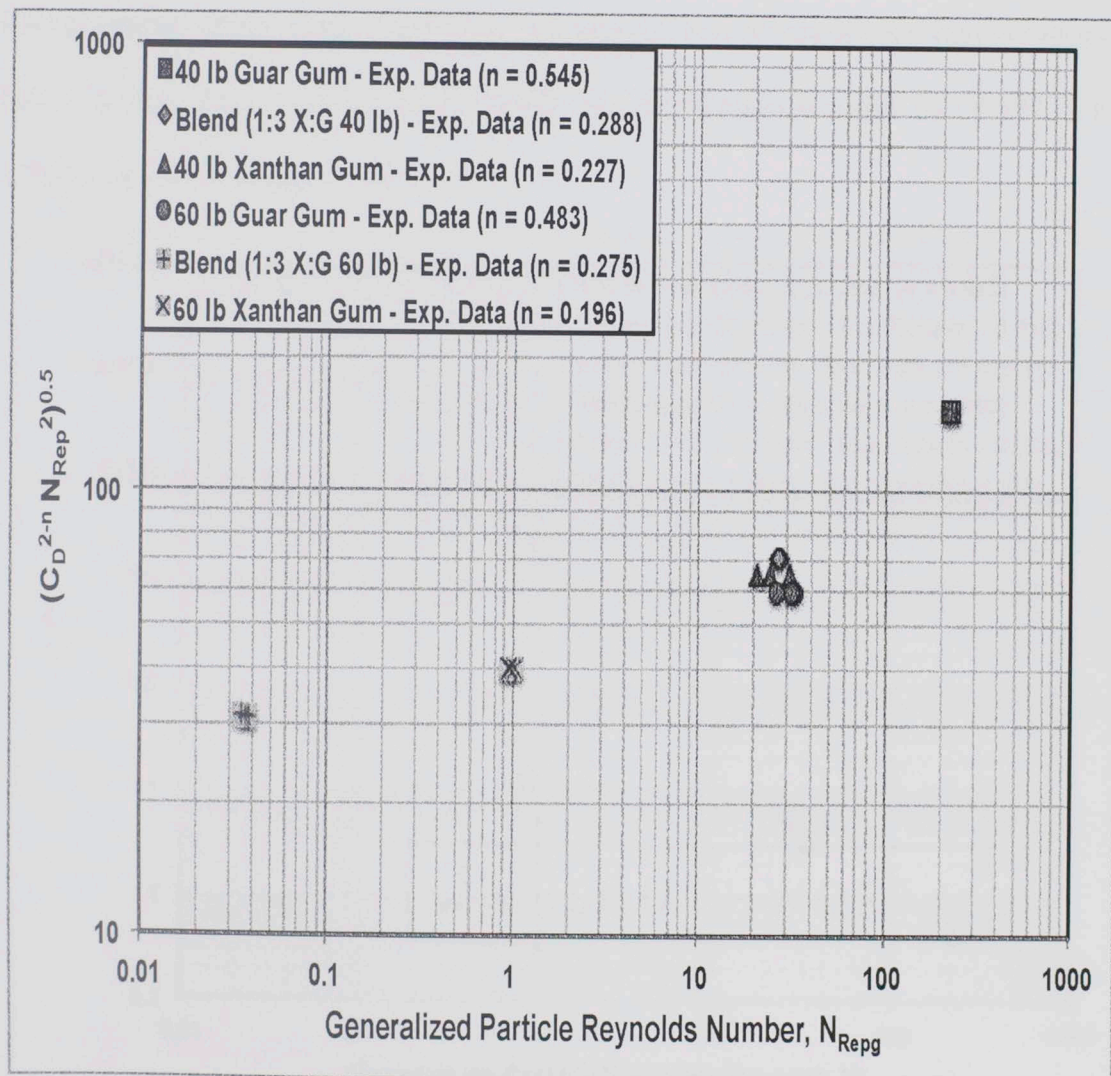
Fig. 5.28: Effect of non-Newtonian parameter n on $\sqrt{C_D^{2-n}N_{Repg}^2}$

Effect of flow behavior index, n, on drag coefficient can be seen in both Fig. 5.28 and 5.29. For each value of 'n', a family of curves can be generated in these figures. Theoretically, effect of 'n' on drag coefficient diminishes with increasing particle Reynolds number and when flow turns turbulent ($N_{Repg} > 500$) drag coefficient is independent of n. Not enough experimental data is shown in these figures to see this transition. However, it can be seen that for the same generalized particle Reynolds number, values of both $\sqrt{C_D^{2-n} N_{Repg}^2}$ and C_D^{2-n} decrease with increasing value of n. Using similar plots, drag coefficient correlation that accounts for non-Newtonian behavior was developed by Shah (1982). His correlation is valid for: $0.281 < n < 1.000$ and $0.01 < N_{Repg} < 500$.
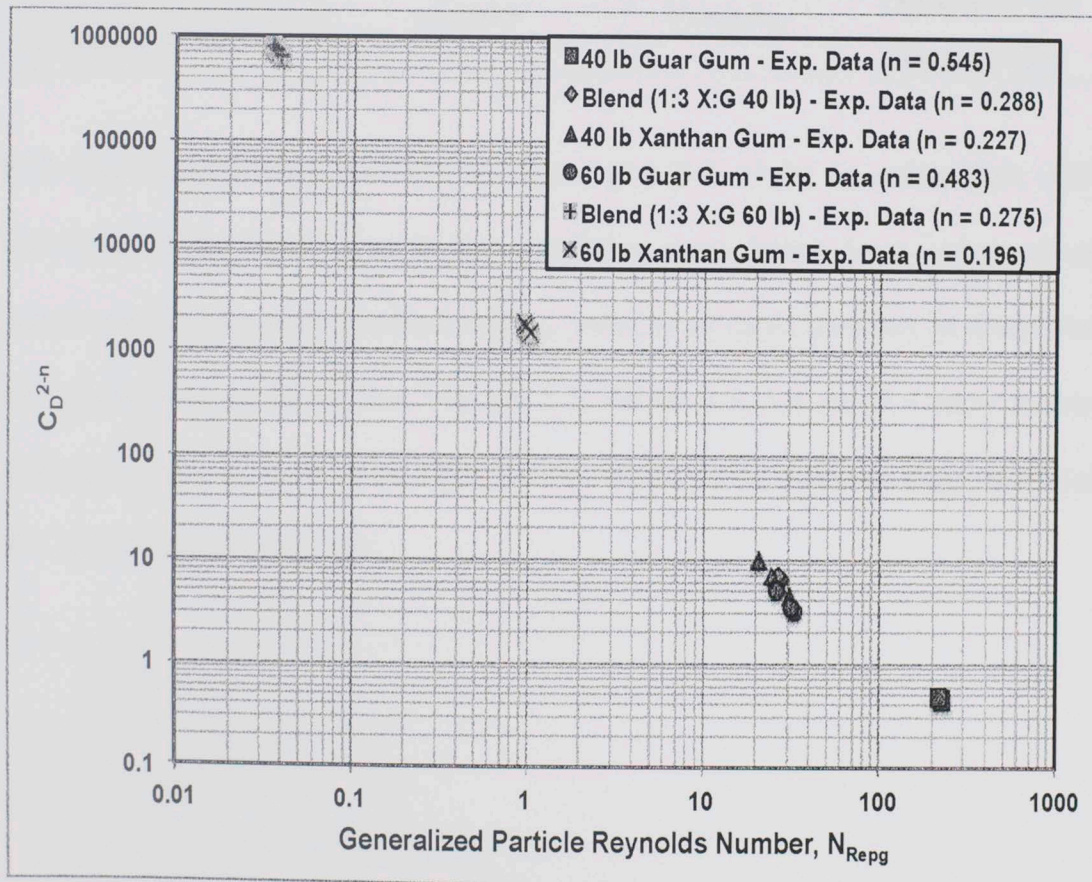
Fig. 5.29: Effect of non-Newtonian parameter n on C_D^{2-n}

Since the experiments were carried out in a cylindrical column, the fluid cannot be considered infinite and terminal-settling velocity data obtained was corrected for wall effects. Table 5.3 lists correction factor, flow regime and empirical correlation used to account for wall effects on particle settling in these fluids.

Table 5.3: Correction factor used to account for wall effects

Fluid	Correction Factor	Flow Regime	Empirical Correlation
40 lb Guar Gum	0.8989		
40 lb Xanthan Gum	0.8542	Intermediate	De Felice (1996)
Blend (1:3 X:G 40	0.8523		
60 lb Guar Gum	0.8581		
60 lb Xanthan Gum	0.6874	Creeping	Haberman and Sayre (1958)
Blend (1:3 X:G 60			

40 lb Guar Gum, 60 lb Guar Gum and Blend (1:3 X:G 40 lb) lie within Shah (1982) correlation limits. Predictions of this correlation have, hence, been compared with experimentally observed terminal settling velocity of three particles in these fluids and can be seen in Tables 5.4, 5.6 and 5.7. Tables 5.5, 5.8 and 5.9 show terminal settling velocity of particle in 40 lb Xanthan Gum, 60 lb Xanthan Gum and Blend (1:3 X:G 60 lb), respectively.

Table 5.4: Terminal Settling Velocity of Particle in 40 lb Guar Gum

Particle	Terminal Settling Velocity, ft/s	
	Experimental	Predicted
1	2.274	2.239
2	2.299	2.244
3	2.227	2.248

Table 5.5: Terminal Settling Velocity of Particle in 40 lb Xanthan Gum

Particle	Terminal Settling Velocity, ft/s
1	1.341
2	1.175
3	1.071

Table 5.6: Terminal Settling Velocity of Particle in Blend (1:3 X:G 40 lb)

Particle	Terminal Settling Velocity, ft/s	
	Experimental	Predicted
1	0.981	0.957
2	1.006	0.959
3	0.988	0.962

Table 5.7: Terminal Settling Velocity of Particle in 60 lb Guar Gum

Particle	Terminal Settling Velocity, ft/s	
	Experimental	Predicted
1	1.190	1.086
2	1.156	1.088
3	1.023	1.090

Table 5.8: Terminal Settling Velocity of Particle in 60 lb Xanthan Gum

Particle	Terminal Settling Velocity, ft/s
1	0.052
2	0.051
3	0.050

Table 5.9: Terminal Settling Velocity of Particle in Blend (1:3 X:G 60 lb)

Particle	Terminal Settling Velocity, ft/s
1	0.322
2	0.335
3	0.319
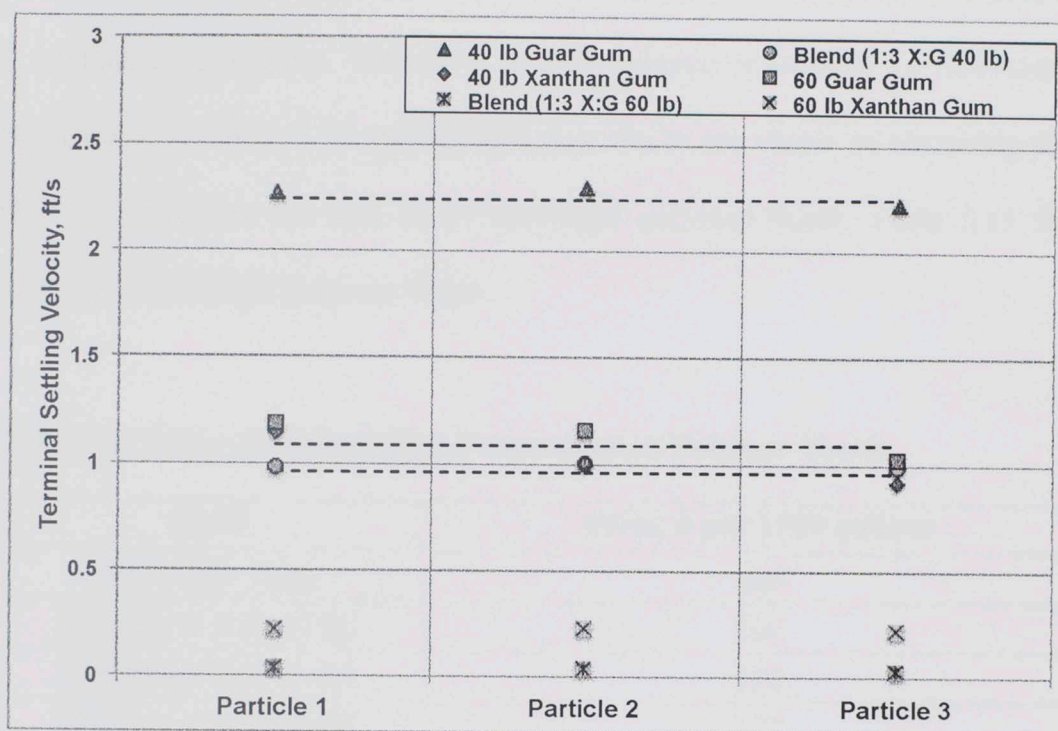
Fig. 5.30 Terminal Settling Velocity of Particle in Polymers and Blends

The average terminal settling velocities of particle in four polymer fluids and two blends are shown in Fig. 5.30. The least velocity was observed with Blend (1:3 X:G 60 lb) and the highest was displayed by 40 lb Guar Gum. Particle settling velocity in Blend (1:3 X:G 40 lb) were close to that of 40 lb Xanthan Gum and lower than 60 lb Guar Gum. Lower single particle terminal settling velocity in a fluid indicates that the fluid would display high viscosity at low shear rate. From this figure it can be,

therefore, inferred that at low shear rates, Blend (1:3 X:G 40 lb) has higher viscosity than 60 lb Guar Gum and comparable viscosity to 40 lb Xanthan Gum.

5.3 Cost Analysis

As stated earlier, price is an important driving factor when selecting a suitable fluid for hydraulic operations. Therefore, a cost analysis is integral to this study to investigate if the blends of xanthan and guar fluids are viable as fracturing fluids. Table 5.10 presents the cost of 40 lbm/Mgal polymer fluids. Table 5.11 shows prices of 60 lbm/Mgal polymer fluids.

Table 5.10: Price of 40 lbm/Mgal Concentration Polymer Fluids

Fluid	Price, $ per 1000 gallons
40 lb Guar Gum	160
Blend (1:4 X:G 40 lb)	200
Blend (1:3 X:G 40 lb)	210
Blend (1:2 X:G 40 lb)	227
Blend (2:3 X:G 40 lb)	240
Blend (1:1 X:G 40 lb)	260
Blend (3:2 X:G 40 lb)	280
Blend (3:1 X:G 40 lb)	310
Blend (4:1 X:G 40 lb)	320
40 lb Xanthan Gum	360

Table 5.11: Price of 60 lbm/Mgal Concentration Polymer Fluids

Fluid	Price, $ per 1000 gallons
60 lb Guar Gum	240
Blend (1:4 X:G 60 lb)	300
Blend (1:3 X:G 60 lb)	315
Blend (1:2 X:G 60 lb)	340
Blend (2:3 X:G 60 lb)	360
Blend (1:1 X:G 60 lb)	390
Blend (3:2 X:G 60 lb)	420
Blend (3:1 X:G 60 lb)	465
Blend (4:1 X:G 60 lb)	480
60 lb Xanthan Gum	540

The cost of one pound of xanthan gum was considered as the cost of FLO-VIS® by MI SWACO and it is $9. The cost of one pound of guar gum was taken from RockWater Energy Solutions as $4. However, it is important to note that the price of guar gum is extremely volatile. India produces 80% of the world's supply of guar gum. Normally, 60% of its exports go to the oil industry and 40% to the global food industry, according to *The Wall Street Journal (WSJ)* newspaper. In May 2012, the export price of a metric ton (MT) of guar gum was $27,000, according to *WSJ*, and it plunged to $7,000/MT in December 2012.

5.4 Discussion

Mixtures of xanthan and guar gum polymer fluids indeed show synergy. The strength of this synergy is dependent upon polymer concentration, polymer ratio, and temperature. Increasing the polymer concentration from 40 to 60 lbm/Mgal,

increased the strength of synergistic interactions of xanthan and guar gum polymer fluids.

On blending these polymer fluids in different ratios, the rheology of resultant fluid was greatly affected. Blend (1:3 X:G 40 lb) and Blend (3:1 X:G 40 lb) showed strong synergy between parent polymers among the 40 lbm/Mgal concentration polymer fluids, taking into account the amount of xanthan polymer added. Although, all blends of 60 lbm/Mgal concentration polymer fluids displayed higher viscosities than 60 lb Guar Gum and 60 lb Xanthan Gum at low shear rates, taking into account the xanthan content Blend (1:3 X:G 60 lb) and Blend (1:1 X:G 60 lb) displayed strong synergy. On increasing the temperature from 77 to 150 °F, the rheology of all polymer fluids was adversely affected except for 60 lb Xanthan Gum, which showed an increase in viscosities at various shear rates. The blends with the highest xanthan content showed the least deviation in viscosity at elevated temperature.

Figure 5.31 compares the apparent viscosities of 40 lb Guar Gum, 60 lb Guar Gum and Blend (1:3 X:G 40 lb) at 77 °F. Blend (1:3 X:G 40 lb) shows about 420% increase in viscosity over 40 lb Guar Gum and 70% increase in viscosity as compared to 60 lb Guar Gum at 5.11 s^{-1} shear rate. At 1021.8 s^{-1} shear rate, the viscosity of Blend (1:3 X:G 40 lb) is 50% lower than 60 lb Guar Gum, indicating higher degree of desirable shear thinning ability of the blend.
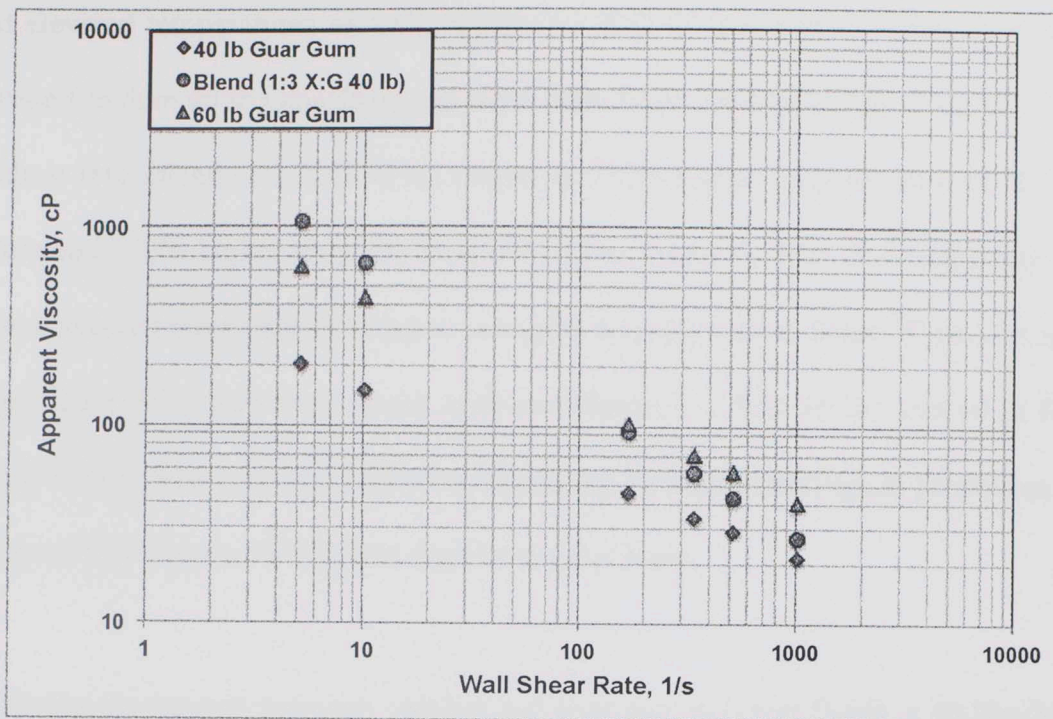
Figure 5.31: Apparent Viscosity of 40 lb Guar Gum, Blend (1:3 X:G 40 lb) and

60 lb Guar Gum at 77 °F
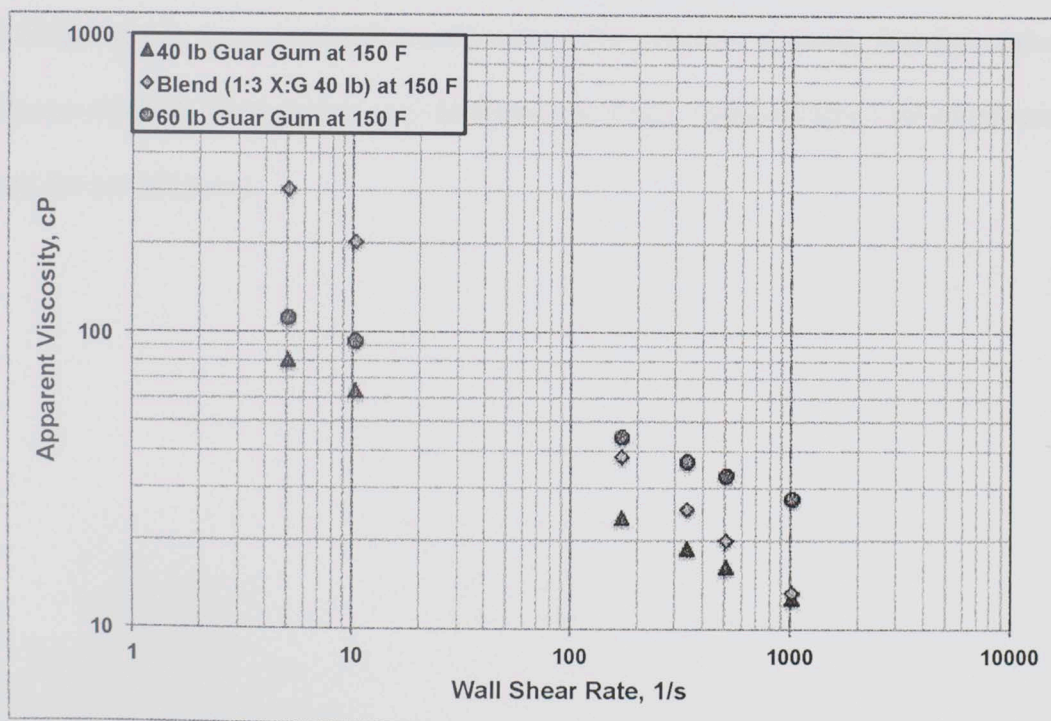
Figure 5.32: Apparent Viscosity of 40 lb Guar Gum, Blend (1:3 X:G 40 lb) and

60 lb Guar Gum at 150 °F

At elevated temperatures as well, Blend (1:3 X:G 40 lb) showed better rheological properties than 40 lb Guar Gum and 60 lb Guar Gum, as seen in Fig. 5.32. At 5.11 s^{-1} shear rate, Blend (1:3 X:G 40 lb) displayed 270% higher viscosity than 40 lb Guar Gum and 170% higher viscosity than 60 lb Guar Gum. At 1021.8 s^{-1} shear rate, this blend showed more than 50% lower viscosity than 60 lb Guar Gum. There was not a significant difference in viscosity between Blend (1:3 X:G 40 lb) and 40 lb Guar Gum at this shear rate. In addition to displaying desirable rheological properties, the price of this blend is 13% lower than 60 lb Guar Gum.

Utilizing the synergy between xanthan and guar gum polymer fluids, a 40 lbm/Mgal concentration polymer blend has been formulated that displays better rheological properties than 60 lb Guar Gum. Making use of Blend (1:3 X:G 40 lb) instead of 60 lbm/Mgal linear guar gum gel, would reduce the polymer content, thereby, reducing polymer residue, show better and desirable rheology, reduce costs, and eliminate the need for crosslinkers.

CHAPTER 6

CONCLUSIONS AND RECOMMENDATIONS

6.1 Conclusions

1. This study constitutes the first step towards utilizing the synergy of xanthan gum and guar gum polymer solutions in the oil and gas industry. Rheology studies were underatken to determine the effect of polymer concentration, polymer ratio and temperature on this synergy.

2. The polymer concentrations investigated were 40 and 60 lbm/Mgal. Eight blends were prepared for each concentration in the xanthan to guar gum fluid ratio of: 1:4, 1:3, 1:2, 2:3, 1:1, 3:2, 3:1, and 4:1. Rheology measurements were made at two temperatures: 77 and 150 °F.

3. The strength of synergistic intercations between these polymer fluids increased with increasing the polymer content from 40 to 60 lbm/Mgal. Blend (3:1 X:G 40 lb) was the only fluid among 40 lbm/Mgal concentration polymer fluids that showed higher viscosity than 40 lb Xanthan Gum at low shear rates. All eight 60 lbm/Mgal concentration polymer blends displayed higher viscosities than 60 lb Guar Gum and 60 lb Xanthan Gum at low shear rates.

4. Apparent viscositites of polymers fluids and blends, except for 60 lb Xanthan Gum, were adversely affected by increase in temperature from 77 to 150 °F. 60 lb Xanthan Gum fluids showed an increase in apparent viscosities on increasing the temperature. Blends with low xanthan gum fluid content displayed the most deviation in apparent viscosities at elevated temperature.

95

5. Based on amount of xanthan gum fluid added, Blend (1:3 X:G 40 lb) and Blend (3:1 X:G 40 lb) showed strong synergy among 40 lbm/Mgal concentration polymer fluids while for 60 lbm/Mgal concentration polymer fluids it was Blend (1:3 X:G 60 lb) and Blend (1:1 X:G 60 lb).

6. Static, single particle settling tests in 40 lb Guar Gum, 40 lb Xanthan Gum, Blend (1:3 X:G 40 lb), 60 lb Guar Gum, 60 lb Xanthan Gum and Blend (1:3 X:G 60 lb) were conducted. Motion of particle in Blend (1:3 X:G 60 lb) was in creeping flow regime. Experimental terminal settling velocity data of particle in 40 lb Guar Gum, 60 lb Guar Gum and Blend (1:3 X:G 40 lb) were in good agreement with predictions of Shah (1982) correlation. Terminal settling velocity of particle in Blend (1:3 X:G 60 lb) was the least while that in 40 lb Guar Gum was the highest. Velocity of particle in Blend (1:3 X:G 40 lb) was comparable to that in 40 lb Xanthan Gum and lower than in 60 lb Guar Gum. This indicates that at low shear rates, Blend (1:3 X:G 40 lb) has higher viscosity than 60 lb Guar Gum.

7. Based on rheology study, static single particle settling tests, and cost analysis, Blend (1:3 X:G 40 lb) was selected as a suitable replacement for guar based polymer fluids. It showed 420% increase in viscosity over 40 lb Guar Gum and 70% increase as compared to 60 lb Guar Gum at 5.11 s^{-1} shear rate. At 1021.8 s^{-1} shear rate, it showed 50% lower viscosity than 60 lb Guar Gum, indicating better shear thinning ability. At elevated temperature of 150 °F, the blend displayed 270% higher viscosity than 40 lb Guar Gum and 170% higher viscosity than 60 lb Guar Gum at 5.11 s^{-1} shear rate. It displayed about 50%

lower viscosity than 60 lb Guar Gum at 1021.8 s^{-1} shear rate, at this temperature. In addition this blend is approximately 13% cheaper than 60 lb Guar Gum.

8. On replacing 25% of 40 lb Guar Gum with 40 lb Xanthan Gum, a blend has been formulated that is less expensive, has better shear thinning property and higher viscosities at low shear rates than 60 lb Guar gum fluid at both ambient and elevated temperature. This synergy between these polymers can be used to increase the viscosity of low polymer concentration guar gum fluids and, thereby, help in reducing polymer residue in fractures without adding chemicals or crosslinkers.

6.2 Recommendations

Recommendations for future work or research are outlined below:

1. A study should be undertaken to investigate if conventional breakers used in fracturing operations to break guar gum fluids are applicable to synergistic blends of xanthan and guar polymer fluids.

2. It would be interesting to check if the polymer residue left behind by xanthan/guar gum fluid blends is dependent upon residue of component guar gum and xanthan gum fluids.

3. It is stated in the literature that for strong synergy, the ideal dissolution temperature for xanthan fluids is < 40 °C and guar fluids is > 80 °C. This relates to the conformation of xanthan and galactose to mannose ratio of guar. The rheology of 40 lb Xanthan Gum and 40 lb Guar Gum blends, when mixed at the

ideal dissolution temperature, should be investigated to determine its effect on synergy.

4. In this study it was found that strength of synergy decreases with decreasing polymer concentration. Synergy of xanthan and guar gum fluids at low polymer concentrations such as 25 or 30 lbm/Mgal needs to be investigated to check if suitable viscosities can be achieved without crosslinking. Reducing the polymer content further would aid in controlling polymer residue problems.

5. Salinity affects the synergy of xanthan and guar gum fluids adversely. A study can be undertaken to see how the rheology of these blends changes with increasing Na^+, K^+ or Ca^{2+} ions.

6. This study focuses on taking advantage of the synergy between xanthan and guar gum fluids to formulate less expensive fracturing fluids. This technology can be extended to any oilfield operations that utilize viscosifiers. For instance, gel strength of these polymer blends can be investigated to check if they display the low-flat gel strength profile desired in drilling fluid applications.

NOMENCLATURE

C_D	Coefficeint of Drag, dimensionless
D_b	Diameter of bob, mm
D_c	Diameter of cup, mm
D_p	Diameter of particle, in.
F_b	Buoyancy force, N
F_g	Gravity force, N
F_v	Viscous drag force, N
K_v	Viscometer consistency index, $lb_f\text{-}s^n/ft^2$
x	Displacement of a particle in a fluid, ft
n	Flow behavior index, dimensionless
t	Time, s
v_t	Terminal-settling velocity, ft/s

GREEK SYMBOLS

β	Ratio of diameter of bob to diameter of cup, dimensionless
ϕ	Void fraction of solids, dimensionless
γ_w	Wall shear rate, s^{-1}
λ	Ratio of diameter of particle to diameter of cylinder, dimensionless
μ_a	Apparent viscosity, cP
θ_i	Dial reading of model 35 Fann viscometer at i^{th} rpm, dimensionless
τ_w	Wall shear stress, lb_f/ft^2

SUBSCRIPTS

a   Apparent

b   Bob

c   Cup

i i^{th}

p   particle

REFERENCES

Fischer, C.C, Navarrete, R.C., Constien, V.G., Coffey, M.D., Asadi, M. 2001. Novel Application of Synergistic Guar/Non-Acetylated Xanthan Gum Mixtures in Hydraulic Fracturing. Presented at the SPE International Symposium on Oilfield Chemistry, Houston, Texas, 13-16 February. SPE 65037.

Higiro, J., Herald, T.J, Alavi, S., Bean, S. 2006. Rheological study of xanthan and locust bean gum interaction in dilute solution: Effect of salt. Food Research International 40 (2007) 435-447, 5 February.

Zhang L.M., Zhou, J.F. 2006. Synergistic viscosity characteristics of aqueous mixed solutions of hydroxypropyl- and carboxymethyl hydroxypropyl-substituted guar gums. Colloids and Surfaces A: Physiochem. Eng. Aspects 279 (2006) 34-39, 19 December.

Tako, M., Nakamura, S. 1984. Synergistic Interaction Between Xanthan and Guar Gum. Carbohydrate Research 138 (1985) 207–213, 10 October.

Copetti, G., Grassi, M., Lapasin, R., Pricl, S. 1997. Synergistic gelation of xanthan gum with locust bean gum: a rheological investigation. Glycoconjugate Journal (1997) 14: 951-961.

Tako, M. 1991. Synergistic Interaction Between Xanthan and Tara-Bean Gum. Carbohydrate Polymers 16 (1991) 239–252, 17 July.

Khouryieh, H.A., Herald, T.J., Aramouni, F., Alavi, S. 2006. Influence of mixing temperature on xanthan conformation and interaction of xanthan-guar gum in dilute aqueous solutions. Food Research International 39 (2006) 964-973.

Casas, J.A., Mohedano, A.F., García-Ochoa, F. 2000. Viscosity of guar gum and xanthan/guar gum mixture solutions. J Sci Food Agric 80:1722-1727.

Morris, E.R., Foster, T.J. 1994. Role of conformation in synergistic interactions of xanthan. Carbohydrate Polymers 23 (1994) 133–135. 3 September.

Zigrye, J.L., Osborne, M.W., Westbrook, G.H. 1986. Delayed Action Crosslinked Fracturing Fluid Systems. Presented at the Annual Technical Conference and Exhibition of the Society of Petroleum Engineers held in New Orleans, Louisianna, 5-8 October. SPE 15633.

Reddy, B.R., Eoff, L., Dalrymple, E.D., Black, K., Brown, D., Rietjens, M. 2002. A Natural Polymer-Based Crosslinker System for Conformance Gel Systems. Presented at the SPE/DOE Improved Oil Recovery Symposium held in Tulsa, Oklahoma, 13-17 April. SPE 75163.

Sun, H., Qu, Q. 2011. High-Efficiency Boron Crosslinkers for Low-Polymer Fracturing Fluids. Presented at the SPE International Symposium on Oilfield Chemistry held in The Woodlands, Texas, 11-13 April. SPE 140817.

Schultheiss, N., Fontenelle, L., Welton, T. 2013. Residue-Free Fracturing Fluid Provides Superior Cleanup and Exceptional Proppant Transport. Presented at the SPE European Formation Damage Conference and Exhibition held in Noordwijk, The Netherlands, 5-7 June. SPE 165128.

Harrington, L.J., Hannah, R.R., Williams, D. 1979. Dynamic Experiments On Proppant Settling in Crosslinked Fracturing Fluids. Presented at the Annual Technical Conference and Exhibition of the Society of Petroleum Engineers of AIME held in Las Vegas, Nevada, 23-26 September. SPE 8342.

Clark, P.E., Quadir, J.A. 1981. Prop Transport in Vertical Fractures. Presented at the Annual Fall Technical Conference and Exhibition of the Society of Petroleum Engineers of AIME held in San Antonio, Texas, 5-7 October. SPE 10261.

Novotny E.J. 1977. Proppant Transport. Presneted at the Annual Fall Technical Conference and Exhibition of the Society of Petroleum Engineers of AIME held in Denver, Colorado, 9-12 October. SPE 6813.

Hannah, R.R., Harrington, L.J. 1981. Measurement of Dynamic Proppant Fall Rates in Fracturing Gels Using a Concentric Cylinder Tester. SPE 7571-PA.

Savins, J.G. 1981. Discussion of Measurement of Dynamic Proppant Fall Rates in Fracturing Gels Using a Concentric Cylinder Tester. 20 May. SPE 9970.

Saha, G., Purohit, N.K., Mitra, A.K. 1992. Spherical particle terminal settling velocity and drag in Bingham liquids. International Journal of Mineral Processing 36 (1992) 273-281. 22 April.

Briscoe, B.J., Luckham, P.F., Ren, S.R. 1993. The settling of spheres in clay suspensions. Powder Technology 76 (1993) 165-174. 25 January.

Dunand, A., Soucemarianadin, A. 1985. Concentration Effects on the Settling Velocities. Presented at the Annual Technical Conference and Exhibition of the Society of Petroleum Engineers held in Las Vegas, Nevada, 22-25 September. SPE 14259.

Roodhart, L.P. 1985. Proppant Settling in Non-Newtonian Fracturing Fluids. Presented at the SPE/DOE Low Permeability Gas Reservoirs held in Denver, Colorado, 19-22 May. SPE/DOE 13905.

Barree, R.D., Conway, M.W. 1994. Experimental and Numerical Modeling of Convective. Presented at the SPE Annual Technical Conference and Exhibition held in New Orleans, Louisiana, 25-28 September. SPE 28564.

Al-quraishi, A.A., Christiansen, R.L. 1999. Dimensionless Groups for Interpreting Proppant Transport in Hydraulic Fractures. Presneted at the Middle East Oil Show held in Bahrain, 20-23 February. SPE 53262.

Shokir, E.M.E., Al-Quraishi, A.A. 2007. Experimental and Numerical Investigation of Proppant Placememnt in Hydraulic Fractures. Presented at SPE Latin American and Carribean Petroleum Engineering Conference held in Buenos Aires, Argentina, 15-18 April. SPE 107927.

Shah, S.N., Fadili, Y.E., Chhabra, R.P. 2006. New model for single spherical particle settling velocity in power law (visco-inelastic) fluids. International Journal of Multiphase Flow 33 (2007) 51-66.

Shah, S.N. 1982. Proppant Settling Correlations for Non-Newtonian Fluids Under Static and Dynamic Conditions. Trans Aime, 273 Part 2, 1982, p. 164-170, also in SPE PE, November 1986, 446-448.

McMehan, D.E., Shah, S.N. 1991. Static Proppant-Settling Characteristics of Non-Newtonian Fracturing Fluids in a Large Scale Test Model. SPE Production Engineering, August.

Shah, S.N. 1985. Proppant-Settling Correlations for Non-Newtonian Fluids. SPE Production Engineering, November. SPE 13835.

Madhav, G.V., Chhabra, R.P. 1995. Drag on non-spherical particles in viscous fluids. Int. J. Miner. Process. 43 (1995) 15-29.

Chhabra, R.P. 1996. Wall effects on terminal settling velocity of non-spherical particles in non-Newtonian polymer solutions. Powder Technoogy 88 (1996) 39-44.

Chhabra, R.P. 1995. Wall effects on free-settling velocity of non-spherical particles in viscosu media in cylinderical tubes. Powder Technology 85 (1995) 83-90.

Arsenijević, Z.L., Grbavčić, Z.B., Garić-Grulović, R.V., Bošković-Vragolović, N.M. 2010. Wall effects on the velocities of a single sphere settling in a stagnant and counter-current fluid and rising in a co-current fluid. Powder Technology 203 (2010) 237-242.

Felice R.D. 1996. A Relationship For The Wall Effect On The Settling Velocity Of A Sphere At Any Flow Regime. Int. J. Multiphase Flow Vol. 22, No. 3, pp. 527-533.

Chhabra, R.P., Agarwal, S., Chaudhary, K. 2002. A note on wall effect on the terminal falling velocity of a sphere in quiescent Newtonian media in cylinderical tubes. Powder Technology 129 (2003) 53-58.

Montgomery, C. 2013. Fracturing Fluids. Intech, http://dx.doi.org/10.5772/56192.

Cunha, P.L.R., Castro, R.R., Rocha, F.A.C., Paula, R.C.M., Judith, P.A.F. 2005. Low viscosity hydrogel of guar gum: Preparation and physiochemical characterization. International Journal of Biological Macromolecules 37 (2005) 99-104.

Bradley, T.D., Ball, A., Harding, S.E., Mitchell, J.R. 1988. Thermal Degradation of Guar Gum. Carbohydrate Polymers 10 (1989) 205-214.

García-Ochoa, F., Santos, V.E., Casas, J.A., Gómez, E. 2000. Xanthan gum: production, recovery, and properties. Biotechnolgy Advances 18 (2000) 549-579.

Cheng, N.S. 2009. Comparison of formulas for drag coefficient and settling velocity of spherical particles. Powder Technology 189 (2009) 395-398.

Chhabra, R.P. 1990. Motion of Spheres in Power Law (Viscoinelastic) Fluids at Intermediate Reynolds Numbers: A Unified Approach. Chemical Engineering and Processing: Process Intensification, Volume 28, Issue 2, October 1990, p. 89-94. Doi:10.1016/0255-2701(90)80004-O.

Elgaddafi, R., Ahmed, R., George, M., Growcock, F. 2012. Settling behavior of spherical particles in fibre-containing drilling fluids. Journal of Petroleum Science and Engineering 84-85 (2012) 20-28. 29 January.

Junin, R., Meng, K.W. 2008. Slurry Transport And Particle Settling In Annulus In Cuttings Reinjection Process. Jurnal Teknologi 49(F) Dis. 2008: 281-295.

Clark, P.E. 2008. Sluury Transport in Hydraulic Fractures: Part II Transport in Settling Slurries and Treatment Design Considerations. Preprint submitted to SPE. 29 January.

Clift, R. 1978. *Bubbles, Drops, and Particles*, second edition. New york: Academic Press.

Brown, G.G. 1950. *Unit Operations*. New York: John Wiley & Sons Inc.

Fink, J.K. 2013. *Hydrauloc Fracturing Chemicals and Fluid Technology*, first edition. Oxford: Elsevier.

Elgaddafi, R.M. 2011. *Hole Cleaning Performance of Water-Based Fiber-Containing Sweep Fluids*. MS thesis, University of Oklahoma, Norman, Oklahoma.

Curr, J., Hallett, B., Sweeney, A. 2012. Formate salt gels and methods for dewatering of pipelines or flowlines. US Patent No. 20120114418 A1.

Makela, C., Makela, C. 2014. Composites for the treatment of herpes and cold sores. US Patent No. 8846114 B1.

Dhole, S.D., Chhabra, R.P., Eswaran, V. 2006. Flow of power law fluids past a sphere at intermediate Reynolds number. Ind. Eng. Chem. Res. 45, 4773-4781.

Heider, A., Levenspiel, O. 1989. Drag coefficient and terminal settling velocity of spherical and nonspherical particles. Powder Technol. 58, 63-70.

Kelessidis, V.C. 2004a. Terminal velocity of solid spheres falling in Newtonian and non-Newtonian liquids. Tech. Chron. Sci., J. T. C.G. 24, 43–54.

Kelessidis, V.C. 2004b. An explicit equation for the terminal velocity of solid spheres falling in pseudoplastic liquids. Chem. Eng. Sci. 59, 4437–4447.

Kelessidis, V.C., Mpandelis, G. 2004. Measurements and prediction of terminal velocity of solid spheres falling through stagnant pseudoplastic liquids. Powder Technol. 147, 117–125.

Koziol, K., Glowacki, P. 1988. Determination of the free settling parameters of spherical particles in power law fluids. Chem. Eng. Proc. 24, 183–188.

Lali, A.M., Khare, A.S., Joshi, J.B., Nigam, K.D.P. 1989. Behavior of solid particles in viscous non-Newtonian solutions: settling velocity, wall effects and bed expansion in solid–liquid fluidized beds. Powder Technol. 57, 39–50.

Machac, I., Cakl, J., Lecjaks, Z. 1987. Fall of spheres through non-Newtonian liquids in transient region. In: 9th CHISA Congr., Prague. Machac, L., Ulbrichova, L., Elson, T.P., Cheesman, D.J. 1995. Fall of spherical particles through non-Newtonian suspensions. Chem. Eng. Sci. 50, 3323–3327.

Peden, J.M., Luo, Y. 1987. Settling velocity of variously shaped particles in drilling

and fracturing fluids. SPE Drill. Eng. 2 (Dec), 337– 343.

Prakash, S. 1983. Experimental evaluation of terminal velocity in non-Newtonian fluids in the turbulent region. Ind. Chem. Eng. 25, 1–4.

Renaud, M., Mauret, E., Chhabra, R.P. 2004. Power law fluid flow over a sphere: average shear rate and drag coefficient. Can. J. Chem. Eng. 82, 1066–1070.

Reynolds, P.A., Jones, T.E.R.,1989. An experimental study of the settling velocities of single particles in non-Newtonian fluids. Int. J. Miner. Process. 25, 47–77.

APPENDIX A

RHEOLOGICAL DATA OF POLYMER BLENDS

Analyzed viscometer data used for the rheological study of polymers and their blends are tabulated below. Temperature and pH of these fluids are listed as well.

Table A.1: Rheological Data of 40 lb Guar Gum

RPM	Dial Reading	Wall Shear Rate, s^{-1}	Wall Shear Stress, lb_f/ft^2	Apparent Viscosity, cP	
3	2	5.11	0.0213	202.58	$n = 0.578$
6	3	10.22	0.0320	151.22	$K_v = 0.00842$ lb_f-s^n/ft^2
100	16	170.30	0.1706	46.15	
200	24	340.60	0.2558	34.45	$T = 77\,^{\circ}F$
300	29	510.90	0.3091	29.03	
600	41	1021.80	0.4371	21.67	

Table A.2: Rheological Data of Blend (1:4 X:G 40 lb)

RPM	Dial Reading	Wall Shear Rate, s^{-1}	Wall Shear Stress, lb_f/ft^2	Apparent Viscosity, cP	
3	8	5.11	0.0853	791.58	$n = 0.349$
6	10	10.22	0.1066	503.97	$K_v = 0.04783$ lb_f-s^n/ft^2
100	27	170.30	0.2878	80.63	
200	34	340.60	0.3624	51.34	$T = 77\,^{\circ}F$
300	39	510.90	0.4157	39.42	
600	51	1021.80	0.5437	25.10	

Table A.3: Rheological Data of Blend (1:3 X:G 40 lb)

RPM	Dial Reading	Wall Shear Rate, s^{-1}	Wall Shear Stress, lb_f/ft^2	Apparent Viscosity, cP	
3	11	5.11	0.1173	1065.60	n = 0.306
6	13	10.22	0.1386	658.78	K_v = 0.06901 lb_f-
100	30	170.30	0.3198	93.55	s^n/ft^2
200	37	340.60	0.3944	57.83	T = 77 °F
300	45	510.90	0.4797	43.65	
600	56	1021.80	0.5970	26.99	

Table A.4: Rheological Data of Blend (1:2 X:G 40 lb)

RPM	Dial Reading	Wall Shear Rate, s^{-1}	Wall Shear Stress, lb_f/ft^2	Apparent Viscosity, cP	
3	7	5.11	0.0746	698.60	n = 0.358
6	9	10.22	0.0959	447.68	K_v = 0.04158 lb_f-
100	24	170.30	0.2558	73.54	s^n/ft^2
200	31	340.60	0.3305	47.12	T = 77 °F
300	38	510.90	0.4051	36.32	
600	46	1021.80	0.4904	23.28	

Table A.5: Rheological Data of Blend (2:3 X:G 40 lb)

RPM	Dial Reading	Wall Shear Rate, s^{-1}	Wall Shear Stress, lb_f/ft^2	Apparent Viscosity, cP	
3	9	5.11	0.0959	878.65	n = 0.312
6	11	10.22	0.1173	545.23	K_v = 0.05640 lb_f-
100	24	170.30	0.2558	78.60	s^n/ft^2
200	32	340.60	0.3411	48.77	T = 77 °F
300	38	510.90	0.4051	36.89	
600	48	1021.80	0.5117	22.89	

Table A.6: Rheological Data of Blend (1:1 X:G 40 lb)

RPM	Dial Reading	Wall Shear Rate, s^{-1}	Wall Shear Stress, lb_f/ft^2	Apparent Viscosity, cP	
3	10	5.11	0.1066	939.13	n = 0.298
6	11	10.22	0.1173	577.38	K_v = 0.06161
100	25	170.30	0.2665	80.16	lb_f-s^n/ft^2
200	32	340.60	0.3411	49.29	
300	40	510.90	0.4264	37.08	T = 77 °F
600	46	1021.80	0.4904	22.80	

Table A.7: Rheological Data of Blend (3:2 X:G 40 lb)

RPM	Dial Reading	Wall Shear Rate, s^{-1}	Wall Shear Stress, lb_f/ft^2	Apparent Viscosity, cP	
3	12	5.11	0.1279	1175.93	n = 0.228
6	14	10.22	0.1492	688.64	K_v = 0.08651
100	24	170.30	0.2558	78.48	lb_f-s^n/ft^2
200	30	340.60	0.3198	45.96	
300	34	510.90	0.3624	33.61	T = 77 °F
600	42	1021.80	0.4477	19.68	

Table A.8: Rheological Data of Blend (3:1 X:G 40 lb)

RPM	Dial Reading	Wall Shear Rate, s^{-1}	Wall Shear Stress, lb_f/ft^2	Apparent Viscosity, cP	
3	16	5.11	0.1706	1609.86	n = 0.167
6	19	10.22	0.2025	903.82	K_v = 0.13078 lb_f-
100	26	170.30	0.2772	86.79	s^n/ft^2
200	32	340.60	0.3411	48.73	
300	36	510.90	0.3838	34.76	T = 77 °F
600	41	1021.80	0.4371	19.52	

Table A.9: Rheological Data of Blend (4:1 X:G 40 lb)

RPM	Dial Reading	Wall Shear Rate, s^{-1}	Wall Shear Stress, lb_f/ft^2	Apparent Viscosity, cP	
3	14	5.11	0.1492	1324.76	$n = 0.203$
6	15	10.22	0.1599	762.44	$K_v = 0.10152$ lb_f-
100	24	170.30	0.2558	80.97	s^n/ft^2
200	30	340.60	0.3198	46.60	
300	36	510.90	0.3838	33.73	$T = 77\,^oF$
600	41	1021.80	0.4371	19.41	

Table A.10: Rheological Data of 40 lb Xanthan Gum

RPM	Dial Reading	Wall Shear Rate, s^{-1}	Wall Shear Stress, lb_f/ft^2	Apparent Viscosity, cP	
3	14	5.11	0.1492	1351.56	$n = 0.141$
6	15	10.22	0.1599	745.26	$K_v = 0.11455$
100	20	170.30	0.2132	66.52	lb_f-s^n/ft^2
200	24	340.60	0.2558	36.68	
300	26	510.90	0.2772	25.89	$T = 77\,^oF$
600	31	1021.80	0.3305	14.28	

Table A.11: Rheological Data of 60 lb Guar Gum

RPM	Dial Reading	Wall Shear Rate, s^{-1}	Wall Shear Stress, lb_f/ft^2	Apparent Viscosity, cP	
3	6	5.109	0.0640	633.34	$n = 0.483$
6	9	10.218	0.0959	442.58	$K_v = 0.03074$ lb_f-
100	38	170.3	0.4051	103.33	s^n/ft^2
200	50	340.6	0.5330	72.21	
300	59	510.9	0.6289	58.55	$T = 77\,^oF$
600	74	1021.8	0.7888	40.91	

Table A.12: Rheological Data of Blend (1:4 X:G 60 lb)

RPM	Dial Reading	Wall Shear Rate, s^{-1}	Wall Shear Stress, lb_f/ft^2	Apparent Viscosity, cP	
3	22	5.109	0.2345	2131.66	n = 0.270
6	25	10.218	0.2665	1285.25	K_v = 0.14642 lb_f-
100	54	170.3	0.5756	164.86	s^n/ft^2
200	66	340.6	0.7036	99.40	
300	75	510.9	0.7995	73.94	T = 77 °F
600	90	1021.8	0.9594	44.58	

Table A.13: Rheological Data of Blend (1:3 X:G 60 lb)

RPM	Dial Reading	Wall Shear Rate, s^{-1}	Wall Shear Stress, lb_f/ft^2	Apparent Viscosity, cP	
3	24	5.109	0.2558	2312.14	n = 0.282
6	27	10.218	0.2878	1405.42	K_v = 0.15581 lb_f-
100	62	170.3	0.6609	186.31	s^n/ft^2
200	75	340.6	0.7995	113.25	
300	86	510.9	0.9168	84.64	T = 77 °F
600	103	1021.8	1.0980	51.44	

Table A.14: Rheological Data of Blend (1:2 X:G 60 lb)

RPM	Dial Reading	Wall Shear Rate, s^{-1}	Wall Shear Stress, lb_f/ft^2	Apparent Viscosity, cP	
3	20	5.109	0.2132	1937.57	n = 0.286
6	23	10.218	0.2452	1180.89	K_v = 0.12975 lb_f-
100	52	170.3	0.5543	158.26	s^n/ft^2
200	64	340.6	0.6822	96.45	
300	72	510.9	0.7675	72.20	T = 77 °F
600	90	1021.8	0.9594	44.00	

Table A.15: Rheological Data of Blend (2:3 X:G 60 lb)

RPM	Dial Reading	Wall Shear Rate, s^{-1}	Wall Shear Stress, lb_f/ft^2	Apparent Viscosity, cP	
3	22	5.109	0.2345	2121.71	n = 0.272
6	25	10.218	0.2665	1280.77	K_v = 0.14533 lb_f-
100	53	170.3	0.5650	165.08	s^n/ft^2
200	66	340.6	0.7036	99.65	
300	75	510.9	0.7995	74.17	T = 77 ^{o}F
600	92	1021.8	0.9807	44.78	

Table A.16: Rheological Data of Blend (1:1 X:G 60 lb)

RPM	Dial Reading	Wall Shear Rate, s^{-1}	Wall Shear Stress, lb_f/ft^2	Apparent Viscosity, cP	
3	26	5.109	0.2772	2458.52	n = 0.249
6	28	10.218	0.2985	1460.66	K_v = 0.17482 lb_f-
100	56	170.3	0.5970	176.50	s^n/ft^2
200	69	340.6	0.7355	104.86	
300	79	510.9	0.8421	77.33	T = 77 ^{o}F
600	95	1021.8	1.0127	45.94	

Table A.17: Rheological Data of Blend (3:2 X:G 60 lb)

RPM	Dial Reading	Wall Shear Rate, s^{-1}	Wall Shear Stress, lb_f/ft^2	Apparent Viscosity, cP	
3	24	5.109	0.2558	2291.43	n = 0.221
6	26	10.218	0.2772	1335.69	K_v = 0.17042 lb_f-
100	47	170.3	0.5010	149.38	s^n/ft^2
200	57	340.6	0.6076	87.08	
300	65	510.9	0.6929	63.50	T = 77 ^{o}F
600	77	1021.8	0.8208	37.02	

Table A.18: Rheological Data of Blend (3:1 X:G 60 lb)

RPM	Dial Reading	Wall Shear Rate, s^{-1}	Wall Shear Stress, lb_f/ft^2	Apparent Viscosity, cP	
3	26	5.109	0.2772	2609.51	$n = 0.205$
6	31	10.218	0.3305	1504.28	$K_v = 0.19921$ lb_f-s^n/ft^2
100	51	170.3	0.5437	160.81	
200	61	340.6	0.6503	92.70	$T = 77\ ^oF$
300	67	510.9	0.7142	67.17	
600	81	1021.8	0.8635	38.72	

Table A.19: Rheological Data of Blend (4:1 X:G 60 lb)

RPM	Dial Reading	Wall Shear Rate, s^{-1}	Wall Shear Stress, lb_f/ft^2	Apparent Viscosity, cP	
3	26	5.109	0.2772	2485.40	$n = 0.197$
6	28	10.218	0.2985	1424.48	$K_v = 0.19234$ lb_f-
100	46	170.3	0.4904	148.75	s^n/ft^2
200	56	340.6	0.5970	85.26	
300	62	510.9	0.6609	61.56	$T = 77\ ^oF$
600	75	1021.8	0.7995	35.28	

Table A.20: Rheological Data of 60 lb Xanthan Gum

RPM	Dial Reading	Wall Shear Rate, s^{-1}	Wall Shear Stress, lb_f/ft^2	Apparent Viscosity, cP	
3	16	5.109	0.1706	1556.74	$n = 0.202$
6	18	10.218	0.1919	895.34	$K_v = 0.11949$
100	29	170.3	0.3091	94.83	lb_f-s^n/ft^2
200	36	340.6	0.3838	54.54	
300	40	510.9	0.4264	39.46	$T = 77\ ^oF$
600	48	1021.8	0.5117	22.70	

Table A.21: Rheological Data of 40 lb Guar Gum at 150 ^{o}F

RPM	Dial Reading	Wall Shear Rate, s^{-1}	Wall Shear Stress, lb_f/ft^2	Apparent Viscosity, cP	
3	1	5.11	0.0107	81.51	n = 0.651
6	1	10.22	0.0107	64.00	K_v = 0.00301
100	8	170.30	0.0853	23.98	lb_f-s^n/ft^2
200	13	340.60	0.1386	18.83	T = 150 ^{o}F
300	17	510.90	0.1812	16.35	
600	25	1021.80	0.2665	12.84	

Table A.22: Rheological Data of Blend (1:3 X:G 40 lb) at 150 ^{o}F

RPM	Dial Reading	Wall Shear Rate, s^{-1}	Wall Shear Stress, lb_f/ft^2	Apparent Viscosity, cP	
3	3	5.11	0.0320	301.59	n = 0.410
6	4	10.22	0.0426	200.38	K_v = 0.01648 lb_f-
100	13	170.30	0.1386	38.12	$s^n/ft2$
200	17	340.60	0.1812	25.33	
300	20	510.90	0.2132	19.94	T = 150 ^{o}F
600	26	1021.80	0.2772	13.25	

Table A.23: Rheological Data of Blend (3:1 X:G 40 lb) at 150 ^{o}F

RPM	Dial Reading	Wall Shear Rate, s^{-1}	Wall Shear Stress, lb_f/ft^2	Apparent Viscosity, cP	
3	10	5.11	0.1066	966.62	n = 0.236
6	11	10.22	0.1173	569.34	K_v = 0.07015 lb_f-
100	22	170.30	0.2345	66.42	s^n/ft^2
200	26	340.60	0.2772	39.12	
300	29	510.90	0.3091	28.70	T = 150 ^{o}F
600	34	1021.80	0.3624	16.91	

Table A.24: Rheological Data of 40 lb Xanthan Gum at 150 °F

RPM	Dial Reading	Wall Shear Rate, s^{-1}	Wall Shear Stress, lb_f/ft^2	Apparent Viscosity, cP	
3	11	5.11	0.1173	1114.94	n = 0.195
6	13	10.22	0.1386	638.04	K_v = 0.08659
100	22	170.30	0.2345	66.22	
200	25	340.60	0.2665	37.89	lb_f-s^n/ft^2
300	28	510.90	0.2985	27.34	T = 150 °F
600	31	1021.80	0.3305	15.65	

Table A.25: Rheological Data of 60 lb Guar Gum at 150 °F

RPM	Dial Reading	Wall Shear Rate, s^{-1}	Wall Shear Stress, lb_f/ft^2	Apparent Viscosity, cP	
3	1	5.109	0.0107	112.40	n = 0.735
6	2	10.218	0.0213	93.54	K_v = 0.00362
100	17	170.3	0.1812	44.39	lb_f-s^n/ft^2
200	26	340.6	0.2772	36.94	
300	34	510.9	0.3624	33.18	T = 150 °F
600	47	1021.8	0.5010	27.61	

Table A.26: Rheological Data of Blend (1:3 X:G 60 lb) at 150 °F

RPM	Dial Reading	Wall Shear Rate, s^{-1}	Wall Shear Stress, lb_f/ft^2	Apparent Viscosity, cP	
3	8	5.109	0.0853	790.79	n = 0.390
6	10	10.218	0.1066	518.21	K_v = 0.04465 lb_f-
100	33	170.3	0.3518	93.21	s^n/ft^2
200	42	340.6	0.4477	61.08	
300	46	510.9	0.4904	47.70	T = 150 °F
600	61	1021.8	0.6503	31.26	

Table A.27: Rheological Data of Blend (1:1 X:G 60 lb) at 150 ^{o}F

RPM	Dial Reading	Wall Shear Rate, s^{-1}	Wall Shear Stress, lb$_f$/ft^2	Apparent Viscosity, cP	
3	12	5.109	0.1279	1170.11	n = 0.285
6	14	10.218	0.1492	712.61	K$_v$ = 0.07850 lb$_f$-
100	31	170.3	0.3305	95.20	s^n/ft^2
200	39	340.6	0.4157	57.98	T = 150 ^{o}F
300	43	510.9	0.4584	43.38	
600	54	1021.8	0.5756	26.42	

Table A.28: Rheological Data of Blend (3:1 X:G 60 lb) at 150 ^{o}F

RPM	Dial Reading	Wall Shear Rate, s^{-1}	Wall Shear Stress, lb$_f$/ft^2	Apparent Viscosity, cP	
3	20	5.109	0.2132	2021.73	n = 0.211
6	24	10.218	0.2558	1170.36	K$_v$ = 0.15282
100	41	170.3	0.4371	127.27	lb$_f$-s^n/ft^2
200	49	340.6	0.5223	73.68	T = 150 ^{o}F
300	55	510.9	0.5863	53.51	
600	62	1021.8	0.6609	30.98	

Table A.29: Rheological Data of 60 lb Xanthan Gum at 150 ^{o}F

RPM	Dial Reading	Wall Shear Rate, s^{-1}	Wall Shear Stress, lb$_f$/ft^2	Apparent Viscosity, cP	
3	19	5.109	0.2025	1932.94	n = 0.214
6	23	10.218	0.2452	1120.75	K$_v$ = 0.14556
100	41	170.3	0.4371	122.67	lb$_f$-s^n/ft^2
200	47	340.6	0.5010	71.12	T = 150 ^{o}F
300	51	510.9	0.5437	51.71	
600	61	1021.8	0.6503	29.98	

\

Table A.30: Approximate Shear Rates for Various Processes

Process	Shear Rate, s^{-1}
Static drilling mud	0.001
Fracture flow	0.01 – 500
Very low stirring	0.01 - 0.1
Reservoir flow in oil recovery	1 – 5
Mixing	10 – 100
Pumping	100 – 1000
Flow in tubing	6,000 – 10,000
Flow of drilling mud at bit nozzle	10,000 – 100,000

APPENDIX B

SINGLE PARTICLE SETTLING TESTS

Rheological measurements made prior to single particle setting tests, temperature, pH and data used to estimate terminal settling velocity of particle in polymer fluids and blends are tabulated in this appendix.

Table B.1: Rheological Data of 40 lb Guar Gum

RPM	Dial Reading	
3	2	
6	3	**pH:** 7.70
100	14	
200	20	**T:** 68.54 °F
300	25	
600	36	

Table B.2: Rheological Data of Blend (1:3 X:G 40 lb)

RPM	Dial Reading	
3	10	
6	12	**pH:** 7.72
100	23	
200	30	**T:** 64.40 °F
300	37	
600	50	

Table B.3: Rheological Data of 40 lb Xanthan Gum

RPM	Dial Reading	
3	13	
6	15	**pH:** 7.61
100	25	
200	31	**T:** 64.58 °F
300	37	
600	46	

Table B.4: Rheological Data of 60 lb Guar Gum

RPM	Dial Reading	
3	14	
6	18	**pH:** 7.67
100	59	
200	65	**T:** 55.22 °F
300	76	
600	96	

Table B.5: Rheological Data of Blend (1:3 X:G 60 lb)

RPM	Dial Reading	
3	22	
6	29	**pH:** 7.81
100	59	
200	71	**T:** 59.72 °F
300	80	
600	100	

Table B.6: Rheological Data of 60 lb Xanthan Gum

RPM	Dial Reading	
3	24	
6	26	**pH:** 7.53
100	40	
200	49	**T:** 57.02 °F
300	57	
600	72	

Table B.7: Specifications of Particles

Particle	Mass, g	Particle Diameter, cm	Specific Gravity
1	3.9599	1.438	
2	3.8898	1.436	2.50
3	3.8385	1.434	

Table B.8: Single Particle Settling Data in 40 lb Guar Gum

Particle	Displacement, ft	Time, s
1	1	0.43
	1	0.45
2	1	0.44
	1	0.43
3	1	0.43
	1	0.47

Table B.9: Single Particle Settling Data in Blend (1:3 X:G 40 lb)

Particle	Displacement, ft	Time, s
1	1	1.05
	1	0.99
2	1	0.97
	1	1.02
3	1	0.96
	1	1.07

Table B.10: Single Particle Settling Data in 40 lb Xanthan Gum

Particle	Displacement, ft	Time, s
1	1	0.88
	1	0.87
2	1	1.03
	1	0.97
3	1	1.09
	1	1.10

Table B.11: Single Particle Settling Data in 60 lb Guar Gum

Particle	Displacement, ft	Time, s
1	1	0.84
	1	0.84
2	1	0.85
	1	0.88
3	1	0.93
	1	1.03

Table B.12: Single Particle Settling Data in Blend (1:3 X:G 60 lb)

Particle	Displacement, ft	Time, s
1	1	27.98
	1	28.03
2	1	28.45
	1	29.35
3	1	28.66
	1	29.53

Table B.13: Single Particle Settling Data in 60 lb Xanthan Gum

Particle	Displacement, ft	Time, s
1	1	4.65
	1	4.35
2	1	4.15
	1	4.57
3	1	4.38
	1	4.78